



National Library of Canada

Cataloguing Branch  
Canadian Theses Division

Ottawa, Canada  
K1A 0N4

Bibliothèque nationale du Canada

Direction du catalogage  
Division des thèses canadiennes

## NOTICE

The quality of this microfiche is heavily dependent upon the quality of the original thesis submitted for microfilming. Every effort has been made to ensure the highest quality of reproduction possible.

If pages are missing, contact the university which granted the degree.

Some pages may have indistinct print especially if the original pages were typed with a poor typewriter ribbon or if the university sent us a poor photocopy.

Previously copyrighted materials (journal articles, published tests, etc.) are not filmed.

Reproduction in full or in part of this film is governed by the Canadian Copyright Act, R.S.C. 1970, c. C-30. Please read the authorization forms which accompany this thesis.

**THIS DISSERTATION  
HAS BEEN MICROFILMED  
EXACTLY AS RECEIVED**

## AVIS

La qualité de cette microfiche dépend grandement de la qualité de la thèse soumise au microfilmage. Nous avons tout fait pour assurer une qualité supérieure de reproduction.

S'il manque des pages, veuillez communiquer avec l'université qui a conféré le grade.

La qualité d'impression de certaines pages peut laisser à désirer, surtout si les pages originales ont été dactylographiées à l'aide d'un ruban usé ou si l'université nous a fait parvenir une photocopie de mauvaise qualité.

Les documents qui font déjà l'objet d'un droit d'auteur (articles de revue, examens publiés, etc.) ne sont pas microfilmés.

La reproduction, même partielle, de ce microfilm est soumise à la Loi canadienne sur le droit d'auteur, SRC 1970, c. C-30. Veuillez prendre connaissance des formules d'autorisation qui accompagnent cette thèse.

**LA THÈSE A ÉTÉ  
MICROFILMÉE TELLE QUE  
NOUS L'AVONS REÇUE**



UNIVERSITÉ D'OTTAWA  
UNIVERSITY OF OTTAWA

3

A RIGOROUS APPLICATION OF THE UNIFIED  
MODEL TO SOME DEFORMED NUCLEI

by

Kuen Hwang Huang

Submitted to the Faculty of Graduate Studies  
In Partial Fulfillment of the Requirements  
For the Degree of Doctor of Philosophy

Department of Physics  
Faculty of Science and Engineering  
University of Ottawa  
Ottawa, Canada

1975

Anyone wishing to explore in detail the work which is described in this thesis is strongly advised to consult the following publications directly.

Hird, B. 1971, Can. J. Phys., 49, 302,

Hird, B., 1973, Comp. Phys. Comm., 6, 30.

Hird, B. and Huang, K. H., 1973, Can. J. Phys., 51,956.

Hird, B. and Huang, K. H., 1975, Can. J. Phys., 53,559.

Hird, B. and Huang, K. H., Comp. Phys. Comm., to be published.

## ABSTRACT

The major shell mixed Nilsson model which includes hexadecapole deformations predicts states from the  $1g_{7/2}$  subshell in the low-lying energy level spectra of  $Mg^{25}$ - $Al^{25}$  in a way which is not found experimentally. The ground state spin cannot be explained with this model for reasonable values of the deformation. These difficulties are removed when a Saxon-Woods function is used for the radial dependence of the one body potential. A good fit to the experimental levels is then produced for accepted deformations, but only if the RPC term is considerably reduced. With the pairing correction the model has been used to predict the full low lying rotational band spectrum of the nuclei with  $N = 91$  to  $97$ . Only three adjustable parameters were used to each nucleus to fit the complete spectrum. It was possible in several nuclei to obtain the correct level sequence and in most to confirm level assignments, and the adjusted parameters were in good agreement with accepted values. However, the accuracy of this method is insufficient, in most nuclei, to provide a

reliable prediction for as yet unidentified bands. The lack of good overall agreements in the low lying spectra of these nuclei confirms that the core shape parameters do change from one band to another. The stripping and pickup differential cross section are in reasonable agreement with experimental data.

## ACKNOWLEDGEMENTS

I would like to thank my supervisor, Prof. B. Hird, for his useful suggestions and discussions about this thesis and for some financial support.

I would also like to thank Prof. R. J. W. Hodgson for his valuable discussions in some theoretical background in chapter I of this thesis.

Appreciation is also extended to Prof. Tuncer I. Oren for his MAGE program which was used to type this thesis by computer.

## TABLE OF CONTENTS

	Page
I INTRODUCTION	
(A) The Theoretical Background	I
(B) General Considerations	9
II DESCRIPTION OF THE MODEL	
(A) The Hamiltonian	22
(B) The Solution of The Hamiltonian	26
(C) Matrix Elements	30
(D) The Differential Cross Sections	34
III NUMERICAL CALCULATIONS	
(A) The Mass-25 Calculation	37
(B) The Mass-153 to 165 Calculation	40
IV RESULTS AND CONCLUSION	
(A) Comparison of The Energy Levels of Mass-25 using a Saxon-Woods Potential with those using a Harmonic Oscillator Potential	43
1. The Nilsson Diagram for Quadruple Deformations only	43
2. RPC and Band Mixing	46
3. The Hexadecapole Deformation	48

	Page
4. Conclusion	53
(B) The Energy Levels and the Stripping and Pick-up Differential Cross Sections for Mass-153 to 165	
1. General Discussion of The Level Systematics	54
2. Discussion of Individual Isotone Groups	
(a) N=91	58
(b) N=93	61
(c) N=95	65
(d) N=97	69
3. Conclusion	72
V TABLES AND FIGURES	77
VI REFERENCES	II3
VII APPENDIX	II8
(A) The Matrix Elements and Quasi-Particle Transformations	II8
(B) The Computer Program with Its Flow Chart	I23

## (A) Theoretical Background

In order to explain the structure of the nucleus, many models have been introduced. Most of them were developed from two aspects: 1) The nucleons in the nucleus are described by considering that they move independently of each other in a potential well and 2) The nucleus is described by the collective motion of all of the nucleons and independent particle motion is ignored.

The nuclear shell model mainly represents the development of the independent particle aspect. There are three models derived from the shell model: The extreme single particle model, the single particle model, and the individual (independent) particle model. In the extreme single particle model the nucleons in the nucleus move independently in a mean potential. Most of the nucleons are paired so that a pair of nucleons contribute zero spin and zero magnetic moment. The paired nucleons thus form an inert core, and this model therefore predicts that the spins

and the magnetic moments of the even-even nuclei are zero. In the case of odd mass nuclei the properties of the nucleus are characterized by the unpaired nucleon, and for odd-odd nuclei, by the unpaired proton and neutron. Very strong experimental evidence exists which supports this point of view, when a nucleus contains the so-called "Magic Number". The model also predicts the electromagnetic and the nuclear ground state properties of the nucleus in terms of the uncorrelated motion of a single particle in the specified mean potential.

A refinement of the extreme single particle model is the single particle model in which states of several particles are involved. The nucleus consists of filled shells which contain the maximum number of neutrons or protons allowed by the Pauli principle and of unfilled shells containing "loose" particles. All the loose particles are considered in describing the properties of the nucleus. The nuclear wave function is represented by the configuration of its loose particles and is given by the Slater determinant. It is found that this model can explain many nuclear properties such as the spin, the magnetic moment, nuclear isomerism, and stripping reaction

spectroscopic factors.

In the individual particle model all the nucleons in the nucleus are taken into account. This model is also referred to as the many-particle shell model. The wave function for one configuration of the nucleus is the properly antisymmetrized Slater determinant of the single particle wave functions of all the nucleons in the nucleus. This model has been successfully applied in the prediction of the energy levels and also the binding energies of light nuclei.

The liquid drop model (Bohr and Kalckar 1937) was based on several properties of the nucleus which are similar to the properties of a liquid drop: The nucleons in the nucleus correspond to the molecules of which a liquid is composed. The similarity can be visualized in three alternative ways. The density of nucleus which is independent of its mass is analogous to the density of a liquid drop which is independent of its size. The radius of a nucleus which is proportional to the cube root of its mass number is analogous to the radius of a liquid drop which is proportional to the cube root of the number of the molecules. The binding energy of a nucleus which is proportional to the

mass number can be compared to the energy needed to evaporate the drop of the liquid into separate molecules, this is surface energy of thermodynamics. And hence the energy is proportional to the number of molecules.

Both the nuclear shell model and liquid drop model achieved respectability by their overwhelming success. The shell model has been most successful in explaining only a certain number of nuclear features, and it does not provide a complete description of the nucleus. It was particularly successful in the case of nuclei composed of a closed shell plus one or a few additional nucleons. In the closed shell configuration the nucleus is spherical. The addition of one or more nucleons produces only a small deformation. However, midway between closed shells the situation is different. The nuclei depart appreciably from the spherical form and collective motion involving many nucleons becomes important.

Criticism of the liquid drop model were based on the unliquid like nature of nuclear matter. Molecules in a liquid have long-range interactions and are essentially localized, whereas nucleons have short-range interactions and

are not localized. Even so, we nowadays believe that the liquid drop like collective motion plays a very important part in nuclear spectroscopy. Its existence is demonstrated most forcefully by the systematic appearance, throughout the periodic table, of the low lying  $2^+$  excited states in even-even nuclei (Scharff-Goldhaber (1953), Scharff-Goldhaber and Weneser (1955)). These states have ground state transition strengths of very many single-particle magnitudes. Such large strengths can only be envisaged as the cooperative effect of many particles, that is as a collective motion. For the rare-earth and actinide nuclei, these strengths are especially large and the excited state also have large quadrupole moments. The interpretation is that these nuclei have highly deformed equilibrium shapes and should consequently exhibit rotational spectra. Other nuclei have little or no static quadrupole moment, but still show large transition strength, which are interpreted as being derived from a collective vibration of the nucleus about its spherical equilibrium shape.

The unified (collective) model (Bohr and Mottelson, 1952, 1953) encompasses some properties of both the shell

model and the liquid drop model. Their contribution was to shift the collective motion of the particle density to the collective motion of the independent particle field. In this way the collective and particle aspects of the nucleus could coexist quite naturally. The shape of the nucleus based on this model is influenced by the field force (which correspond to the long-range part of the two-body interaction) which tends to align the nucleon orbits and create a deformed nucleus, while the short-range pairing force tends to scatter nucleons isotropically and stabilize the spherical shape. The equilibrium shape of the nucleus depends therefore on the balance between these two principal ingredients. The deformation in the shape of the nucleus leads to modes of excitation which are classified as vibrational and rotational.

Under the unified model, there are two main aspects: One is that the aligned wave function is derived phenomenologically by combining the single particle wavefunctions of a deformed potential well, it may be described as the deformed shell model, a particular example of which is the Nilsson model (Nilsson 1955). The other aspect is where the aligned wave functions and the field are

derived by self-consistent methods, this is called the Hartree-Fock (HF) self-consistent field method in which an approximation is made for reducing the problem of many interacting particles to one of a non-interacting particle in a field. It neglects a large part of the interaction force which is called the residual interaction.

In considering the residual interaction the HF method has been extended by the several theories: The quasi-particle theory (which is called the BCS theory after Bardeen, Cooper, and Schrieffer, 1957 and which can be regarded as a generalized HF theory) is designed to take account of the short-range part of the residual interaction. The time dependent Hartree Fock theory (TDHF theory) is made to describe the excited states and, in particular, to take account of the long-range or field-producing part of the residual interaction. This theory goes under the other name RPA (which stands for the random-phase approximation), the quasi-boson approximation, and the method of linearized equations. The TDHF theory has been used most extensively in the calculation of nuclear collective vibrational excitations, particularly for the low-lying quadrupole and octupole vibration and for the high-lying giant dipole

excitation.

This thesis and the papers (Hird and Huang, 1973, 1975) are based on the unified model in which the Nilsson model with a Saxon-Woods potential was used to calculate the long-range interaction and the BCS theory was chosen to represent the short-range interaction.

## (B) General Considerations

One of the features of the half-filled shells of both neutrons and protons is to favour the aligned coupling of their wave functions to form a stable deformed nucleus. There are three deformed mass regions:  $A=25$  (Region I),  $152 < A < 190$  (Region II), and  $A > 224$  (Region III). When nucleons are added outside a closed shell they first occupy the  $3$ -projection,  $\Omega$ , of the empty  $j$ -shell at  $\Omega = 1/2 \ll j$  which have a density distribution concentrated along the polar axis, so that prolate deformation is found in nuclei with less than half filled shells. On the other hand, beyond half filled shells the holes in the complete shell tend to be in orbits with  $\Omega \approx j$  which have a density distribution concentrated in the equatorial plane, the shapes of these nuclei therefore favour the oblate deformation. So the prolate shape is favoured for  $0 < n < j + 1/2$  and the oblate for  $j + 1/2 < n < 2j + 1$ , where  $n$  is the number of nucleons within the valence shell.

Another feature of the half filled shell is that the residual interaction, that is the interaction which cannot

be described in terms of the average field potential well, plays an important role in a discussion of the deformed odd-A nuclei. The BCS theory was used to treat the short-range component of this residual nucleon-nucleon interaction. The theory provides a mathematical formalism for describing the experimental fact that the nucleons prefer to exist as correlated pairs and that these pairs continuously scatter from one orbit to another. According to this model, which has strong experimental support, the Fermi surface in a real nucleus is not sharp, but diffuse, with the consequence that the elementary excitations of odd-A nuclei should be thought of as one quasiparticle states, not as single particle states (Nathan and Nilsson 1965, Ogle etc. 1971). The effect of this treatment provides much more realistic predictions of reaction cross sections and transition probabilities than does the single particle model without pairing correlation which often form the main basis for a particular state assignment.

Some nuclei in the region of a half filled shell are believed to follow more the aligned coupling scheme than the pairing coupling scheme because their pairing strengths are not strong enough to generate a diffuse Fermi surface and it

## II

is not appropriate to apply the BCS theory to these nuclei. Mass number  $A=25$  (Region I) is in this picture. The low energy structures of the odd- $A$  deformed nuclei in the rare-earth mass (Region II), where the examples of both the aligned and the pairing coupling schemes exist, are remarkably well described by a unified model which takes into account not only the independent particle motion (Nilsson 1955) but also pairing correlation and collective phenomena (Nathan and Nilsson, 1965). For example, in nearly all the well studied cases, the first few energy levels in these nuclei are describable as rather pure Nilsson one-quasiparticle states with their associated rotational excitations.

Nilsson (1955) made in this pioneering work an analysis of nonspherical nuclei which are characterized by the presence of the rotational bands in their structure. His model has been very successful in understanding the low lying single particle levels of many odd mass number nuclei which have permanent deformations.

Because of its success, the original formulation of the model has been extended in several ways. Some examples

of these are, 1) The inclusion of the interaction between particle states and core excitations, so that both may be considered simultaneously. The interaction is known by the names of Rotation Particle Coupling, RPC, and band mixing (Kerman 1965). 2) The particle states which are eigenstates of an ellipsoidal potential in which all three principal axes are different have been calculated (Newton 1960, Hecht and Satchler 1962, Chi and Davidson 1963). This is described as the triaxial model. 3) Higher deformations in the symmetric core have been added. The next higher order of deformation beyond the spheroidal shape which retains axial symmetry is the hexadecapole term  $Y_4^0$  (Kjallquist 1958/59, Harada 1964). It has been established that in certain mass regions one or more of these extensions to the model has important consequences and in all cases the existence of these extra terms has been detected experimentally.

The extensions to the Nilsson model have so far mostly been confined to the angular part of the Hamiltonian. In almost all published calculations the harmonic oscillator radial dependence of the original model has been retained. There are computational advantages to using the harmonic oscillator potential. It is the lowest order even parity

potential and the matrix elements all have simple algebraic forms. The centre of mass effects, which are usually neglected, can be separated in a unique way from the internal motion (De-Shalit and Talmi 1963). However even in the original formulation some modification of the simple  $r^2$  dependence is required to match the observed single particle level spacings and Nilsson added a term  $CL^2$  to simulate the level ordering of a somewhat flatter radial potential than the harmonic oscillator. The  $j$  splitting of the shell model was generated by adding a spin-orbit interaction  $Dl \cdot s$  which also was assumed to have a harmonic radial dependence in the early theories. These two terms introduce two arbitrary constants  $C$  and  $D$ , or alternatively the constants  $k = C/(2\hbar\omega)$  and  $\mu = 2D/C$  of Nilsson. It is interesting to notice that the  $L^2$  interaction represents a modification to the angular dependence which is introduced in order to minimize a deficiency in the radial part of the potential.

A further computational advantage of the harmonic oscillator potential is that  $N$ , the radial quantum number is approximately a good quantum number for the spheroidal potential states. Nilsson showed that the  $N$  mixing matrix elements are relatively small, and he neglected them in his

numerical calculations. He also provided an alternative representation which, though it is exactly diagonal in  $N$  is only approximately diagonal in the angular quantum numbers. It has been verified by direct calculation that the  $N$  mixing does not qualitatively change the Nilsson diagram, for example there are no changes in the level ordering, so that in most situations this approximation is quite justified. However there are three experimentally relevant applications of the Nilsson model where  $N$  mixing plays a decisive role, and there is reason to believe that the poor agreement which occurs after including the  $N$  mixing interactions originates in the harmonic oscillator assumption. The first, and the obvious requirement for including an interaction between different  $N$  shells is where two levels from shells differing by 2 in  $N$  cross each other. In the mass region  $A=153$  to  $171$  it is found that the large positive deformations which occur there cause the highest two levels from the  $N=4$  shell to cross the lowest two levels from the  $N=6$  shell. The  $1/2^+$  levels in several of these nuclei have been identified as strongly mixed states of  $[400]$  and  $[600]$  and two  $3/2^+$  levels as mixed  $[402]$  and  $[651]$  states. Calculations using harmonic oscillator functions fail to predict the mixing by an order of magnitude at the observed energy separation of

these levels (Anderson 1968, Kanestrom, Tjom and Bang 1971). The required mixing can however be obtained by adding a hexadecapole term  $Y_4^0$ . The higher multipole terms  $Y_n^0$  introduce direct mixing across  $N$  major shells and the  $N \leftrightarrow N+2$  matrix elements are much larger. No general investigation of the  $N$  diagonal approximation has been made, though the presence of hexadecapole and possibly higher terms has been established in several mass regions, however some conclusions which are obtained by adding the  $Y_4^0$  term to a single shell Hamiltonian (Turner and Trainer 1968) are found to be changed when a larger basis involving several  $N$  shells is used (Hird 1971). It may be that calculations which are made to compare the hexadecapole and higher deformations with experiment may be, at most, qualitatively valid (Harada 1964, Rebel et al. 1972, Hendrie et al. 1968) when harmonic oscillator states are assumed. The third area where  $N$  mixing is important, but where the model does not give agreement is in a reaction mechanism which is specially sensitive to the nuclear surface. In neutron pick-up reactions the  $N$  mixing has the effect of changing spectroscopic factors between mixed Nilsson states in the 1d-2s shell by about a factor of 2 (Kroon et al 1971). The

effect of the harmonic oscillator assumption (Rost 1967) is not too serious on the strongest transitions, but those which go by way of N mixing, and are otherwise j-forbidden, are quite unreliably predicted. In the calculation of two neutron pick-up spectroscopic factors the predictions using the technique developed by Bayman and Kallio (1967) for Saxon-Woods bound states are quite different from those using a reaction theory where the bound states are described by harmonic oscillator wave function matched to a hankel tail (Glendenning 1965).

In more recent calculations, where detailed fits to experimental levels were made, the excitations of pairs of nucleons from the core were taken into account by the quasiparticle transformation. In the region of large permanent deformations, this transformation generates Nilsson quasiparticle states which are significantly closer together than they are in the Nilsson diagram, so that their separations have the correct order of magnitude to fit the experimental band head energy spacing. When the particle states have the same order of spacings as the rotational bands spacings, then the Coriolis coupling, which mixes bands, becomes important and this can make detailed changes

in the level spacings, and also significantly change the spectroscopic factors of nucleon transfer reactions.

This thesis describes calculations in two mass regions: One is mass-25 and the other is mass-153 to 165. The Nilsson diagram of the deformed harmonic oscillator potential was compared with the deformed Saxon-Woods potential in calculating the energy levels of the mass-25 nuclei. After the comparison of two potentials in the mass-25 region, the deformed Saxon-woods potential was chosen to calculate the mass-153 to 165 region.

The single particle model with the deformed Saxon-Woods potential adopted for nonspherical nuclei with axial symmetry is described in Section II. The formulation of the Hamiltonian of the deformed Saxon-woods potential with a pairing force is given. The assumption of the incompressibility of nuclear matter is taken into account by making small changes in the mean nuclear radius up to second order in the deformation parameters. The deformed wave functions are given in terms of the spherical Saxon-woods potential basis. The BCS theory is used to calculate the core energy.

In Section III, two computer programs are described which were used for the numerical calculation. In the mass-25 region the total wave function and its associated energy were obtained by three successive diagonalizations of different terms in the Hamiltonian. The spherically symmetric part is first diagonalized in a harmonic oscillator basis by using the numerically integrated radial matrix elements. The second diagonalization generates the deformed single particle states in a basis of the spherically symmetric eigenstates of the first diagonalization, and finally the core and RCP terms are diagonalized in a basis of the deformed states. Only two successive steps were used to diagonalize the matrix elements of the Hamiltonian for calculating the mass-153 to 165. The deformed part was first diagonalized in a basis of the spherical Saxon-Woods eigenstates, and then, the core and RCP terms with the pairing force were diagonalized in a basis of the deformed states.

The results and conclusions are described in Section IV. There were two subdivisions: (A) The energy levels of  $Mg^{25}$  and  $Al^{25}$  using a Saxon-Woods potential are compared with the levels using a harmonic oscillator potential. The

Nilsson diagrams for these potentials both of which have quadruple deformations, are similar, but the Nilsson diagram is quite different when a hexadecapole deformation is added. The Saxon-Woods potential yields a more correct level sequence for the deformed states than the harmonic oscillator potential. (B) The results of the energy level, stripping and pick-up cross section of  $\text{Sm}^{153}$ ,  $\text{Gd}^{155, 157, 159, 161}$ ,  $\text{Dy}^{157, 159, 161, 163}$ , and  $\text{Er}^{161, 163, 165}$  were calculated by the deformed Saxon-Woods potential. The number of adjustable parameters were kept to the minimum which is needed to completely specify the model. For example, a single energy parameter  $\hbar^2/2g_0$ , which represents the quantum of core rotational energy, completely determines the Coriolis Coupling between bands, and the decoupling parameter within  $K=1/2$  bands, and hence determines the level spacing within bands. The shape of the core and the rotational energy are expected to change with the number of nucleons in the core, so the three parameters  $\beta_2$ ,  $\beta_4$  and  $\hbar^2/2g_0$  were allowed to vary from one nucleus to another. many well defined rotational bands have been identified in this region of the permanent deformation; there is considerable interband mixing and some major shell mixing. On the other hand many levels remain to be incorporated into

the model. A particular difficulty in fitting this range of nuclei, containing several different neutron numbers is that the odd valence neutron is found to occupy the same  $3/2-[521]$  orbital in nuclei with different numbers of core neutrons so that level crossing must occur between such isotopes. The problem of the positive parity states is more complicated than for the negative parity states, with more band mixing among more closely spaced levels. These positive parity states were not considered in the calculations, except where the ground state has positive parity, in which case the relative excitation of this particle state was also included in the theoretical predictions. The single particle states had to be calculated for both positive and negative-parity states in order to determine the Fermi energy in the quasiparticle transformation, but only the negative parity states were afterwards retained for the subsequent diagonalisations.

There are seventeen tables and twelve figures in Section V. The References are in Section VI. The two appendices are in Section VII. The detail calculation of the matrix elements of a Hamiltonian with a spherical Saxon-Woods potential basis and the quasi-particle

transformation are included in Appendix (A). The computer program, which was written for the mass-153 to 165 calculation, with its flow chart, is shown in Appendix (B).

## II DESCRIPTION OF THE MODEL

### (A) Hamiltonian

The total Hamiltonian, in which the last odd nucleon is added to the deformed even-even core of the nucleus, can be schematically written

$$H = H_p + H_c + H_{rot} + H_{rpc} \text{ ----- (1)}$$

Where  $H_p$  represents the single particle motion with respect to the core in the body fixed coordinates,  $H_c$  is the Hamiltonian operator for particle states occupied by the core nucleons,  $H_{rot}$  describes the rotational motion of the nucleus, and  $H_{rpc}$  is the Coriolis interaction coupling the intrinsic and the rotational motion of the deformed even-even nuclear core. The eq(1) may be expressed as follows

$$H_p = H_{sp} - V_0 R_0 \frac{\partial f(r, R, \theta)}{\partial R} \Big|_{R=R_0} \left[ \beta_{-2} Y_{-2}^0(\theta) + \beta_{+2} Y_{+2}^0(\theta) - \frac{\beta_{-2}^2}{4\pi} - \frac{\beta_{+2}^2}{4\pi} \right]$$

$$- V_0 \frac{R_0^2}{2} \frac{\partial^2 f(r, R, \theta)}{\partial^2 R} \Big|_{R=R_0} \left\{ \beta_{-2}^2 [Y_{-2}^0(\theta)]^2 + \beta_{+2}^2 [Y_{+2}^0(\theta)]^2 \right\} \text{ ----- (2)}$$

Where

$$H_{sp} = -\frac{\hbar}{2m} \nabla^2 - V_0 f(r) + \left(\frac{\hbar}{m_\pi c}\right) z v_{z0} \frac{1}{r} \frac{\partial f(r)}{\partial r} \vec{l} \cdot \vec{\sigma} \quad (3)$$

With

$$f(r, R, \theta) = \{1 + \exp[(r-R)/a_d]\}^{-1} \quad (4)$$

$$f(r) = \{1 + \exp[(r-R_0)/a_d]\}^{-1} \quad (4a)$$

$$R = R_0 \left[ 1 - \frac{\beta_2^2}{4\pi} - \frac{\beta_4^2}{4\pi} + \beta_2 Y_2^0(\theta) + \beta_4 Y_4^0(\theta) \right] \quad (5)$$

And

$$\left. \frac{\partial f(r, R, \theta)}{\partial R} \right|_{R=R_0} = \frac{1}{a_0} \exp\left(\frac{r-R_0}{a_0}\right) \left[ 1 + \exp\left(\frac{r-R_0}{a_0}\right) \right]^{-2} \quad (6)$$

$$\left. \frac{\partial^2 f(r, R, \theta)}{\partial R^2} \right|_{R=R_0} = \frac{-1}{a_0^2} \exp\left(\frac{r-R_0}{a_0}\right) \left[ 1 - \exp\left(\frac{r-R_0}{a_0}\right) \right] \left[ 1 + \exp\left(\frac{r-R_0}{a_0}\right) \right]^{-3}$$

$$\text{-----} \quad (6b)$$

Here the deformed Saxon-Woods potential is used for calculating the single particle energy and wave function. The  $\hbar/m_\pi c$  in the spin-orbit term of eq(3) is the  $\pi$ -meson

Compton wavelength. The Pauli-spin operator  $\vec{\sigma}$  and orbital angular momentum operator  $\vec{l}$  are given in units of  $\hbar$ . The parameters in the Saxon-Woods potential are the nuclear radius  $R=r A^{1/3}$ , the surface thickness  $a_0$ , and the depth of the central potential  $V_0$ .  $V_{so}$  is the spin-orbit constant. The  $\beta_2$  and  $\beta_4$  in eq(2) are quadrupole and hexadecapole deformation parameters respectively. The term  $-\left(\frac{\beta_2^2}{4\pi} + \frac{\beta_4^2}{4\pi}\right)$  in R guarantees volume conservation to second order in the deformation parameters.

The  $H_{rot}$  and  $H_{rpc}$  for a symmetric rotor about the 3-axis of the deformed even-even core of the nucleus are

$$H_{rot} = \frac{\hbar^2}{2g_0} [I^2 + j^2 - I_3^2 - j_3^2] \text{-----} (7)$$

$$H_{rpc} = -\frac{\hbar^2}{2g_0} [I^+ j^- + I^- j^+] \text{-----} (8)$$

With

$$j^\pm = j_r \pm i j_a$$

$$I^\pm = I_r \pm i I_a$$

Here  $I=R+J$  is the total angular momentum which consists of the rotation part  $R$  and the total intrinsic part  $J$ . Because

of the assumed symmetry about the 3-axis the relation  $R_3=0$  or  $I_3=J_3$  holds. The total spin  $I$  is a constant of motion, but  $J$  is not because of the presence of  $H_{rpc}$ .

The particle states occupied by the core nucleons feel a short-range force which tends to couple the particles pairwise to form a stable  $J=0$  configuration. The short-range Hamiltonian operator (BCS) is

$$H_c = \sum_{\nu \neq \mu} (\epsilon_\nu - \chi^{(\mu)}) (a_{\nu}^+ a_{\nu} + a_{-\nu}^+ a_{-\nu}) - G \sum_{\nu, \mu \neq \mu} a_{\nu}^+ a_{-\nu}^+ a_{-\mu} a_{\mu} \quad (9).$$

In the notation,  $\epsilon_\nu$  is the single particle energy of eq(2).  $\chi^{(\mu)}$  is the Fermi energy for which the state  $|\mu\rangle$  of the last odd particle outside the core is blocked,  $a_\nu$  and  $a_\nu^+$  are the annihilation and creation operators, and  $G$  is the strength of the pairing force.

## (B) The Solution of The Hamiltonian

The approximation which is made to obtain the solution of eq(1) is that the rotation of the nucleus is slow enough that the intrinsic motion can be considered to be independent of the rotational motion at any moment, that is the eigenfunction can be separated except for the RPC term. Under this assumption, the eigenfunction of eq(1) in the absence of RPC can be expressed as follows

$$|\bar{\Phi}_{K,\mu}\rangle = \left(\frac{2I+1}{16\pi^2}\right)^{1/2} [D_{M,K}^I(\theta) a_{\pm,\mu}^\dagger + (-1)^{I-1/2} D_{M,-K}^I(\theta) a_{\mp,\mu}^\dagger] \varphi_c \quad (10)$$

Here M and K are, respectively, the 3-projection of the rotation wavefunction in the space-fixed and body-fixed coordinate.  $\varphi_c$  is the wavefunction of the core corresponding to a solution of eq(9) and is obtained using a trial wavefunction method employed by the BCS theory to satisfy

$$\varphi_c = \prod_{\nu \neq \mu} (U_\nu^{(\mu)} + V_\nu^{(\mu)} a_\nu^\dagger a_{-\nu}^\dagger) |0\rangle \quad (11)$$

and

$$|\mu\rangle = |jQ\rangle = a_{\mu}^{\dagger} \phi_{\nu} \text{-----} (12)$$

Here  $|0\rangle$  is the bare-particle vacuum and  $\nu$  is the index of the particle inside the core. The requirement for normalization of the  $U_{\nu}^{(\mu)}$  and  $V_{\nu}^{(\mu)}$  is

$$(U_{\nu}^{(\mu)})^2 + (V_{\nu}^{(\mu)})^2 = 1 \text{-----} (13)$$

The single particle state of the spherical nucleus  $|jQ\rangle$ , which is the solution of eq(3), is

$$|jQ\rangle = |\bar{p}jQ\rangle = \frac{1}{r} U_{\bar{p}jQ}(r) \sum_{\Lambda \Sigma} \langle \Lambda \frac{1}{2} \Sigma | jQ \rangle Y_{\Lambda \Lambda}(\theta, \phi) f_{\frac{1}{2} \Sigma} \text{-----} (14)$$

where  $\frac{1}{r} U_{\bar{p}jQ}(r)$  is the radial eigenfunction of eq(3),  $Y_{\Lambda \Lambda}(\theta, \phi)$  is the angular part and  $f_{\frac{1}{2} \Sigma}$  is the spin function.  $\Lambda$  and  $\Sigma$  are the projections of the orbital angular momentum and the spin  $s = \frac{1}{2}$ .  $\bar{p}$  is related to the radial quantum number of the harmonic oscillator  $N$  by mean of the equation

$$\bar{p} = (N - l) / 2 + 1 \text{-----} (15)$$

the  $\langle \Lambda \frac{1}{2} \Sigma | jQ \rangle$  in eq(14) is Clebsch-Gordan coefficient.

The eigenfunction of eq(2),  $\chi_{\mu}$ , is calculated by expanding in the spherical basis function  $|jq\rangle$ , that is

$$\chi_{\mu} = \chi_{\Omega, \mu} = \sum_j C_{j, \Omega, \mu} |jq\rangle \text{-----} (16a)$$

For the negative projection

$$\chi_{-\mu} = \chi_{-\Omega, \mu} = \sum_j (-1)^{j-1/2} C_{j, \Omega, \mu} |j-\Omega\rangle \text{-----} (16b)$$

with its eigenvalue  $\epsilon_{\mu}$ . The extra index  $t$  is introduced to distinguish between different Nilsson levels in the same oscillator shell having the same projection quantum number  $\Omega$ .

The wavefunction of eq(1) when the Coriolis interaction is included is

$$\begin{aligned} \Psi(I, M) &= \sum_{K=\Omega} \sum_{\mu} C_{K, \mu} |\Phi_{K, \mu}\rangle \\ &= \left(\frac{2I+1}{16\pi^2}\right) \sum_{K=\Omega} \sum_{\mu} C_{K, \mu} [D_{M, K}^I(\theta) a_{\Omega, \mu}^{\dagger} + (-1)^{I-1/2} D_{M, -K}^I(\theta) a_{-\Omega, \mu}^{\dagger}] \\ &\cdot \varphi_c \text{-----} (17) \end{aligned}$$

where the coefficients  $C_{\kappa u}$  are determined after the diagonalization of the matrix.

## (C) Matrix Elements

The matrix element of eq (1) is calculated by using as a basis the eigenfunctions of eq(10)

$$\begin{aligned}
 \langle \bar{\Phi}_{k',\mu} | H | \bar{\Phi}_{k,\mu} \rangle &= \langle \bar{\Phi}_{k',\mu} | (H_p + H_c + H_{rot} + H_{rpc}) | \bar{\Phi}_{k,\mu} \rangle \\
 &= \epsilon_{\mu} \delta_{k'k} \delta_{\mu\mu} + \epsilon_c^{\mu} \delta_{k'k} \delta_{\mu\mu} + \frac{\hbar^2}{2I} \left\{ [I(I+1) \right. \\
 &\quad \left. - 2Q^2] \delta_{k'k} \delta_{\mu\mu} + \sum_j c_{j\mu} c_{j\mu} j(j+1) \delta_{k'k} \right\} + \langle \bar{\Phi}_{k',\mu} | H_{rpc} | \bar{\Phi}_{k,\mu} \rangle
 \end{aligned}$$

----- (18)

Where the matrices of  $H_p$  and  $H_c$  are diagonal, and their expectation value are, respectively,  $\epsilon_{\mu}$  and  $\epsilon_c^{\mu}$ . The  $j^2$  term contributes both to the diagonal and off diagonal elements. By using a variational method (Rowe 1970) for eq(9) the total energy of even-even core with state  $\mu$  being blocked is

$$\epsilon_c^{\mu} = \langle \bar{\Phi}_{k,\mu} | H_c | \bar{\Phi}_{k,\mu} \rangle = \langle \psi_c | H_c | \psi_c \rangle$$

$$= \sum_{\nu \neq \mu} [2(\mathcal{E}'_{\nu} - \chi^{(\mu)}) (v_{\nu}^{(\mu)})^2 - G(v_{\nu}^{(\mu)})^4] \text{-----} (19)$$

with

$$N = 2 \sum_{\nu \neq \mu} (v_{\nu}^{(\mu)})^2 \text{-----} (20)$$

$$\mathcal{E}_{\nu}^{(\mu)} = [(\mathcal{E}'_{\nu} - \chi^{(\mu)})^2 + (\Delta^{(\mu)})^2]^{1/2} \text{-----} (20a)$$

$$u_{\nu}^{(\mu)} = \left\{ \frac{1}{2} [1 + (\mathcal{E}'_{\nu} - \chi^{(\mu)}) / \mathcal{E}_{\nu}^{(\mu)}] \right\}^{1/2} \text{-----} (20b)$$

$$v_{\nu}^{(\mu)} = [1 - (u_{\nu}^{(\mu)})^2]^{1/2} \text{-----} (20c)$$

where

$$\Delta^{(\mu)} = G \sum_{\nu \neq \mu} u_{\nu}^{(\mu)} v_{\nu}^{(\mu)} \text{-----} (20d)$$

$$\mathcal{E}'_{\nu} = \mathcal{E}_{\nu} - Gv^2 \text{-----} (20e)$$

Here  $N$  is the true particle number in the system and  $Gv^2$ , which is small in comparison with  $\mathcal{E}_{\nu}$  in eq(20e), can be neglected through eq(19) to eq(20d) in the self-consistent calculation.

From eq (A-8) (see appendix), the eq (10) can be written as

$$\begin{aligned}
 \langle \Phi_{\kappa', \mu'} | H | \Phi_{\kappa, \mu} \rangle = & \mathcal{E}_{\mu} + \mathcal{E}_{\xi}(\mu) + \frac{\hbar^2}{2g_0} [I(I+1) \\
 & - 2Q^2] \delta_{\kappa'=\Omega, \kappa} \delta_{\mu', \mu} + \frac{\hbar^2}{2g_0} \left\{ \sum_j C_{j, \mu'} C_{j, \mu} j(j+1) \delta_{\kappa'=\Omega, \kappa} \right. \\
 & \left. - [(I \mp Q)(I \pm Q + 1)]^{1/2} \sum_j (-1)^{I-j} C_{j, \mu} C_{j, (\mu \pm 1), \mu} [(j \mp Q)(j \pm Q + 1)]^{1/2} \right. \\
 & \left. \cdot P(\mu', \mu) \right\} \text{-----} (21)
 \end{aligned}$$

Here  $P(\mu', \mu)$  is given by eq (A-3), it can be written for  $\tau = +$  as follows

$$P(\mu', \mu) = \frac{(\mathcal{U}_{\mu'}(\mu) \mathcal{U}_{\mu}(\mu') - \mathcal{V}_{\mu'}(\mu) \mathcal{V}_{\mu}(\mu'))}{\prod_{\lambda \neq \mu', \mu} (\mathcal{U}_{\lambda}(\mu') \mathcal{U}_{\lambda}(\mu) + \mathcal{V}_{\lambda}(\mu') \mathcal{V}_{\lambda}(\mu))} \text{----} (22)$$

For numerical calculation, it is convenience to separate the diagonal and off-diagonal matrices of eq (21).

$$\begin{aligned}
 \langle \Phi_{\kappa, \mu} | H(D) | \Phi_{\kappa, \mu} \rangle = & \mathcal{E}_{\mu} + \mathcal{E}_{\xi}(\mu) + \frac{\hbar^2}{2g_0} [I(I+1) + \sum_j (C_{j, \mu})^2 j(j+1) - 2Q^2] \\
 & - \frac{\hbar^2}{2g_0} (I + \frac{1}{2}) \sum_j (-1)^{I-j} (C_{j, \frac{1}{2}, \mu})^2 (j + \frac{1}{2}) \delta_{\mu, \frac{1}{2}} \text{-----} (23)
 \end{aligned}$$

and

$$\langle \bar{\Phi}_{K,\mu} | H(OD) | \bar{\Phi}_{-(K\pm 1),\mu} \rangle = -\frac{\hbar^2}{2g_0} [ (I\mp Q) (I\pm Q + 1) ]^{1/2}$$

$$\sum_j (-1)^{I-j} C_{j\pm\mu} C_{j-(Q\pm 1)\mu} [ (j\mp Q) (j\pm Q + 1) ]^{1/2} P(\mu', \mu) \text{ ----- (24)}$$

$$\langle \bar{\Phi}_{K,\mu} | H(OD) | \bar{\Phi}_{K,\mu} \rangle = \left( \frac{\hbar^2}{2g_0} \right) \sum_j C_{j\pm\mu} C_{j\pm\mu} [ j(j+1) ] P(\mu', \mu) \text{ ----- (25)}$$

#### (D) Differential Cross Sections

A relatively new and powerful technique for identifying Nilsson single particle states is high resolution spectroscopy of single nucleon transfer reactions, such as  $(d,p)$ ,  $(d,t)$ ,  $(^3\text{He},d)$ ,  $(^3\text{He},\alpha)$ ,  $(\alpha,t)$ , etc. The reactions employed most widely to date are the  $(d,p)$  "stripping" and  $(d,t)$  "pick-up" reactions on even-even target nuclei. The  $(d,p)$  reaction is useful as a spectroscopic tool because the process can be viewed as the transfer of a neutron into a definite single particle orbital in the final nucleus without excitation of other degrees of freedom. On the other hand, the  $(d,t)$  reaction represents pick up a neutron from a definite single particle orbital leaving a hole in that orbital in the final nucleus. According to the theory (Satchler 1958, Vergnes and Sheline 1963, Burke etc. 1966, Elbek and Tjom 1969), the differential cross section for a single nucleon transfer reaction leading from the ground state of an even-even target nucleus to a specified member of the rotational band built on a pure one quasiparticle state of an odd-A deformed nucleus is given by the simple relation

---

$$\frac{d\sigma(\theta)}{d\omega} = 2k C_{j,\ell}^2 V^2 \sigma_{\ell}(\theta) \text{-----} (26)$$

where the  $C_{j,\ell}$  is the expansion coefficient in a spherical Saxon-Woods potential basis,  $V$  is calculated from eq(20),  $\sigma_{\ell}(\theta)$  is the intrinsic single particle cross section obtained from the DWBA (which stands for Distorted Wave Born Approximation) calculation for an angular momentum transfer  $\ell$  at the angle  $\theta$ ,  $k$  is a normalization constant to the DWBA theory. For a stripping reaction  $V$  is replaced by  $U$

In the reactions under consideration, the even-even target has spin zero so that the total angular momentum,  $j$ , of the transferred nucleon must equal the spin,  $I$ , of the final state. Consequently, as implied in eq(26), the differential cross section for exciting a particular rotational band member is expected to be proportional to the square of a single  $C_{j,\ell}$  coefficient (the one for which  $j=I$ ).

If the wave function for a level contains admixtures of the other levels, the eq(26) which applies only for pure one quasiparticle Nilsson states has to be modified, then the

pick-up differential cross section for n'th level is taken to be

$$\frac{d\sigma_n(\theta)}{d\omega} = 2k \left( \sum_i c_{j,s}^i v_i a_{i,n} \right)^2 \sigma_x(\theta) \text{-----} (27)$$

Where  $a_{i,n}$  is the mixing amplitude of the i'th levels.

### III NUMERICAL CALCULATIONS.

Two numerical calculations were carried out in two mass regions: The  $T=1/2$  isotopes with mass 25 were chosen for the calculation and no pairing force were included. The odd neutron numbers from 89 to 95 in the nuclei with mass numbers from 153 to 165 were chosen for the calculation with a pairing force included. This is because the pairing force becomes important as the mass number increases.

#### (A) The Mass-25 Calculation

The odd particle of  $Al^{25}$  and  $Mg^{25}$  in the ground state are near the middle of the  $2s-1d$  shell. Their large prolate core deformations are well established and the Nilsson model has been extensively applied to the even parity levels (Kean and Ollerhead 1972 and reference quoted in their paper). A well known anomaly exists that the  $5/2^+[202]$  particle state is the ground state, whereas, for all reasonable quadrupole deformations the  $1/2^+[200]$  state has been predicted to occur at a lower energy. One aim of the calculation is to see whether the use of a more realistic potential removes this

anomaly.

Two alternative optical model parameters for the Saxon-woods potential were used. The systematic nucleon scattering analysis of Hodgson (1963) provides a set of neutron parameters, which were used with the imaginary parts set to zero. A more recent survey by Becchetti and Greenlees (1969) suggested similar systematic parameter, the main difference being a radial dependence with a slightly smaller radius and a thicker surface. These parameters are shown in table 1.

In an early program for this part of the calculation, the single particle state of a spherical nucleus  $|jQ\rangle$ , which is a solution of eq(3), is further expanded in a sum of harmonic oscillator eigenstates (Hird and Huang 1973), that is  $|jQ\rangle = \sum_N C_{Nj}^Q |Nj\rangle$ . A computed set of radial integrals for  $\langle f(r) \rangle$  and  $\langle (df/dr)/r \rangle$  were generated using 300 equally spaced integration steps in the range  $r=0$  to  $r=r_0 A^{1/3} + 8a_0$ . The integral was calculated for all non-zero matrix elements with even  $N$  and  $L$  up to, and including, 12. The energy parameter  $\hbar\omega$  of the basis function was chosen so that the Saxon-woods potential and the harmonic oscillator potential matched at  $r=0$  and  $r=r_0 A^{1/3}$ .

There are three successive steps to diagonalize the matrix elements of the Hamiltonian. The spherically symmetric part is first diagonalized in a harmonic oscillator basis by using the numerically integrated radial matrix elements. The second diagonalization generates the deformed single particle states on a basis of the spherically symmetric eigenstates of the first diagonalization, and finally the core and RPC terms are diagonalized in a basis of the deformed states. A more complete description of the techniques used in the computer code to compute the wavefunctions and energies has been published and a more general version of the program circulated under the name ABOV Nilsson orbits (Hird 1973).

(B) The Mass-163 to 165 Calculation.

As in the mass-25 calculation and discussion (see DISCUSSION), the conventional values  $r = A^{1/3}$  for the radius and surface thickness  $a_s$  of Saxon-Woods potential are, respectively, chosen as  $r_s = 1.25$  fm and  $a_s = 0.65$  fm. The potential depth is chosen as  $V_0 = (-51 + 33(N-Z)/A)$  MeV, (Bohr and Mottelson 1969), which give an average value of  $-44.9$  MeV for all the nuclei. The spin-orbit potential parameter was estimated in a similar way and a common value of  $V_{ls} = -9.5$  MeV adopted for all the nuclei.

The level density increases as the mass number increases. In this region the pairing force must be taken into account to calculate the core energy, energy gap and Fermi energy by including both odd and even parity of Nilsson particle states. So that much longer computer time is required. A faster computer program was written by improving the early program, including the second order Saxon-Woods potential of  $H_{sp}$  and adding the pairing force calculation subroutine. The computer program with its flow chart for this calculation is shown in APENDIX (B). The program has been further developed to automatically search

for the wavefunctions and energies to first order in the Saxon-Woods potential (Hird and Huang). The subroutine WAFEN directly calculates the spherical Saxon-Woods eigenstates by radial integration of the Schrodinger equation  $H_{sp}$  (Caswell 1966). In the subroutine a table of  $SDW = V_c R_c \langle j_1 m_1 | df/dr | j_2 m_2 \rangle$  and  $SDDW = 0.5 \cdot V_c R_c^2 \langle j_1 m_1 | d^2 f/dr^2 | j_2 m_2 \rangle$  was generated. There are only two successive steps to diagonalize the matrix elements of the Hamiltonian: The deformed part is first diagonalized in a basis of the spherical Saxon-Woods eigenstates, and then, the core and RPC terms with the pairing force are diagonalized in a basis of the deformed states. Both negative and positive parity states were necessary for the variational calculation to determine  $U_{\nu}^{(\mu)}$ ,  $V_{\nu}^{(\mu)}$ , the Fermi energy  $\lambda^{(\mu)}$  and the  $P(\mu', \mu)$  of each deformed quasi-particle state. The pairing strength value of  $G = (25/A)$  MeV is chosen for calculation in this mass region.

For the numerical calculation of the differential cross section of eq(27), a simple computer program was separately written. The coefficients  $C_{j_1, l}^i$  which are obtained from  $C_{j_1, l}^i$  of eq(16) and  $a_{j_1, l}$  which is obtained after diagonalization the matrix of eq(18) are punched out for the

input data of eq(27). The normalization factors  $k$ , which are 3.0 for (d,t) and 1.5 for (d,p) reactions, and the intrinsic single particle cross sections  $\sigma_k(\theta)$ , which are given in table 2, are taken from Tjon and Elbek (1967).

IV RESULTS AND CONCLUSION

(A) Comparison of The Energy Levels of Mass-25 Nuclei using a Saxon-woods Potential with Those using a Harmonic Oscillator Potential.

1. Nilsson Diagram for Quadruple Deformations only.

The well-known Nilsson energy level diagrams associated with single particle wave function are obtained by diagonalizing the deformed Hamiltonian of the Saxon-Woods potential eq(2) with  $\beta_4 = 0.0$  and the deformed Hamiltonian of harmonic oscillator potential eq(12) of Nilsson (1955). The diagrams appropriate for odd nucleon nuclei of mass-25 are shown in figure 1a, 1b and 1c which are labeled with the set of quantum number  $K^\pi [N n, \Lambda]$  defined by Nilsson. Each level can accommodate two particles. The two orbitals have degenerate eigenvalues associated with the wave function which has reflection symmetric with respect to a plane perpendicular to the nuclear symmetry axis.

It can be seen immediately that the general shape of

all three figures agrees very well as should be expected from the large overlap between the two types of wave function. The difference in detail are mainly due to the energy spacings which occur at zero deformation. A way to compare these energy spacings is to take the ratio  $[E(d_{3/2}) - E(s_{1/2})] / [E(s_{1/2}) - E(d_{5/2})]$ . In the harmonic oscillator states the simple analytic form of the  $\langle l \cdot s \rangle$  interaction produces 1.5 for this ratio when  $\mu \langle L^2 \rangle = 0$ . In the Saxon-Woods states the ratio varies considerably; with the Hodgson parameters it is 0.85, whereas with the Becchetti and Greenless parameters it is 1.98. Nilsson introduced the  $\mu \langle L^2 \rangle$  term into his Hamiltonian in order to bring the ratio nearer to the shell model value since he found that the matrix elements between larger  $L$  states are increased by the  $\langle L^2 \rangle$  term in a way which simulates the radial dependence of a more hard-edged potential than harmonic oscillator. With the Saxon-Woods potential it is possible to vary the shape of the potential in this respect arbitrarily by varying the surface thickness parameter  $a_0$ . The two optical sets therefore probably produce the very different energy ratios through difference in the  $a_0$  parameter. To verify this, a calculation was made with  $a_0$  reduced in the Hodgson parameters. The dotted line

in figure 1b shows that the ratio is reduced to 0.51 for  $a_0 = 0.55$  fm from 0.85 for  $a_0 = 0.65$  fm of solid line. The Hodgson and the Becchetti and Greenlees parameters produce energy ratios which straddle the harmonic oscillator value, so that, at least in this respect, the harmonic oscillator is a good compromise to represent the experimental situation.

## 2. RPC and Band Mixing

The way to compare the energy levels calculated by the Saxon-woods potential and by the harmonic oscillator potential with the experimental situation is to include all members of the bands, rather than just the band head. A large number of states are then generated in the 2s-1d shell. Because of this, it is sometimes difficult to identify a particular state. An ambiguity of this type can be resolved by plotting the energies of the states as a function of moment of inertia  $\hbar^2/2g_0$ , when all the members of the same band become degenerate at  $\hbar^2/2g_0 = 0.0$ . The energy spacings of the band heads are mainly produced by the core deformation, whereas the energy spacing of the states within the band is mainly produced by the moment of inertia. By choosing an appropriate quadrupole deformation and moment of inertia for the RPC and Band mixing calculation, the best result for fitting the experiment situation can be obtained.

The band mixed states with total spin up to  $I=9/2$  in the 2s-1d shell are plotted in figure 2. The curves show the way in which the energy levels in a band spread and

overlap one another as the rotational energy increase. The core particle interaction is apparent in the repulsion between states of the same spin when  $K$  differs by 1. And the very uneven spacing, with inversions, in the  $K=1/2^+$  bands. A fixed quadrupole deformation  $\beta_2=0.2$  was chosen. This is smaller than the deformation suggested by the intrinsic quadrupole moment of  $Mg^{25}$ , but it is apparent from figure 1 that a higher value would invert the  $5/2^+[202]$  and  $1/2^+[211]$  levels in all calculations. To achieve the experimental spacing of all band heads and the states within the ground state  $5/2^+$  band a moment of inertia about  $\hbar^2/2g_0 = 0.15$  MeV is required. While the harmonic oscillator calculation gives the  $1/2^+$  level as the ground state even with this modest deformation, the Saxon-Woods potential shows a quite good general level order. The most serious discrepancy which remains between the deformed Saxon-Woods levels and experiment is, apart from the small deformation, that the  $1/2^+[200]$  band derived from the  $d_{3/2}$  spherical particle state is at too high an energy, and the spacing of the  $K=1/2^+$  band is too uneven.

### 3. Hexadecapole Deformation

In order to retain the correct level order and spacing at  $\beta_2=0.4$  which is obtained from the experimental static quadrupole moment (Lurio 1962), a hexadecapole deformation  $\beta_4$  is introduced to this calculation. It is expected intuitively for a core which shows evidence of being made up of four alpha-particles. Inelastic alpha-particle scattering (Rebel et al. 1972) and electron scattering (de Swiniarski et al. 1969) to the  $2^+$  and  $4^+$  states of  $Mg^{2+}$  both confirm the larger  $\beta_2$  value and predict a significant hexadecapole deformation.

For making a direct comparison between the harmonic oscillator and the Saxon-Woods potential, the same radial  $r^2$  dependence was taken for the  $\beta_4$  as for the  $\beta_2$  deformation in the deformed harmonic oscillator so that the Hamiltonian is  $H=H_0-K\hbar\omega(\beta)r^2(\beta_2Y_2^0+\beta_4Y_4^0)$ . A frequently used alternative is to take the next higher order in the radial term as well as in the angular term. The hexadecapole term is then proportional to  $\beta_4 r^4 Y_4^0$ . Trial calculation with an  $r^4$  radial dependence was found to produce qualitatively similar results to those with an  $r^2$  dependence if the coefficient  $\beta_4$

is scaled by a factor which was about equal to the square of the nuclear radius.

The energy levels dependence on  $\beta_2$  and  $\beta_4$  for the harmonic oscillator potential was shown in figure 3. The left hand side is exactly the same as the right hand side of the figure 1a. The  $1/2+[440]$  state which belong to the  $1g_{9/2}$  subshell approaches the  $1/2+[200]$  state of the  $d_{3/2}$  subshell when  $\beta_2$  increases to 0.4. The right hand side of the figure shows the  $\beta_4$  dependence of the energy levels assuming a constant value for  $\beta_2=0.4$ . The  $1/2+[440]$  was found to descend in energy as  $\beta_4$  increase so that it crossed the  $1/2+[200]$  level of the  $1d_{3/2}$  subshell at about  $\beta_4=0.05$  and the  $1/2+[211]$  level of the  $2s_{1/2}$  subshell at about  $\beta_4=0.3$ . It shows that the hexadecapole term has now introduced considerable N mixing so that there is significant displacement of the energies and mixing of the spherical configuration over a wide range of  $\beta_4$  values. Clearly one of the two available  $K=1/2+$  level is first filled before the  $5/2+[202]$  level for any value of the hexadecapole deformation greater than  $\beta_4=0.2$ . The introduction of a hexadecapole deformation therefore makes it more difficult rather than easier to explain the  $5/2+$  ground state when

using a harmonic oscillator radial dependence.

The similar calculation for the hexadecapole variation of the Saxon-Woods potential eigenstates was made and is shown in figure 4. The left hand side of this figure shows the  $\beta_2$  variation when  $\beta_4=0$ , and the central region is obtained when a constant  $\beta_2=0.4$  is assumed and  $\beta_4$  is varied. The  $5/2+[202]$  and  $1/2+[211]$  are seen to cross back to their original order which occurred at smaller  $\beta_2$  values. There seems to be no other significant change in the spectrum of the unfilled levels in contrast to the deformed harmonic oscillator states.

Both bound and unbound spherical Saxon-Woods states are generated as a result of diagonalizing a Hamiltonian oscillator basis. Then the deformed Saxon-Woods states were calculated by diagonalizing its spherical basis. The dotted line in figure 4 were calculated using only bound states from the spherical Saxon-Woods basis in the diagonalization, whereas the continuous line included all the  $N=4$  states. It was found that there was little mixing with the  $N=2$  shell by the quadrupole deformation and more shell mixing by the hexadecapole interaction. The differences, which are mostly a common energy displacement for the  $\beta_2$  deformation, begin

to show a change of spacing with the  $\beta_4$  deformation. It is interesting to see whether the higher shell states were brought down in energy by the hexadecapole interaction to provide some extra bound states in the energy region of interest as occurs with the harmonic oscillator potential. It was found that the  $1/2+[440]$  component from the  $1g_{9/2}$  subshell in the deformed Saxon-Woods potential remained well above zero energy at all the  $\beta_2$  and  $\beta_4$  values considered and no extra bound state was introduced.

The right hand side of figure 4 shows the effect of adding the core excitation and band mixing to the Hamiltonian assuming a constant deformation with  $\beta_2=0.4$  and  $\beta_4=0.4$ . The level spectrum is qualitatively similar to that previously found with  $\beta_2=0.2$  and  $\beta_4=0.0$ , and the correct separations of the members of the ground state band were obtained when  $\hbar^2/2g_0$  was about 0.15 MeV. The energy levels with these parameters were compared with previous calculations and with the experimental spectrum in figure 5. The overall fit is not very different from that obtained with  $\beta_2=0.2$  and  $\beta_4=0.0$ , however the upper  $K=1/2+$  band head energy is in better agreement with the experimental value than in previous calculation. Table 3 shows the expansion

coefficients  $C_{Nj\Omega}$  of the lowest two states of  $Mg^{25}$  and  $Al^{25}$  in terms of the spherical harmonic basis, that is  $|ja\rangle = \sum_{Nj\Omega} C_{Nj\Omega} |Nj\rangle$ . The band mixing which is produced when  $\hbar^2/2g_0 = 0.15$  Mev in the bound states in term of the unmixed Saxon-woods states with  $\beta_2 = 0.4$  and  $\beta_4 = 0.4$  are shown in table 4.

In an attempt to remove the discrepancy which predicts the  $K=1/2^+$  bands as more unevenly spaced than their experimental bands, the value of  $\hbar^2/2g_0$  was reduced by a factor of five in the band mixing and decoupling term while retaining the value  $\hbar^2/2g_0 = 0.2$  MeV which gives the best fit to in-band spacing at  $\beta_2 = 0.4$   $\beta_4 = 0.4$ . The improvement to the fits to the three known experimental band of  $Mg^{25}$  and  $Al^{25}$  are displayed together in figure 5.

#### 4. Conclusion

The energy levels produced by the harmonic oscillator potential in the Nilsson model agree substantially with those predicted by Saxon-Woods potential both for the spherical symmetric potential and for a quadrupole deformed shape. However when a hexadecapole deformation is included there is so much N mixing with higher shells that the levels from the N=4 shell are predicted to occur well down in the 1s-2d shell and even below the  $5/2+[202]$  in a way which is quite inconsistent with experiment. So it is impossible to fit the experimental energy levels by including RPC and band mixing at  $\beta_2=0.4$   $\beta_4=0.4$  when using a harmonic oscillator potential.

The Saxon-Woods potential removes these anomalies and predicts good band head spacing to fit the experiment at  $\beta_2=0.4$   $\beta_4=0.4$ . The spacing of the levels within each  $K=1/2+$  band are found to be too uneven so that better agreement can be obtained by arbitrarily reducing the  $\hbar^2/2g_0$  value by about a factor of five in the  $\langle I \cdot j \rangle$  term compare to its value in the  $\langle \vec{I}^2 - 2R^2 \rangle$  term.

(B) The Energy Levels and the Stripping and Pick-up  
Differential Cross Sections for Mass-153 to 165

1. General Discussion of The Level Systematics

The  $\text{Sm}^{153}$ ,  $\text{Gd}^{155, 157, 159, 161}$ ,  $\text{Dy}^{157, 159, 161, 163}$ , and  $\text{Er}^{161, 163, 165}$ , are grouped according to the neutron number  $N=91, 93, 95$ , and  $97$ . The ground states of these nuclei, except  $3/2+[651]$  for  $\text{Sm}^{153}$  and  $5/2+[642]$  for  $\text{Dy}^{161}$ , are  $3/2-[521]$  for  $\text{Gd}^{155, 157, 159}$ ,  $\text{Dy}^{157, 159}$ ,  $\text{Er}^{161}$ , and  $5/2-[523]$  for  $\text{Gd}^{161}$ ,  $\text{Dy}^{163}$ ,  $\text{Er}^{163, 165}$ . The occurrence of the same band as the ground state in nuclei with different neutron numbers is a somewhat remarkable fact and shows that the  $3/2-[521]$  and  $5/2-[523]$  states must cross the  $3/2+[651]$  and  $5/2+[642]$  states at experimentally occurring deformations. The other remarkable fact is that the  $11/2-[505]$  always stays as a hole state in the nuclei under consideration and shows a quite different variation in its energy as the deformation is varied compared to any of the other low lying states. The long life (Borggreen and Sletten 1970) and the strong  $l_n=5$  neutron transfer angular distribution in stripping and pick-up reactions (Lovhoden et al 1971, Tjom and Elbek 1967, Yagy et al 1969; Joskola et al 1969, Grotdal

et al 1970) make this state relatively easy to identify experimentally, and it is known in all the nuclei under consideration except  $Gd^{161}$ .

The figure 6 shows the model prediction for the single particle energies as a function of the deformation with the second order of  $\beta_2$  and  $\beta_4$  in the deformed Saxon-Woods potential being omitted. On the left hand side, only the quadrupole deformation  $\beta_2$  is considered from 0 to 0.25. On the right, the quadrupole deformation is frozen at  $\beta_2=0.25$  and a variable hexadecapole deformation  $\beta_4$  is added from 0 to 0.2. The optical parameters for the calculation of figure 6 are taken from  $Gd^{157}$  and are qualitatively very similar for the other nuclei. The main difference in the energy levels of the various nuclei comes from the difference of the  $\beta_2$ ,  $\beta_4$  and neutron number. In this region near  $\beta_2=0.25$  the levels  $3/2-[521]$ ,  $5/2-[523]$ ,  $3/2+[651]$  and  $11/2-[505]$  all lie close together so that slight  $\beta_2$  changes can modify the order of fitting of these states, and therefore the state of the last odd neutron. The most important effect in this Nilsson diagram is that the  $3/2-[521]$  and  $11/2-[505]$  levels change very significantly and in the opposite direction as  $\beta_2$  and  $\beta_4$

change, which allows the  $3/2-[521]$  level to become the ground state of six nuclei and the  $11/2-[505]$  level to become a hole state for all the nuclei under consideration as the experimental evidences requires. The number inside the circles in figure 6 refer to the average number of neutrons in the deformed core when the Fermi energy lies within each region between the Nilsson orbit energies.

The Nilsson diagram predicts the correct spin for the ground state and most of the the particle or hole excitation states are in the correct order if the neutron number,  $\beta_2$ , and  $\beta_4$  are properly chosen. But it was not possible fit the energy spacings among the band heads and among the energy levels within a rotational band unless the transformation to quasiparticle states was performed. A complete calculation including all the RPC and the pairing force was made before attempting a comparison with the experimental energy levels of a particular nucleus. The ground state band and the band head energy of  $11/2-[505]$  were considered to be the most firmly established parameters, and a search was made to find the best  $\hbar^2/2g$ ,  $\beta_2$  and  $\beta_4$  parameters to fit these levels. The levels of all the other bands therefore represent predictions of the model and provide a test of its accuracy.

The resulting data was used to analyze the differential cross section from the ground state towards deeper hole states by mean of the (d,t) reaction and then the ground state towards higher particle states by mean of the (d,p) reaction. The comparision of theoretical differential cross section with experiment is shown in table 5 to 16. The parenthesis indicates that the differential cross section has been shared with another level which was too close in energy to be experimentally separated.

## 2. Discussion of Individual Isotone Groups

### (a) N=91

The levels schemes of N=91 nuclei is shown in figure 7. In  $Dy^{157}$  the  $3/2$ -[521] ground state band and  $11/2$ -[505] state are well established. The  $5/2$ -[523],  $3/2$ -[523] and  $1/2$ -[530] assignments are reasonably certain and the  $5/2$ -[512] and  $1/2$ -[510] assignments somewhat less so (Tuli 1973a). Our calculation, by fitting the ground state band and the  $11/2$ -[505] state, predicts quite well the level ordering of all five other bands. The main discrepancies are that the  $5/2$ -[523] band head is depressed in energy so that it comes slightly below the  $11/2$ -[505] state, and that the  $1/2$ -[521] band head energy is lower than predicted. Only the  $7/2$ - number of the  $1/2$ -[530] band has been firmly established and it is almost degenerate with  $7/2$ - level of the  $1/2$ -[521] band. We find that the  $1/2$ -[530] band has the larger interband spacing. So our calculation suggest that  $1/2$ -[530] band head should be found below the  $1/2$ -[521] band head as in the other N=91 isotones.

In  $Gd^{155}$  the experimental level scheme is less well

established. Tjom and Elbek (1967) found that the  $5/2-[523]$  band head occurs at a similar excitation and that the  $1/2-[521]$  band at a slightly higher excitation than in  $Dy^{157}$ , so that the  $5/2-[523]$  band is again predicted at too low an energy and the  $1/2-[521]$  band too high by this calculation. The  $1/2-[530]$  band is better experimentally established in this nucleus and its band head appears below the band head of the  $1/2-[521]$ . This is in agreement with the calculation. The decoupling parameter and the RPC interaction in this calculation are strong enough in the  $1/2-[530]$  to cause an inverted spin ordering in this band, however the experimental spin assignments show the normal consecutive spin values, and the uneven spacing within this band is in the opposite sense to that produced by this calculation. (Tjom and Elbek 1967, Jaskora, Tjom and Elbek 1969). The  $3/2-[532]$  and the  $5/2-[512]$  band are predicted at closely similar energies to those in  $Dy^{157}$ , but in  $Gd^{155}$  there is insufficient experimental information to identify them.

In  $Sm^{155}$  the ground state is  $3/2+[651]$  (Kroger and Reich 1973) and the first excited state is the band head of  $3/2-[521]$  which is 35.843 KeV above the ground state. By

using slightly higher values for  $\beta_2$  and  $\beta_4$  a fit to the energy spacing between the band head of the  $3/2$ -[521] and the  $11/2$ -[505] states the ground state was predicted. however, the  $1/2$ -[521] state is found at a slightly higher energy than experimental level and the  $1/2$ -[530] state is predicted considerably too high. There is no indication of the experimental lower energy of the  $3/2$ -[532]. In view of the discrepancies in the energies of all the higher levels it is difficult to make a prediction about the  $5/2$ -[523] or the  $5/2$ -[512] band from this calculation.

The comparison of theoretical differential cross sections with experiment in this group is shown in table 5 to 7. The differential cross section of the band head of the  $1/2$ -[530] is extremely weak, that is why this band head is difficult to confirm. Both experiment and theory indicate that the pick-up differential cross section is large compared with stripping in the band head of  $11/2$ -[505]. The theory agrees excellently with the experiment in predicting that the  $3/2$ - and  $7/2$ - members of the  $3/2$ -[521] band are stronger than the other members of this band both in the pick up and stripping differential cross sections.

(b) N=93

The single particle energies of figure 6 show that the  $3/2^-$ -[521] state ought to be the ground state and the  $3/2^+$ [651] ought to be a hole state in the N=91 isotones, the  $3/2^-$ -[521] state must cross over the  $3/2^+$ [651] state. It is necessary simultaneous to increase both  $\beta_2$  and  $\beta_4$  to meet these requirements.

The best known level systematics again occur with the Dysprosium and Gadolinium isotopes. In  $Dy^{159}$  several members of  $3/2^-$ -[521],  $11/2^-$ -[505],  $1/2^-$ -[521] and  $5/2^-$ -[523] bands are established with reasonable certainty (Tuli 1973a). The  $1/2^-$ -[530] band head is missing, and this band and the  $3/2^-$ -[532] band assignments are somewhat less certain. Our model fit, show in figure 8 which fits the energy spacing between the ground state band and the  $11/2^-$ -[505] energy level, again predicts the correct band ordering but with the higher bands too high in energy particularly for the  $1/2^-$ -[530] band. The pick-up and stripping differential cross section calculated for the band head of  $1/2^-$ -[530], which are shown in table 9, is predicted as zero, which is why this band head is missing in experimental measurements.

In  $Gd^{157}$  the experimental status of the bands is quite similar (Tuli 1973b). The  $3/2-[532]$  and  $1/2-[530]$  bands are again less certain than other band assignments. Compared to  $Dy^{159}$  the energies of the bands are changed in that the  $11/2-[505]$  and the  $5/2-[523]$  band heads are higher in energy and closer together. Similarly the  $3/2-[532]$  and the  $1/2-[521]$  bands are at higher energies and almost degenerate. One is a hole state, whereas the other is a particle state, so there is little band mixing between them. This calculation fits excellently the ground state,  $5/2-[523]$  and  $11/2-[505]$  bands by choosing the proper value of  $\beta_2$ ,  $\beta_4$  and  $\hbar^2/2g_0$ . It predicts an increased energy for the higher bands compared to their position in  $Dy^{159}$ . However, this increase is more than occurs experimentally and the prediction are all too high.

In  $Er^{161}$  the work of Hjorth and Ryde (1970) has established several member of the  $3/2-[521]$ ,  $11/2-[505]$  and the  $5/2-[523]$  bands, but other low lying negative parity bands have not been identified. Since this calculation fits the energy spacing between the band head of  $3/2-[521]$  and  $11/2-[505]$ , only the higher member of the  $11/2-[505]$  band

and the  $5/2^-$ -[523] band energies can be considered a test of the model. The agreement is excellent. The model also places the  $3/2^-$ -[532],  $5/2^-$ -[512] and the  $1/2^+$ -[530] bands at lower excitation than in the other isotopes. So if the estimates are again too high, these bands should occur experimental at quite low excitations.

The experimental stripping and pick-up differential cross sections in  $Gd^{157}$  and  $Dy^{159}$ , which are shown in table 8 and table 9, are in rough agreement with the theory, but there is no experimental stripping data in  $Er^{161}$  with which to compare with the theoretical results as shown in table 10. The differential cross sections of the  $3/2^-$ - and  $7/2^-$ - members of the  $3/2^-$ -[521] band, which is the ground state band for the  $N=93$  group, are stronger than the other members of this band in good agreement with the experiment. The extremely weak experimental (d,p) and (d,t) differential cross sections for the band head of the  $1/2^-$ -[530] band and the strong (d,t) differential cross section for the  $3/2^-$ - member in this band also show good agreement between the theory and experiment. However there is disagreement in the  $1/2^-$ -[521] band where the experiment shows that the  $5/2^-$ - member is stronger than the  $3/2^-$ - and  $7/2^-$ - members in the (d,p)

differential cross section, in contrast to the theoretical prediction.

(c) N=95

The general trend in the deformations is to increase with the value of N in the Gd, Dy and Er isotopes, corresponding to the increase in the number of neutrons beyond the spherical region which ends near N=88. This trend is confirmed for N=95 by the continuing low energy of the 3/2-[521] configuration. It forms the ground state in Gd<sup>159</sup>, has 74.6 KeV excitation in Dy<sup>161</sup> and 104 KeV excitation in Er<sup>163</sup>. Because of the generally increased deformation, the second order terms in the deformed Saxon-Woods potential expansion for  $H_p$  were included for the N=95 and the N=97 calculation. The effect of this term can be seen by comparing figure 9 with figure 6. The most important effect, is that the 11/2-(505) is raised in energy more dramatically and 3/2-[521] falls in energy more slowly as  $\beta_2$  is increased, however the 3/2-[521], 5/2-[523] and 11/2-[505] energies remain in good agreement in N=95 and N=97 at these larger deformations. Because of the large deformation the variation of  $\beta_2$  has been extended to  $\beta_2=0.3$  in figure 9.

In Gd<sup>159</sup> the 3/2-[521] ground state band, and the

5/2-[523], 1/2-[521] and 5/2-[512] bands have been identified with reasonable certainty (Tuli 1973a). The 11/2-[505] band head occurs at a higher excitation than in any of the N=91 or N=93 isotones. The value of  $\beta_2$  must be therefore increased sufficiently to make the 3/2-[521] level cross the 5/2+[642] level so that it becomes the ground state, simultaneously the value of  $\beta_4$  must be increased to make the 11/2-[505] state become a higher excited hole state. Under these requirements the model makes a good fit to the energy spacing between 3/2-[521] and 11/2-[505] band head and predicts excellent agreement for the 1/2-[521] and 5/2-[523] bands, however the 5/2-[512] energy is about 400 Kev too high. The levels scheme of  $Gd^{159}$  is shown in figure 10. The effect of the decoupling parameter appear to be again in the opposite sense to that found in the experimental level spacing.

Somewhat less is known about the negative parity state of  $Dy^{161}$  where the ground state has the configuration 5/2+[642]. The lowest two negative parity bands are well established from the  $\gamma$ -ray decay spectrum following  $\beta$  decay (Funke et al 1966, Berg and Malmskog 1969) and following the ( $\alpha, 3n$ ) reaction (Hjorth, Johnson and Ehrling 1972) which

assigned to them the  $5/2-[523]$  and  $3/2[521]$  orbitals. Neutron transfer reaction measurements have tentatively assigned the  $5/2-[512]$  and  $1/2-[530]$  band heads to levels near 800 KeV (Grotdal et al 1970). In comparison with  $Gd^{159}$  the  $11/2-[505]$  band is somewhat lower in energy which suggests a smaller deformation. The simultaneous fitting of the  $5/2+[642]$  ground state, the  $3/2-[521]$  band energies, which appear as a hole state, and the  $11/2-[505]$  band head energy also give good agreement for the  $5/2-[523]$  band and the  $1/2-[521]$  band energies except that the uneven spacing within the latter band again disagrees with experiment. The tentative  $5/2-[512]$  assignment near 900 KeV is supported by the model, but not the  $1/2-[530]$  band, which is predicted at a much higher energy.

The decrease in deformation through the  $N=95$  isotones from  $Gd^{159}$  to  $Dy^{161}$  continues with  $Er^{163}$  where the  $5/2-[523]$  configuration here occurs as the ground state. This nucleus has been well explored and several members of each of the  $5/2-[523]$ ,  $3/2-[521]$ ,  $1/2-[521]$ ,  $11/2-[505]$ ,  $5/2-[512]$  and the  $1/2-[530]$  are well established. The  $1/2-[530]$  band assignments are less certain (Buyrn 1972). The model results are not in as good agreement as in the other  $N=95$

isotones in that there is a discrepancy of about 100 KeV in the energies of the  $5/2-[512]$  and the  $1/2-[521]$  bands but the experimental band ordering is maintained. No low spin states were predicted between 800 KeV and 900 KeV where the lower members of the  $1/2-[530]$  band have been tentatively identified. However a common feature of the model systematics seems to be an overestimate of the excitation energy of this band.

The differential cross section of the  $N=95$  isotones were shown in table 11 to table 13. In  $Gd^{159}$  and  $Dy^{161}$  the differential cross sections seem to be quite good agreement in proportion between theory and experiment. But the differential cross section of  $Er^{163}$  is not in such good agreement. The main reason is because the energy level fit in the  $Gd^{159}$  and  $Dy^{161}$  is better than in  $Er^{163}$ .

(d)  $N=97$

All the  $N=97$  isotones under consideration have a  $5/2-[523]$  ground state.

In  $Gd^{161}$  the  $11/2-[505]$  state has not been identified however the  $3/2-[521]$ ,  $1/2-[521]$  and the  $5/2-[512]$  bands have been proposed above the ground state band (Groshev et al 1971, Tjom and Elbek 1967). The model was made to fit the energy spacing between the ground state and the band head of the  $3/2-[521]$ . The resulting level scheme places the  $1/2-[521]$  band lower than the  $3/2-[521]$  band in disagreement with experiment. The  $5/2-[512]$  band head was predicted about 100 KeV below the experiment result. Since both the  $1/2-[521]$  and  $5/2-[512]$  band heads are particle states whereas the  $3/2-[521]$  band head is a hole state, this implies that the discrepancy in the theory is really in the  $5/2-[523]$  orbit energy being too high.

In  $Dy^{163}$  many measurements have been made (Buyrn 1972). The ground state  $5/2-[523]$ , the  $3/2-[521]$  and the  $1/2-[521]$  bands are all reasonably certain. The  $5/2-[512]$  band, which the band head is missing and the  $11/2-[505]$  assignments are based on neutron transfer data only and are

somewhat less certain. The model predicts the correct level ordering with the  $1/2-[521]$  band head below that of the  $3/2-[521]$  orbit, though both are somewhat higher in energy than predicted. The  $5/2-[512]$  band is excellent agreement with the two experimentally identified members.

The recent compilation of  $\text{Er}^{165}$  levels (Burn 1974) identified the  $5/2-[523]$  ground state band and the  $3/2-[521]$ ,  $1/2-[521]$ ,  $5/2-[512]$  and the  $1/2-[510]$  bands as having firm assignment for several of each of these members. The state of  $11/2-[505]$  is somewhat less certain, and the  $3/2-[512]$  is only tentatively assigned. The  $1/2-[521]$  particle state which occurs above the  $3/2-[521]$  hole state in  $\text{Gd}^{161}$ , and below this state in  $\text{Dy}^{163}$  again occurs above it in  $\text{Er}^{165}$ . The theoretical fit which here use the  $3/2-[523]$  band energy and the  $11/2-[505]$  state predicts excellent agreement in the  $5/2-[512]$  band and about 40 KeV difference in the  $3/2-[521]$  band, but the  $1/2-[521]$  band is predicted as the lowest band above the ground state and the  $1/2-[510]$  band is predicted too high.

The experimental (d,t) differential cross section is not available in  $\text{Gd}^{161}$  (Tjon and Elbek 1967) and its (d,p)

differential cross section is less certain. It is difficult to make a comparison in  $Gd^{161}$  which is shown in table 14. The (d,t) and (d,p) differential cross section of the  $Dy^{163}$  and the  $Er^{165}$  are shown in table 15 and table 16. There are very rough agreement between experiment and theory.

### 3. Conclusion

The present analysis, which gives first priority to a rigorous application of the axially symmetric collective model, and makes few concessions towards providing a parameterization of the experimental data, was able to achieve a limited success in correctly predicting the band ordering in many nuclei. By choosing the proper  $\beta_2$  and  $\beta_4$  and fitting the neutron number  $N$ , the ground state of the nuclei under consideration are correctly determined in the Nilsson diagram. Then, by fitting the energy spacing between the ground state and the most confirmed band head, the rest of the low energy bands in several nuclei are predicted in the right order. Certain of the collective band energies are predicted consistently with reasonable accuracy, for example the  $5/2$ -[523] band, and the  $3/2$ -[521] band when this is not the ground state, are usually predicted within a few KeV. The exceptions occur in the  $N=91$  isotones where there is a difference between theory and experiment of 100 KeV to 150 KeV.

The energy differences which depend primarily on the rotational quantum of energy  $\hbar^2/2g$ , are generally in good

agreement with experiment. A good fit to the in-band spacings of all the excited state bands is mostly found using the value of  $\hbar^2/2g_0$ , which was obtained from fitting the ground state band. The RPC term contributed significantly to the spacings between bands, and it was necessary to include this term before attempting a fit to the level structure so that it is hard to assess whether this term is mainly responsible for the discrepancies in the position of the band heads.

Some difficulties occurred with the decoupling parameter which is generated in our calculation as a diagonal term in the RPC interaction. This clearly has the wrong sign to account for the observed uneven spacing in the  $1/2$ -[521] band in several of the  $N=91$  and  $95$  nuclei. The decoupling parameter is large enough to depress the  $(2n+1/2)$  spin states below the  $(2n-1/2)$  spin states in the  $1/2$ -[530] band of  $Gd^{155}$ . The experimental data (Tjom and Elbek, 1967) suggests a non-inverted level ordering, but the  $3/2$  and  $5/2$  levels were not completely resolved from levels in other bands and these spin assignments are inconclusive.

The input parameters of the model are listed in table 17 and shown as a function of the atomic weight in figure 12.

The dotted lines connect the nuclei with the same  $N$ , and the continuous lines connect the nuclei the same  $Z$ . In the same  $N$  it show that  $\beta_2$  and  $\beta_4$  decrease with mass increasing and  $k^2/2g_0$  increase with mass except  $Gd^{161}$  and  $Dy^{163}$  which have the same input parameters. It is not meaningful to make a comparison of the values of these parameters with those found by other authors who fitted the collective model parameters individual to each band, since the same experimental information is being compared. However the deformation of several of the nuclei in this mass region have been deduced from some quite different experiments and so provide an independent check. In the tabulation of Lobner, Vetter and Honig (1970) their parameter  $\beta_2$  was mainly obtained from hyperfine structure measurements,  $\mu$ -x rays and coulomb excitation. Their value of  $\beta_2$  for the odd-A nuclei are shown crosses in figure 12. Apart from  $Er^{165}$  where there is a large error on  $\beta_2$ , the agreement is very good. The hexadecupole have been obtained from  $\mu$ -x ray and inelastic scattering measurements (Erb et al 1972, Davidson, Close and Malanify 1974, Hendrie et al 1968) but only for even-even nuclei. These deformations are quite similar to those found in the present analysis, but the spread in

values and the absence of odd A data make it difficult to pick out any overall difference. There is no indication in our  $\beta_4$  parameters value of the change in sign which occurs beyond A=166.

There is a striking similarity in the shapes of the  $\beta_2$  and  $\beta_4$  distributions in figure 12, where the variations in  $\beta_2$  from one nucleus to another are mirrored by similar changes in  $\beta_4$ . This suggests that our method of choosing these parameters selects some aspect of the nuclear shape which is not directly related to its expansion as a truncated series of spherical harmonics. Thus it turns out that all our nuclear shapes have the same minimum value of  $R(\pi\theta\phi)/R_0$  within 1.5%.

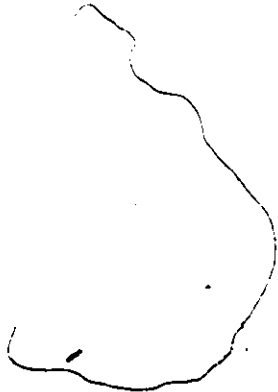
It is evident that there is no smooth variation in the parameters with either A, N or Z, and that the nuclear shape depends on the number and type of nucleons within it in such a complicated way as to produce an apparently random fluctuation of these small changes. This being so it seems likely that the assumption of constant nuclear shape for a given nucleus, regardless of the state of excitation of either the orbiting nucleon or the collective core, represents a gross oversimplification and that, to achieve

detailed fits, the shape parameters of the core must be separately adjusted for each collective band.

General speaking the theoretical (d,p) and (d,t) differential cross section of the nuclei under consideration are roughly agreement with experiment, for example, the band head of  $1/2-[530]$  can not be found if the theoretical differential cross section of this level is very small. A rigorous comparison of differential cross section is difficult to make since the four basic parts of the theory [DWBA, Satchler stripping formalism (Satchler 1958), pairing correlation formalism, and independent particle model] involve various approximations and assumptions, and the experimental differential cross sections of some nuclei under consideration can not be confirmed.

V

TABLES AND FIGURES



g

TABLE 1

Saxon-Woods Potential parameters for Mass-25

Reference	$V_0$ (MeV)	$r_0$ (fm)	$a_0$ (fm)	$V_{os}$ (MeV)	Label
Hodgson (1963)	53.0	1.25	0.65	7.2	(a)
Becchetti and Greenlees (1969)	55.3	1.17	0.75	6.2	(b)

TABLE 2

The DWBA single particle cross sections  
 $\sigma_{\ell}(90^{\circ})$  ( $\mu\text{b}/\text{sr}$ ) for (d,t) and (d,p) reaction.

N	$\ell$	(d,t) $Q=-2\text{MeV}$	(d,p) $Q=3\text{MeV}$
4	0	214	
4	2	120	
4	4	234	
5	1	251	500
5	3	88.4	195
5	5	13.7	26.5
6	0	372	580
6	2	222	365
6	4	58.5	102
6	6	6.4	15.5

TABLE 3

$C_{Nj\Omega}$  values for  $\frac{1}{2}^+[211]$  and  $5/2^+[202]$  states with no RPC interaction.

Energy (MeV) =		-8.622	-8.874	-7.888	-11.739	-9.969	-8.910
$\Omega$ =		1/2	1/2	1/2	5/2	5/2	5/2
N	j	$\beta_2 = 0$	$\beta_2 = 0.2$	$\beta_2 = 0.4$	$\beta_2 = 0$	$\beta_2 = 0.2$	$\beta_2 = 0.4$
		$\beta_4 = 0$	$\beta_4 = 0$	$\beta_4 = 0.4$	$\beta_4 = 0$	$\beta_4 = 0$	$\beta_4 = 0.4$
0	1/2	-0.0126	-0.0147	0.0117	0.0	0.0	0.0
2	1/2	0.9896	0.7466	0.7184	0.0	0.0	0.0
4	1/2	0.0890	0.0660	0.0812	0.0	0.0	0.0
6	1/2	0.0955	0.0712	0.0802	0.0	0.0	0.0
8	1/2	0.0579	0.0431	0.0495	0.0	0.0	0.0
10	1/2	0.0050	0.0035	0.0072	0.0	0.0	0.0
12	1/2	0.0046	0.0034	0.0037	0.0	0.0	0.0
2	3/2	0.0	-0.5540	-0.4007	0.0	0.0	0.0
4	3/2	0.0	-0.0203	0.0380	0.0	0.0	0.0
6	3/2	0.0	-0.0557	-0.0553	0.0	0.0	0.0
8	3/2	0.0	-0.0231	-0.0280	0.0	0.0	0.0
10	3/2	0.0	-0.0039	-0.0081	0.0	0.0	0.0
12	3/2	0.0	-0.0030	-0.0029	0.0	0.0	0.0
2	5/2	0.0	-0.3438	-0.5388	0.9982	0.9967	0.9978
4	5/2	0.0	0.0137	0.0367	-0.0021	0.0014	0.0025
6	5/2	0.0	-0.0096	-0.0070	0.0482	0.0499	0.0506
8	5/2	0.0	-0.0065	0.0043	0.0339	0.0352	0.0357
10	5/2	0.0	0.0037	0.0086	-0.0036	-0.0029	-0.0027
12	5/2	0.0	-0.0012	-0.0015	0.0041	-0.0041	0.0042
4	7/2	0.0	-0.0173	-0.0732	0.0	-0.0101	0.0048
6	7/2	0.0	-0.0125	-0.0531	0.0	-0.0073	0.0035
8	7/2	0.0	-0.0100	-0.0424	0.0	-0.0058	0.0028
10	7/2	0.0	-0.0050	-0.0211	0.0	-0.0029	-0.0014
12	7/2	0.0	-0.0011	-0.0048	0.0	-0.0007	0.0003
4	9/2	0.0	-0.0298	-0.0088	0.0	0.0472	-0.0208
6	9/2	0.0	-0.0086	-0.0026	0.0	0.0137	-0.0060
8	9/2	0.0	-0.0081	-0.0024	0.0	0.0128	-0.0057
10	9/2	0.0	-0.0036	-0.0011	0.0	0.0057	-0.0025
12	9/2	0.0	-0.0011	-0.0001	0.0	0.0008	-0.0004



TABLE 5. The differential cross section ( $\mu\text{b}/\text{sr}$ ) of Sm-I53 at  $90^\circ$ 

Assignment Band	Spin	( $\alpha, p$ )		( $d, t$ )	
		Exp.	Theory	Exp.	Theory
I/2- (52I)					
	I/2	I83	396	I7	43
	3/2	52	I70	56	I7
	5/2		42		I4
	7/2		I27		I6
	9/2		I6		I
	II/2		2		0
I/2- (530)					
	I/2		I		5
	3/2		22	622	I44
	5/2		I7		86
	7/2		I3		I04
	9/2		9		39
	II/2		0		5
3/2- (52I)					
	3/2	44	54	23	30
	5/2		I8		7
	7/2	III	II7	2I	78
	9/2		32		I2
	II/2		2		2
3/2- (532)					
	3/2	33	28	39	I25
	5/2		I4	77	55
	7/2	I73	27	I27	I46
	9/2		3		I3
	II/2		I		9
5/2- (5I2)					
	5/2		5		0
	7/2		229		I9
	9/2		43		2
	II/2		I		0
5/2- (523)					
	5/2		30		5
	7/2		200		44
	9/2		29		5
	II/2		4		I
II/2- (505)					
	II/2	I7	I3	I25	8i

TABLE 6. The differential cross section ( $\mu\text{b}/\text{sr}$ ) of Gd-I55 at  $90^\circ$ 

Assignment Band	Spin	(d,p)		(d,t)	
		Exp.	Theory	Exp.	Theory
I/2- (52I)					
	I/2	200	4I7		5I
	3/2	36	I88		2I
	5/2	36	39	4	4
	7/2	98	II5	5	I7
	9/2	II	I4	5	I
	II/2		<del>2</del>		0
I/2- (530)					
	I/2		3		I5
	3/2		I8		I00
	5/2		28		II5
	7/2		I7		90
	9/2		I5		49
	II/2		I		4
3/2- (52I)					
	3/2	43	43	58	29
	5/2	3	25	I	II
	7/2	I38	97	92	77
	9/2	I0	35	I0	I4
	II/2		I		2
3/2- (532)					
	3/2		36		I5I
	5/2		I0		38
	7/2		33		I79
	9/2		I		5
	II/2		I		9
5/2- (5I2)					
	5/2		5		0
	7/2		2I5		2I
	9/2		45		2
	II/2		I		0
5/2- (523)					
	5/2	28	29	95	7
	7/2	90	I96	49	58
	9/2	25	23		5
	II/2		3		2
II/2- (505)					
	II/2		I2	97	8I

TABLE 7. The differential cross section ( $\mu\text{b/sr}$ ) of  
 $\text{Dy-I57}$  at  $90^\circ$ 

Assignment Band	Spin	(d,p)		(d,t)	
		Exp.	Theory	Exp.	Theory
I/2- (52I)					
	I/2	I02	4I8	34	49
	3/2	(36)	I97	(40)	2I
	5/2	(89)	38	(I38)	4
	7/2	(32)	II4	(27)	I7
	9/2		I4		I
	II/2		2		0
I/2- (530)					
	I/2		4		I7
	3/2	(89)	I7	(I38)	90
	5/2	23	3I	I6	I25
	7/2	(32)	I7	(27)	88
	9/2		I7		53
	II/2		I		3
3/2- (52I)					
	3/2	35	39	55	26
	5/2	2	26	0.6	II
	7/2	96	9I	96	74
	9/2	I7	36	9	I3
	II/2		I		I
3/2- (532)					
	3/2		37		I56
	5/2		9	20	29
	7/2		33	I6	I89
	9/2		0		2
	II/2		I		9
5/2- (5I2)					
	5/2		6		0
	7/2	55	207		20
	9/2	6	46		2
	II/2		I		0
5/2- (523)					
	5/2	26	29	I9	7
	7/2	99	204	30	64
	9/2	(36)	22	(40)	5
	II/2		3		2
II/2- (505)					
	II/2	I0	II	30	82

TABLE 8. The differential cross section ( $\mu\text{b}/\text{sr}$ ) of Gd-157 at  $90^\circ$ 

Assignment Band	Spin	(d,p)		(d,t)	
		Exp.	Theory	Exp.	Theory
I/2- (521)					
	I/2	128	339		30
	3/2	20	I34		II
	5/2	70	5I		5
	7/2	39	I50		I7
	9/2	4	I8		I
	II/2		3		I
I/2- (530)					
	I/2		0		0
	3/2	84	I2	260	239
	5/2		4	43	57
	7/2		I	20	II7
	9/2		I	I2	3I
	II/2		0		8
3/2- (521)					
	3/2	55	54	I00	4I
	5/2		6	2	3
	7/2	I32	I30	I50	II7
	9/2	9	2I	I3	II
	II/2	5	2	9	3
3/2- (532)					
	3/2		8	59	89
	5/2		7	I3	80
	7/2		3	I43	9I
	9/2		3	7	26
	II/2		0		IO
5/2- (512)					
	5/2		3		0
	7/2	95	25I		2I
	9/2		4I		3
	II/2		I		0
5/2- (523)					
	5/2	28	25	24	3
	7/2	I03	I79	9	30
	9/2	20	39	II	5
	II/2		5		I
II/2- (505)					
	II/2		8	69	90

TABLE 9. The differential cross section ( $\mu\text{b}/\text{sr}$ ) of Dy-I59 at  $90^\circ$ 

Assignment Band	Spin	(d,p)		(d,t)	
		Exp.	Theory	Exp.	Theory
I/2- {52I}	I/2	I40	367	36	37
	3/2	I9	I35		I2
	5/2	52	48		5
	7/2	(I20)	I4I	(92)	20
	9/2		I7		I
	II/2		3		I
I/2- {530}	I/2		0		0
	3/2	(I20)	I3	(92)	222
	5/2	(I3)	5	(26)	67
	7/2	8	2	3I	II3
	9/2		I		33
	II/2		0		7
3/2- {52I}	3/2	39	52	9I	49
	5/2		8		5
	7/2	I05	I09	I32	I26
	9/2	(47)	2I	(68)	I3
	II/2		2		3
3/2- {532}	3/2		II	I3	I05
	5/2	I2	7	55	76
	7/2	(I3)	4	(I26)	I0I
	9/2		3		23
	II/2		0		9
5/2- {5I2}	5/2		3		0
	7/2		255		24
	9/2		42		3
	II/2		2		I
5/2- {523}	5/2	20	28	I3	4
	7/2	7I	I76	3I	38
	9/2	I7	36	4	5
	II/2		4		2
II/2- {505}	II/2		8	50	87

TABLE IO. The differential cross section ( $\mu\text{b}/\text{sr}$ ) of Er-I6I at  $90^\circ$ 

Assignment Band	Spin	(d,p)		(d,t)	
		Exp.	Theory	Exp.	Theory
I/2- (52I)	I/2		384		46
	3/2		I52		I5
	5/2		44		6
	7/2		I3i		25
	9/2		I6		I
	II/2		2		I
I/2- (530)	I/2		0		3
	3/2		I3		I77
	5/2		8		82
	7/2		3		I05
	9/2		2		37
	II/2		0		6
3/2- (52I)	3/2		44	55	49
	5/2		II		9
	7/2		85	77	I24
	9/2		22	7	I6
	II/2		I	(5)	3
3/2- (532)	3/2		I7		I27
	5/2		8		65
	7/2		4		I25
	9/2		3		I8
	II/2		0		9
5/2- (5I2)	5/2		5		I
	7/2		237		28
	9/2		47		4
	II/2		I		I
5/2- (523)	5/2		28	9	6
	7/2		I84	50	56
	9/2		3I	(5)	6
	II/2		4	9	2
II/2- (505)	II/2		8		87

TABLE II. The differential cross section ( $\mu\text{b}/\text{sr}$ ) of Gd-159 at  $90^\circ$

Assignment Band	Spin	(d,p)		(d,t)	
		Exp.	Theory	Exp.	Theory
I/2- (521)					
	I/2	I99	204	80	23
	3/2	25	I76	7	I9
	5/2	67	I3	I7	I
	7/2	I36	I78	26	23
	9/2	I8	2I		2
	II/2		4		I
I/2- (530)					
	I/2		0		0
	3/2		7	2I9	246
	5/2		2	8	67
	7/2	I5	I		9I
	9/2		I	I3	25
	II/2		0	9	I5
3/2- (521)					
	3/2	66	I9	I9I	28
	5/2		7	4	9
	7/2	88	66	2I9	I45
	9/2		I2	22	I6
	II/2		2	25	6
3/2- (532)					
	3/2		3	54	99
	5/2		4	90	I00
	7/2		I	37	80
	9/2		2	34	28
	II/2		0		I8
5/2- (512)					
	5/2		II		0
	7/2		3		I
	9/2		3I		I
	II/2		0		0
5/2- (523)					
	5/2	22	2I	27	4
	7/2	I36	22I	II8	59
	9/2		30	25	6
	II/2	I8	7	I8	3
II/2- (505)					
	II/2	4	5	I02	9I

TABLE I2. The differential cross section ( $\mu\text{b}/\text{sr}$ ) of Dy-I6I at  $90^\circ$ 

Assignment Band	Spin	(d,p)		(d,t)	
		Exp.	Theory	Exp.	Theory
I/2- {52I}					
	I/2	I52	283	I02	59
	3/2	27	I42	II	28
	5/2	48	II	35	2
	7/2	66	I37	I9	32
	9/2	I2	I8	4	3
	II/2	9	3	I	I
I/2- {530}					
	I/2		I	I2	I2
	3/2	39	9	I48	I79
	5/2		6	26	98
	7/2		3	34	95
	9/2		2		32
	II/2		0		9
3/2- {52I}					
	3/2	29	24	I83	44
	5/2	2	I5	5	2I
	7/2	I24	60	2I7	I39
	9/2	2	I9	6	23
	II/2		I		5
3/2- {532}					
	3/2		II		I5I
	5/2		6		84
	7/2		3		I2I
	9/2		2		2I
	II/2		0		I3
5/2- {5I2}					
	5/2		9		I
	7/2	259	I96		25
	9/2	I3	47		3
	II/2		I		0
5/2- {523}					
	5/2	20	24	23	I2
	7/2	(49)	I55	(84)	I03
	9/2	I0	I9	27	9
	II/2		4		4
II/2- {505}					
	II/2	5	8	58	84

TABLE I3. The differential cross section ( $\mu\text{b}/\text{sr}$ ) of  
 Er-I63 at  $90^\circ$ 

Assignment Band	Spin	(d, p)		(d, t)	
		Exp.	Theory	Exp.	Theory
I/2- (52I)					
	I/2	I03	300	47	90
	3/2	23	I43	II	40
	5/2	38	7		2
	7/2	64	III	34	40
	9/2	8	I7		4
	II/2		2		I
I/2- (530)					
	I/2		4		4I
	3/2	2I	8	63	I04
	5/2	8	I4	4	I40
	7/2		5	I6	8I
	9/2		4		4I
	II/2		0		5
3/2- (52I) *					
	3/2	34	20	I0I	38
	5/2	I	23		32
	7/2	I53	37	I98	II3
	9/2		24	5	27
	II/2	6	I	7	3
3/2- (532)					
	3/2		20		205
	5/2		7		62
	7/2		6		I63
	9/2		I		II
	II/2		0		I2
5/2- (5I2)					
	5/2	7	7	I5	I
	7/2	I58	I97	5	42
	9/2	2	45		4
	II/2		2		I
5/2- (523)					
	5/2	II	20	20	I9
	7/2	I9	I2I		I54
	9/2	I9	I3	I8	II
	II/2		2	I	5
II/2- (505)					
	II/2		8	39	83

TABLE I4. The differential cross section ( $\mu\text{b}/\text{sr}$ ) of  
 Gd-161 at  $90^\circ$ 

Assignment Band	Spin	(d,p)		(d,t)	
		Exp.	Theory	Exp.	Theory
I/2- {521}	I/2	I68	266		84
	3/2	I5	98		31
	5/2	I95	8		3
	7/2	I7	I26		42
	9/2	I3	I7		5
	II/2	I5	3		I
I/2- {530}	I/2		0		4
	3/2		6		247
	5/2		3		88
	7/2		I		86
	9/2		I		29
	II/2		0		I2
3/2- {521}	3/2	52	I6		79
	5/2		6		22
	7/2		24		I68
	9/2		8		25
	II/2	I5	I		8
3/2- {532}	3/2		6		I45
	5/2		26		I02
	7/2		55		84
	9/2		6		23
	II/2		I		I3
5/2- {512}	5/2	~3	7		0
	7/2		229		30
	9/2	I6	40		2
	II/2	II	2		I
5/2- {523}	5/2	20	I8		25
	7/2	~20	79		I35
	9/2	22	I5		20
	II/2	7	2		7
II/2- {505}	II/2		6		85

TABLE I5. The differential cross section ( $\mu\text{b}/\text{sr}$ ) of Dy-I63 at  $90^\circ$ 

Assignment Band	Spin	(d,p)		(d,t)	
		Exp.	Theory	Exp.	Theory
I/2- {52I}	I/2	II5	269	263	8I
	3/2	3	.99		29
	5/2	57	8		3
	7/2	(II6)	I28	(I50)	40
	9/2		I7		4
	II/2		3		I
	I/2- {530}	I/2		0	
3/2			6	60	247
5/2			3	24	88
7/2			I	I5	86
9/2			I		29
II/2			0		I2
3/2- {52I}	3/2	8	I7	22I	80
	5/2	8	5	I4	22
	7/2	28	23	I52	I88
	9/2		8	I3	25
	II/2		I	(24)	8
3/2- {532}	3/2		4		I44
	5/2		5		I06
	7/2		4		68
	9/2		I		I7
	II/2		I		9
5/2- {5I2}	5/2		7		0
	7/2	306	230		29
	9/2	9	40	28	2
	II/2		2		I
5/2- {523}	5/2	II	I7	54	25
	7/2	I8	78	43	I36
	9/2	I9	I5	43	20
	II/2	5	3	I4	7
II/2- {505}	II/2		6		85

TABLE I6. The differential cross section ( $\mu\text{b}/\text{sr}$ ) of  
 Er-I65 at  $90^\circ$ 

Assignment Band	Spin	(d, p)		(d, t)	
		Exp.	Theory	Exp.	Theory
I/2- {52I}					
	I/2	I2I	269	92	I02
	3/2	I8	I06	9	40
	5/2	27	8	~2I	3
	7/2	60	II0		42
	9/2		I5		5
	II/2		2		I
I/2- {530}					
	I/2		I		I4
	3/2		6	96	I94
	5/2		5	8	I07
	7/2		2	I7	89
	9/2		I		32
	II/2		0		9
3/2- {52I}					
	3/2	57	I5	233	69
	5/2		8		29
	7/2	I22	23	2I7	I72
	9/2	4	I2	~5	29
	II/2		I		6
3/2- {532}					
	3/2		8		I7I
	5/2		4		92
	7/2		2		II0
	9/2		I		22
	II/2		0		I3
5/2- {5I2}					
	5/2		8		I
	7/2	I75	2I8	~I8	40
	9/2	7	4I		3
	II/2	7	2	58	I
5/2- {523}					
	5/2	6	I5	34	27
	7/2	7	76	I6	I6I
	9/2	II	I3	33	I9
	II/2		2		6
II/2- {505}					
	II/2		6	~33	85

TABLE I7. The input parameters for Mass I53 to I65.

Nucleus	N	$\beta_2$	$\beta_4$	$\hbar^2/2g_0$
Sm-I53	91	0.249	0.036	0.0125
Gd-I55	91	0.235	0.015	0.0136
Dy-I57	91	0.230	0.013	0.0137
Gd-I57	93	0.290	0.090	0.0118
Dy-I59	93	0.280	0.068	0.0125
Er-I61	93	0.260	0.046	0.0132
Gd-I59	95	0.330	0.145	0.0110
Dy-I61	95	0.280	0.064	0.0116
Er-I63	95	0.250	0.016	0.0127
Gd-I61	97	0.320	0.080	0.0110
Dy-I63	97	0.320	0.080	0.0110
Er-I65	97	0.290	0.050	0.0116

## CAPTIONS TO FIGURES FOR MASS-25

Fig. 1 The energy levels of a particle in a potential well with quadrupole deformation. (a) The central and quadrupole deformations with an  $r^2$  radial dependence. Nilsson parameters  $\kappa = .08$ ,  $\mu(N = 2) = 0$ ,  $\mu(N = 4) = 0.45$ ,  $\hbar\omega = 41/A^{1/3}$  MeV. (b) The Saxon-Woods central, and the derivative of the Saxon-Woods quadrupole radial dependence, with the optical potential parameters of Hodgson (1963)  $V_0 = -53$  MeV,  $r_0 = 1.25$  fm,  $a_0 = 0.65$  fm, for the solid lines. The dashed lines are for  $a_0 = 0.55$  fm with the other parameters unchanged. (c) The Saxon-Woods central, and the derivative of the Saxon-Woods quadrupole radial dependence with the optical potential parameters of Becchetti and Greenlees (1969)  $V_0 = -55.3$  MeV,  $V_{0s} = 6.2$  MeV,  $r_0 = 1.17$  fm,  $a_0 = 0.75$  fm. The half integers on the right of each line are the  $K = \Omega$  values of the state.

Fig. 2 The effect of RPC and band mixing on single particle states in a quadrupole deformed potential for (a) A harmonic oscillator radial dependence with the same parameters are the same as in fig. 1a. (b) A Saxon-Woods radial dependence with the same parameters as for the solid lines in fig. 1b. The half integers on the right of each line are the  $I$  values of each state.

Fig. 3. The effect of applying, first a quadrupole deformation  $\beta_2 r^2 Y_2^0$  on the left side of the figure, and then a hexadecapole deformation  $\beta_4 r^4 Y_4^0$  for a constant quadrupole deformation  $\beta_2 = 0.4$  on the right side of the figure, to a harmonic oscillator potential well. continued.....

The other parameters are  $\kappa = 0.08$ ,  $\mu(N = 2) = 0.0$ ,  $\mu(N = 4) = 0.45$ .  
 All states with  $N \leq 6$  were included in the diagonalisation

Fig. 4 The eigenstates in a deformed Saxon-Woods potential in which, on the left  $\beta_4 = 0$  and  $\beta_2$  is varied, in the centre  $\beta_2 = 0.4$  and  $\beta_4$  is varied, and on the right core rotational energy and band mixing is introduced and varied through the parameter  $\hbar^2/2J_0$  with constant  $\beta_2 = 0.4$  and  $\beta_4 = 0.4$ .

Fig. 5 The energy levels of the three lowest even parity bands in  $A = 25$ . On the left are the experimental levels of  $^{25}\text{Mg}$ , and on the extreme right the experimental levels of  $^{25}\text{Al}$ . The theoretical predictions with various assumptions are shown in between. The lowest level has been set to zero excitation in all cases. The symbol SW refers to calculations using a Saxon-Woods radial dependence for the central potential and a derivative Saxon-Woods dependence for the other interactions. The symbol HO refers to the eigenstates of a deformed harmonic oscillator.

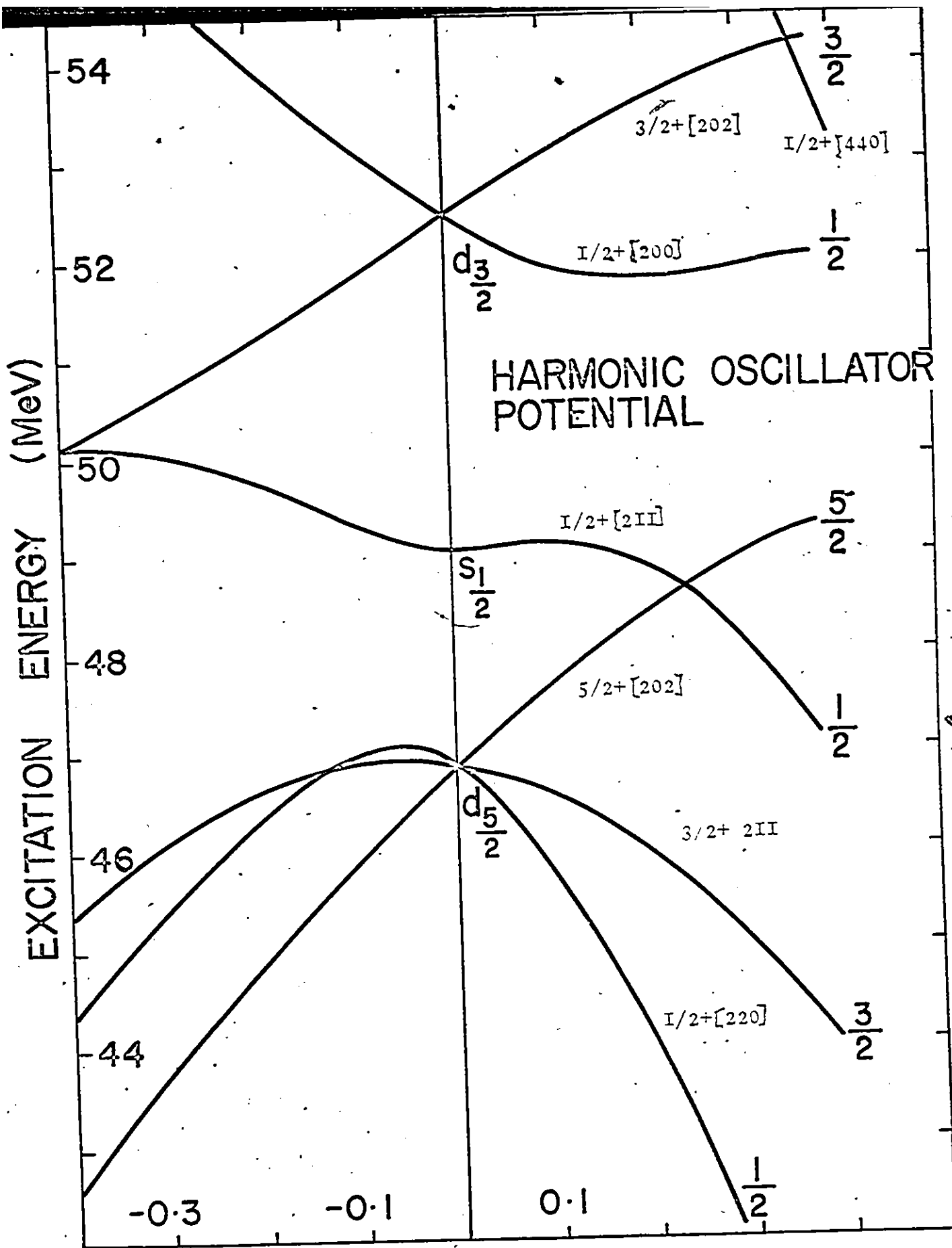


Fig. 1a

DEFORMATION  $\beta_2$

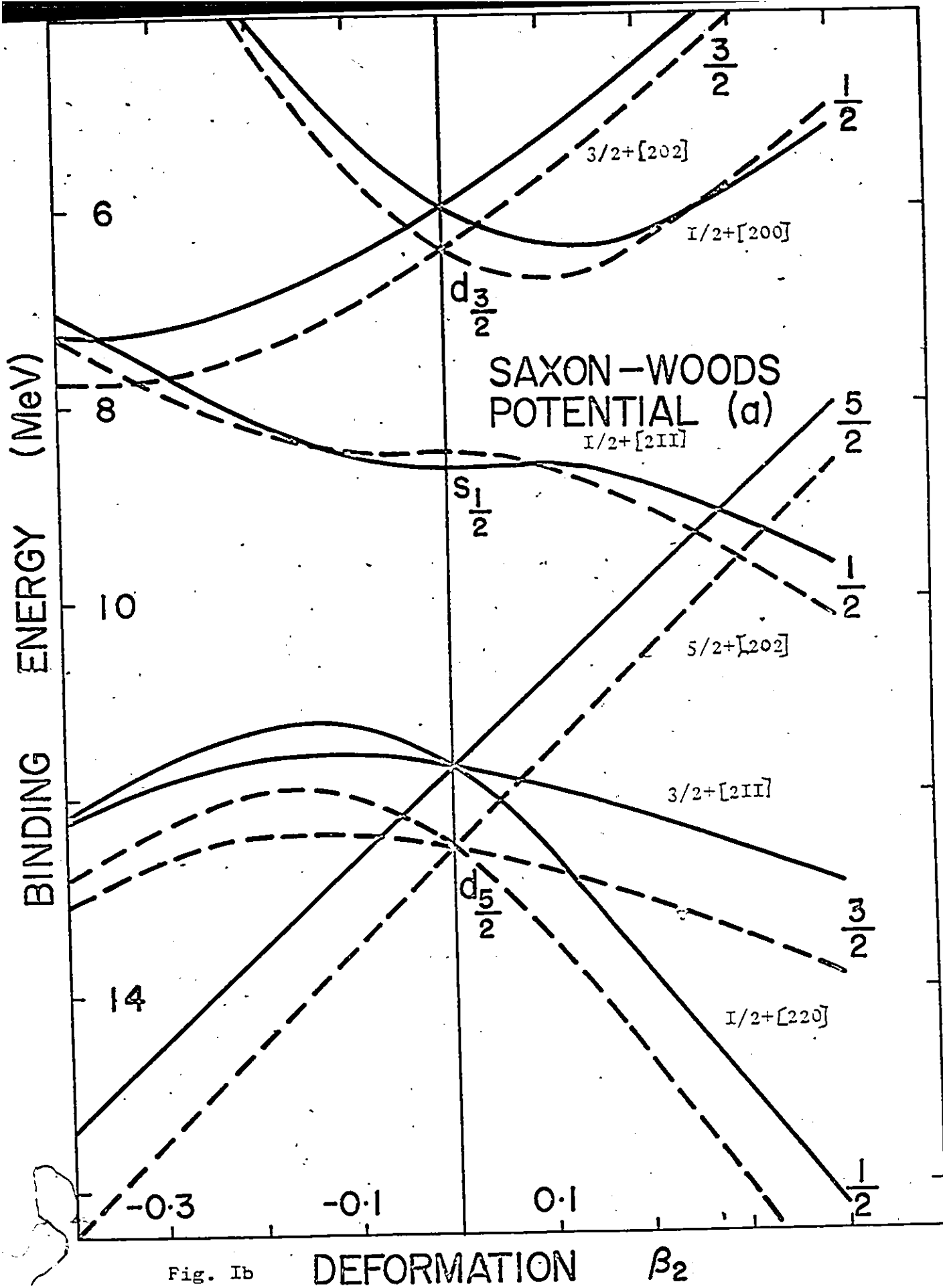


Fig. Ib

DEFORMATION  $\beta_2$

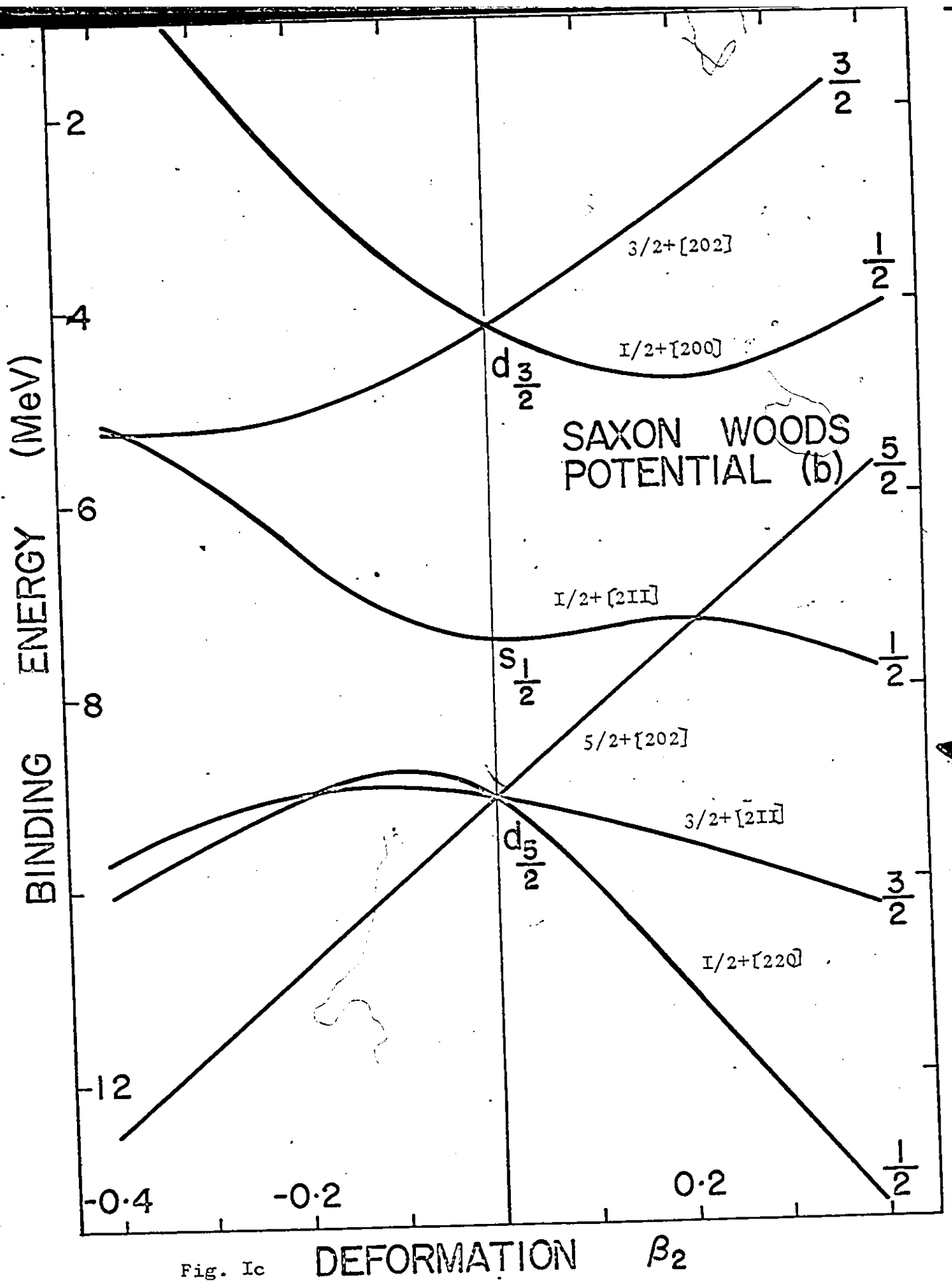
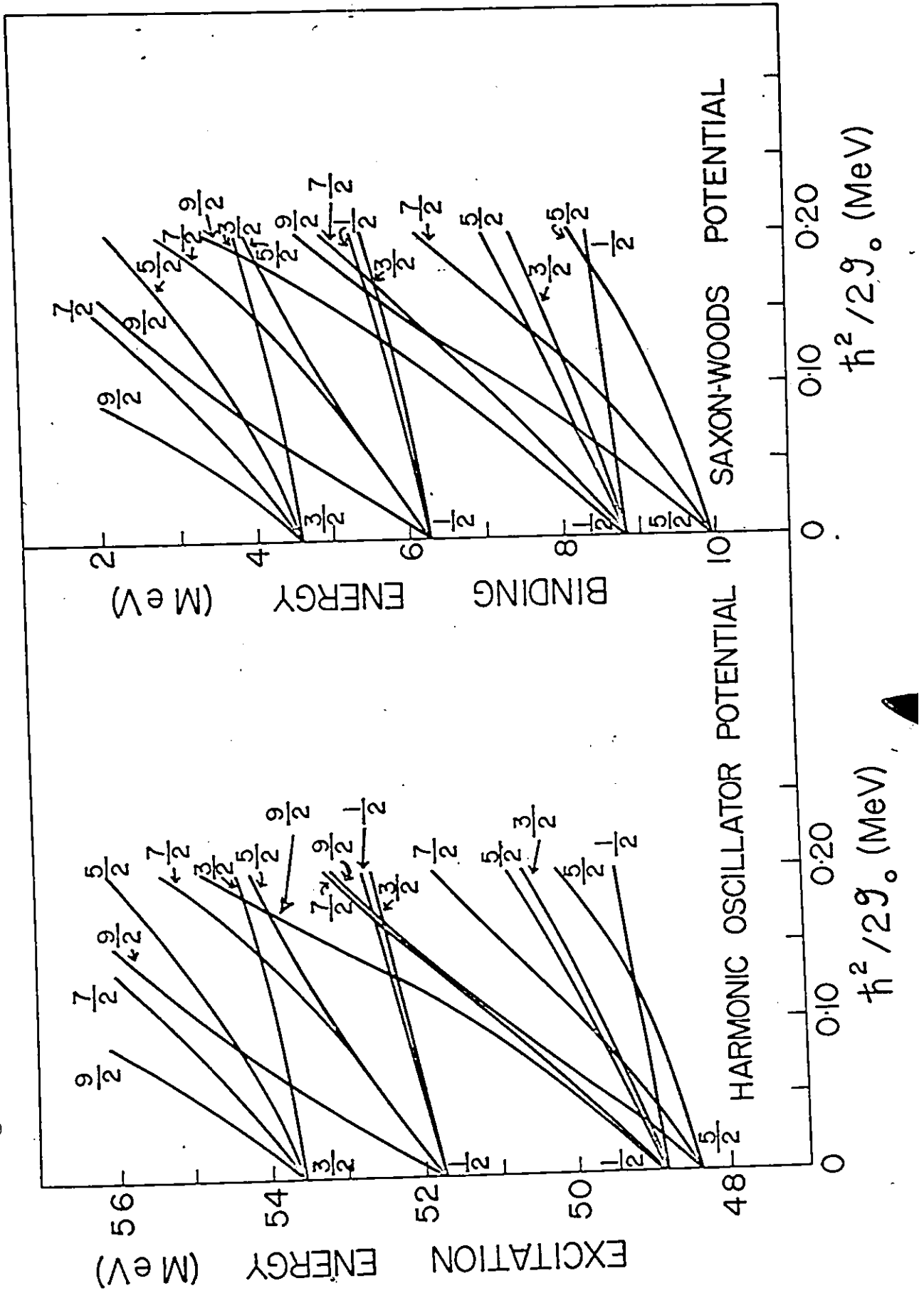


Fig. 1c

DEFORMATION  $\beta_2$

Fig. 2



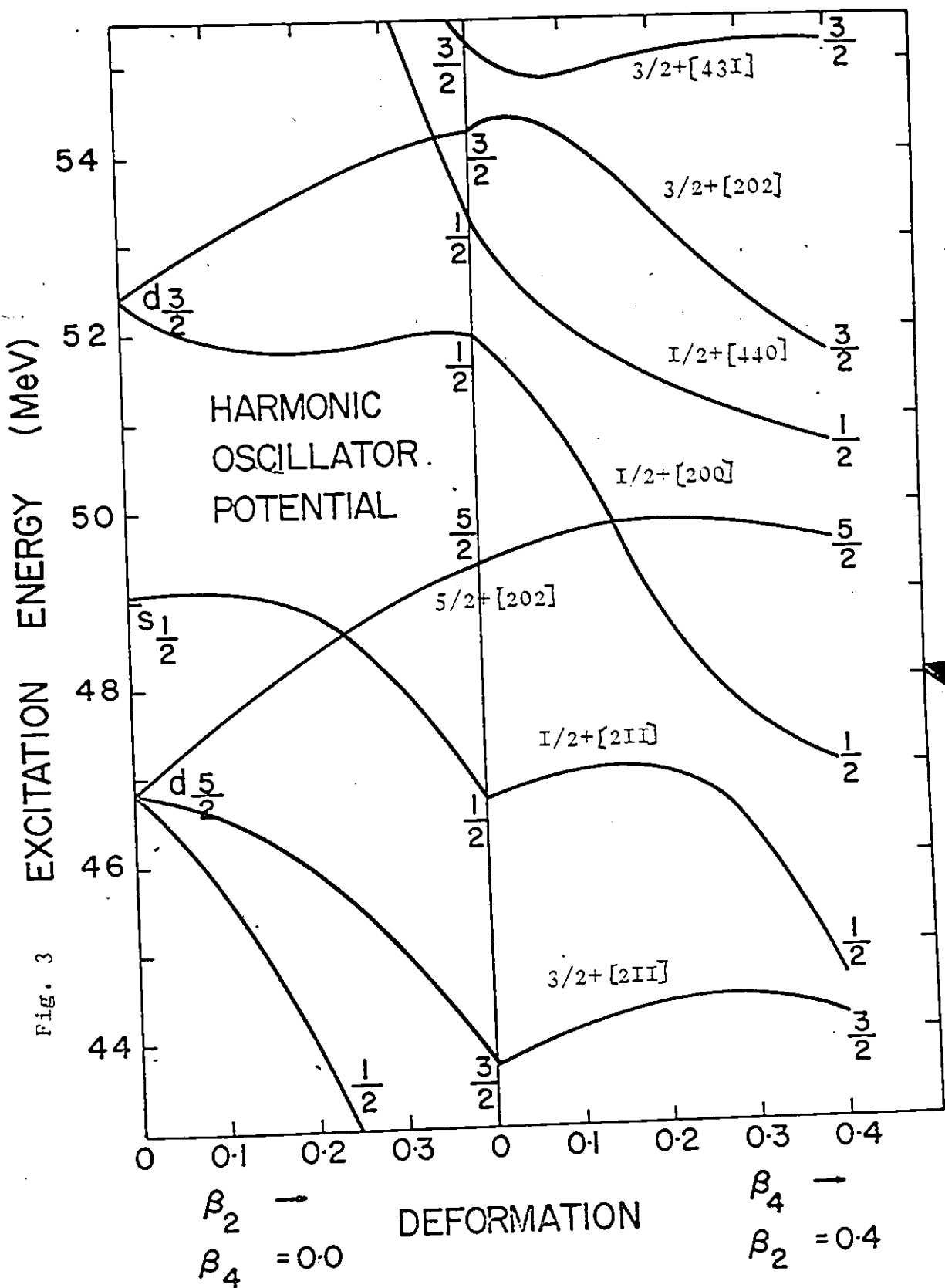
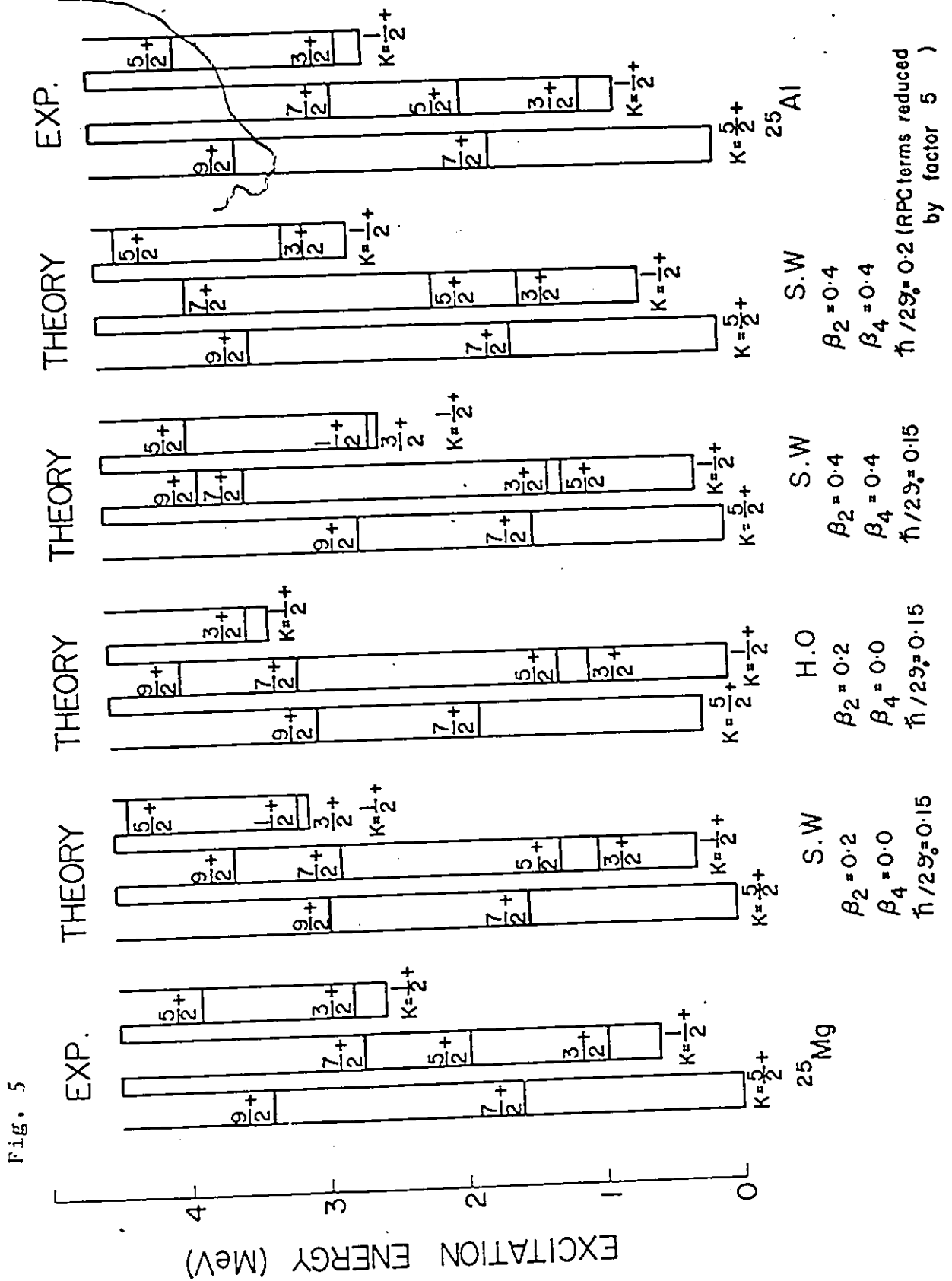


Fig. 3





▲

## CAPTIONS TO FIGURES FOR MASS I53 TO I65

Fig. 6 Single particle energies for a particle in a deformed Woods-Saxon potential with  $r_0 = 1.25$  fm,  $a = 0.65$  fm,  $V_0 = -44.9$  MeV,  $V_l = -9.5$  MeV, where the radius has an angular dependence  $R = r_0 A^{1/3} [1 - (\beta_2^2 + \beta_4^2)/4\pi + \beta_2 Y_2^0(\theta) + \beta_4 Y_4^0(\theta)]$ . On the left the  $\beta_2$  variation is shown for  $\beta_4 = 0$ ; on the right the  $\beta_4$  variation is shown for  $\beta_2 = 0.25$ . The calculation was made for  $A = 157$ , but is very similar for neighbouring nuclei. The term in  $H_p$  which is proportional to  $d^2V(rR\theta)/dr^2$  was omitted.

Fig. 7 The model predictions for the  $N = 91$  isotones compared to the experimentally identified bands. Level energies are given above the  $3/2^- [521]$  band head which forms the ground state. In each nucleus the experimental levels are shown on the left and the theoretical predictions on the right. The single digits refer to twice the  $j$  value of each level.

Fig. 8 The model predictions for the  $N = 93$  isotones compared to the experimentally identified bands. Level energies are measured from the  $3/2^- [521]$  band head which forms the ground state. The experimental levels are shown to the left of the theoretical predictions for each isotope. The single digits refer to twice the  $j$  value of each level.

Fig. 9 Single particle energies for a particle on a deformed Woods-Saxon potential. The calculation and parameters were identical to those of fig. 1., except that the  $d^2V(rR\theta)/dr^2$  term was here included.

Fig. I0      The model predictions for the  $N = 95$  isotones compared to the experimentally identified bands. Level energies are measured from the band head energy of the ground state band in each nucleus. The single digits refer to twice the  $j$  value of each level.

Fig. II      The model predictions for the  $N = 97$  isotones compared to the experimentally identified bands. Level energies are measured from the band head energy of the ground state band in each nucleus. The single digits refer to twice the  $j$  value of each level.

Fig. I2      The variation of the input parameters of the model with atomic weight. The nuclei having the same  $N$  are connected by dotted lines; the nuclei having the same  $Z$  value are connected by continuous lines. The crosses on the graph for the quadrupole deformation  $\beta_2$  show the average values which were mostly obtained from HFS,  $\mu$ -Xray and Coulomb excitation measurements (Lörner, Vetter and Hönig 1970). The crosses on the graph for the hexadecapole deformation  $\beta_4$  show experimental values (Erb et al. 1972, Davidson, Close and Malonify 1974, Hendrie et.al. 1968).

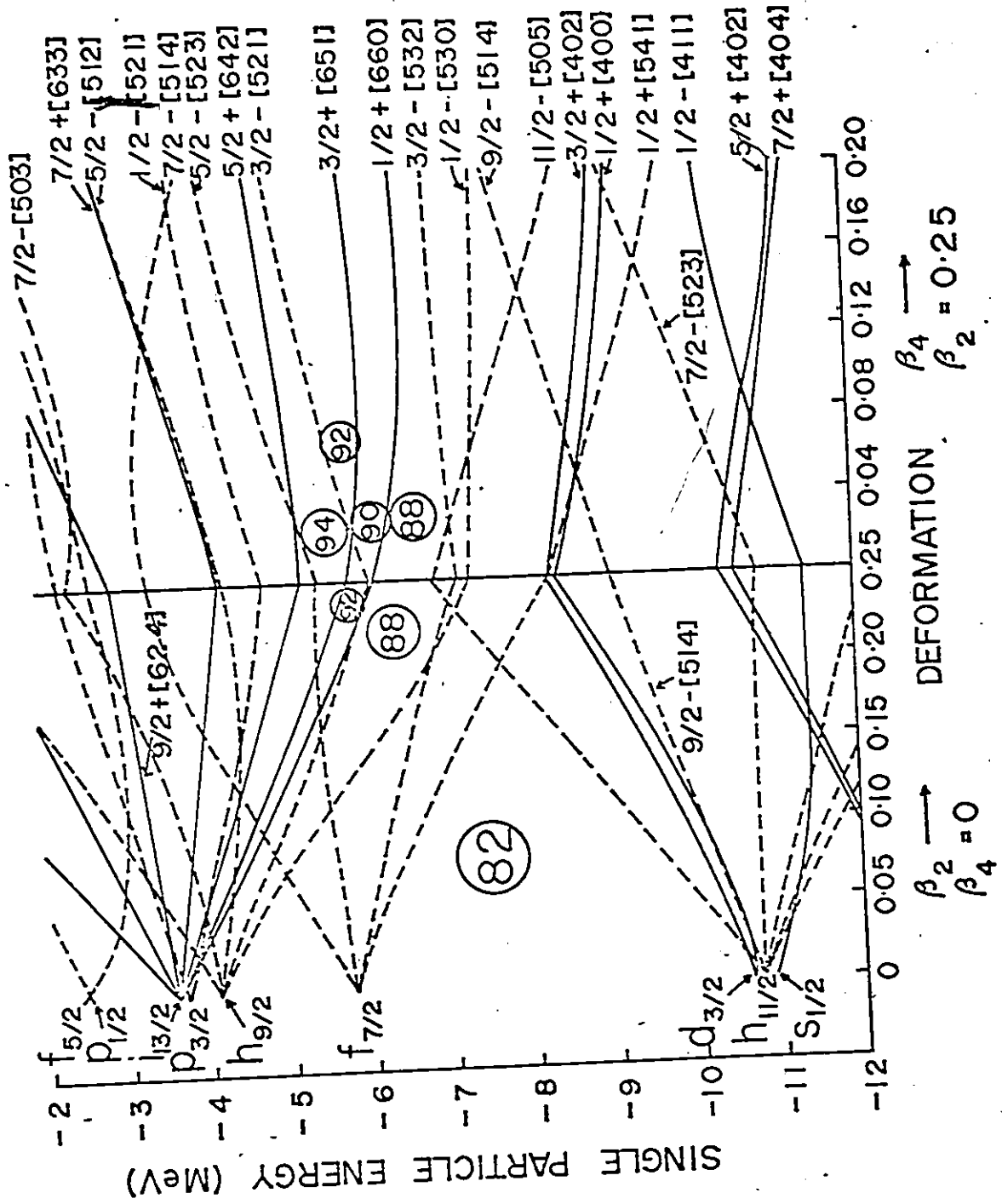


Fig. 6





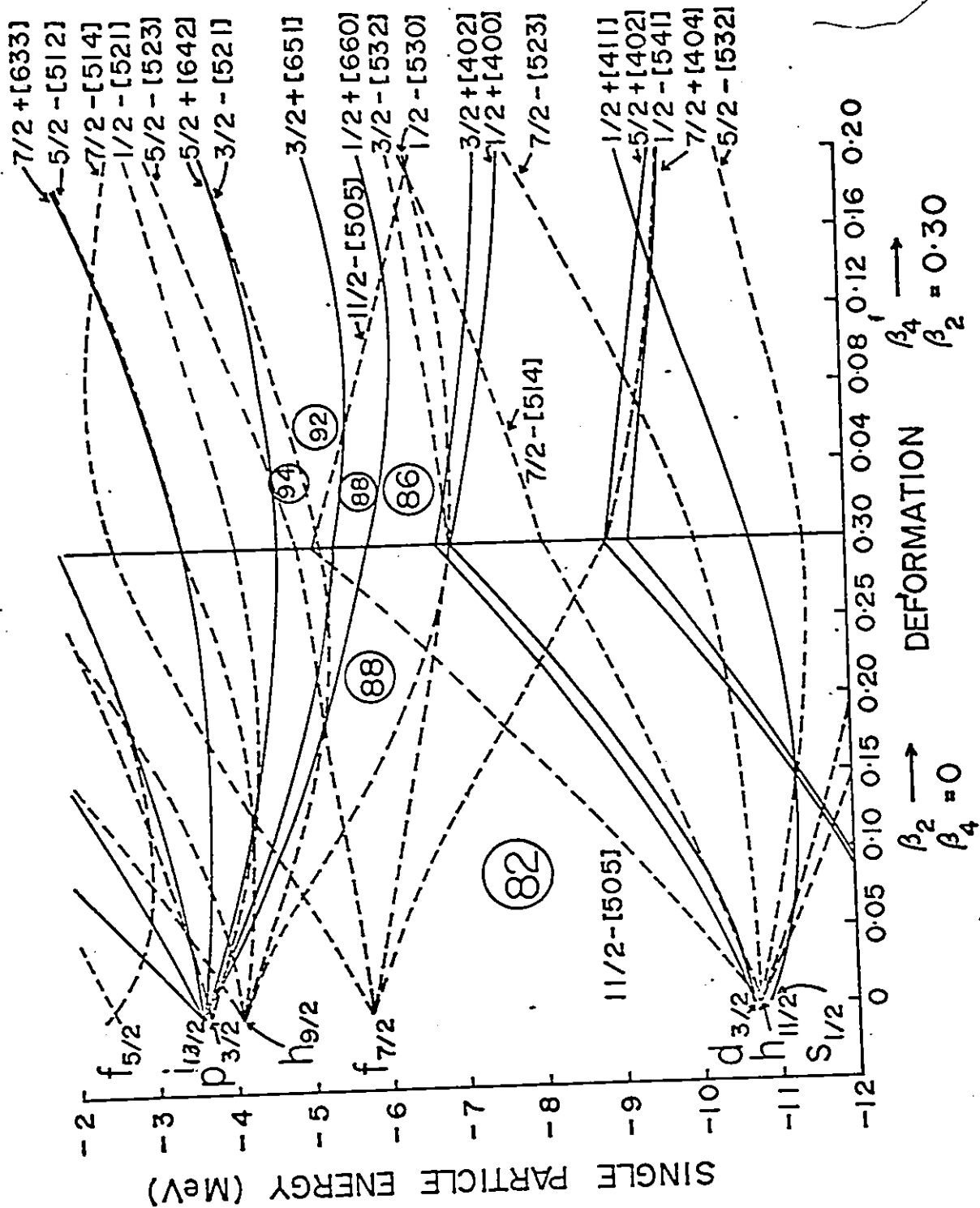


Fig. 9



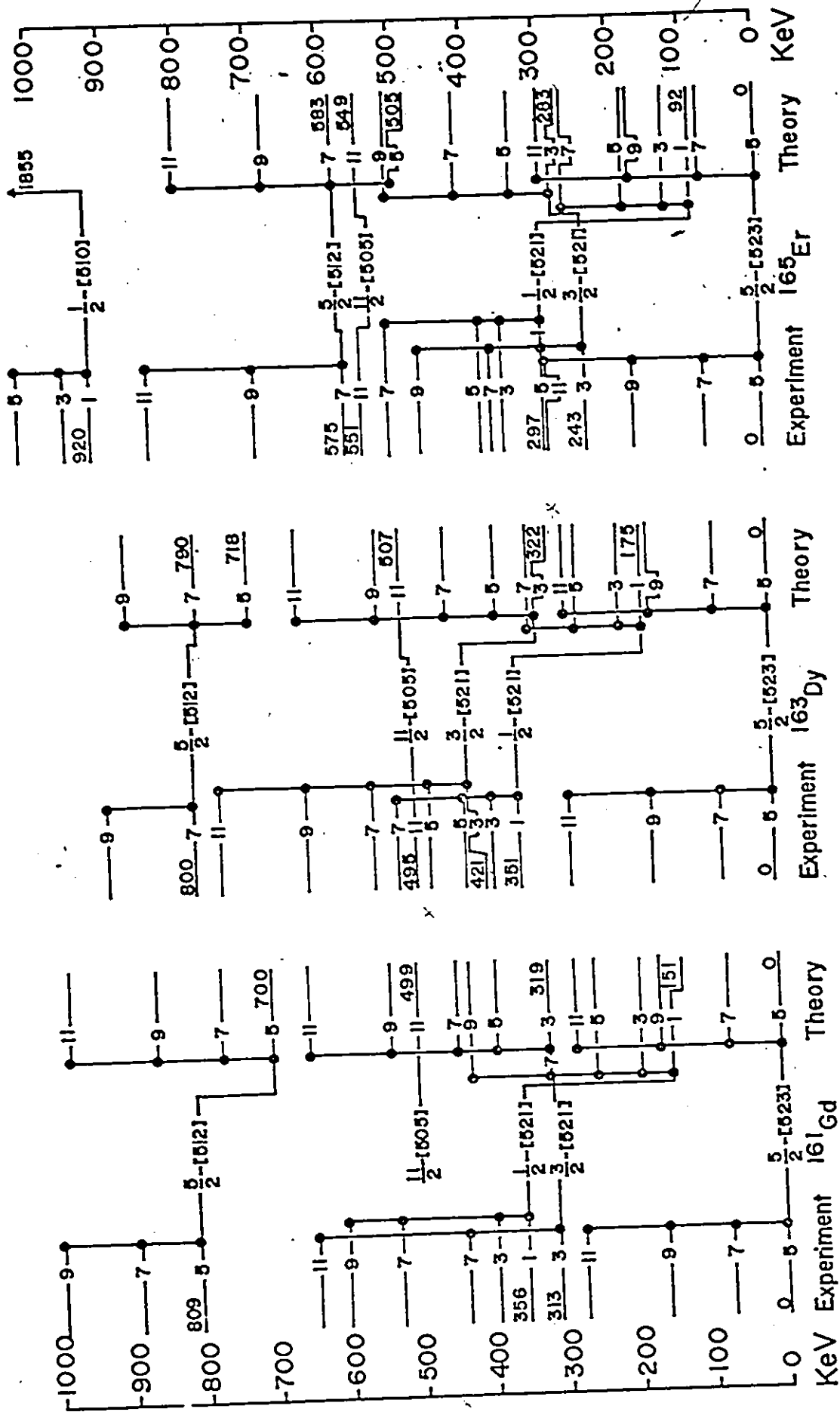
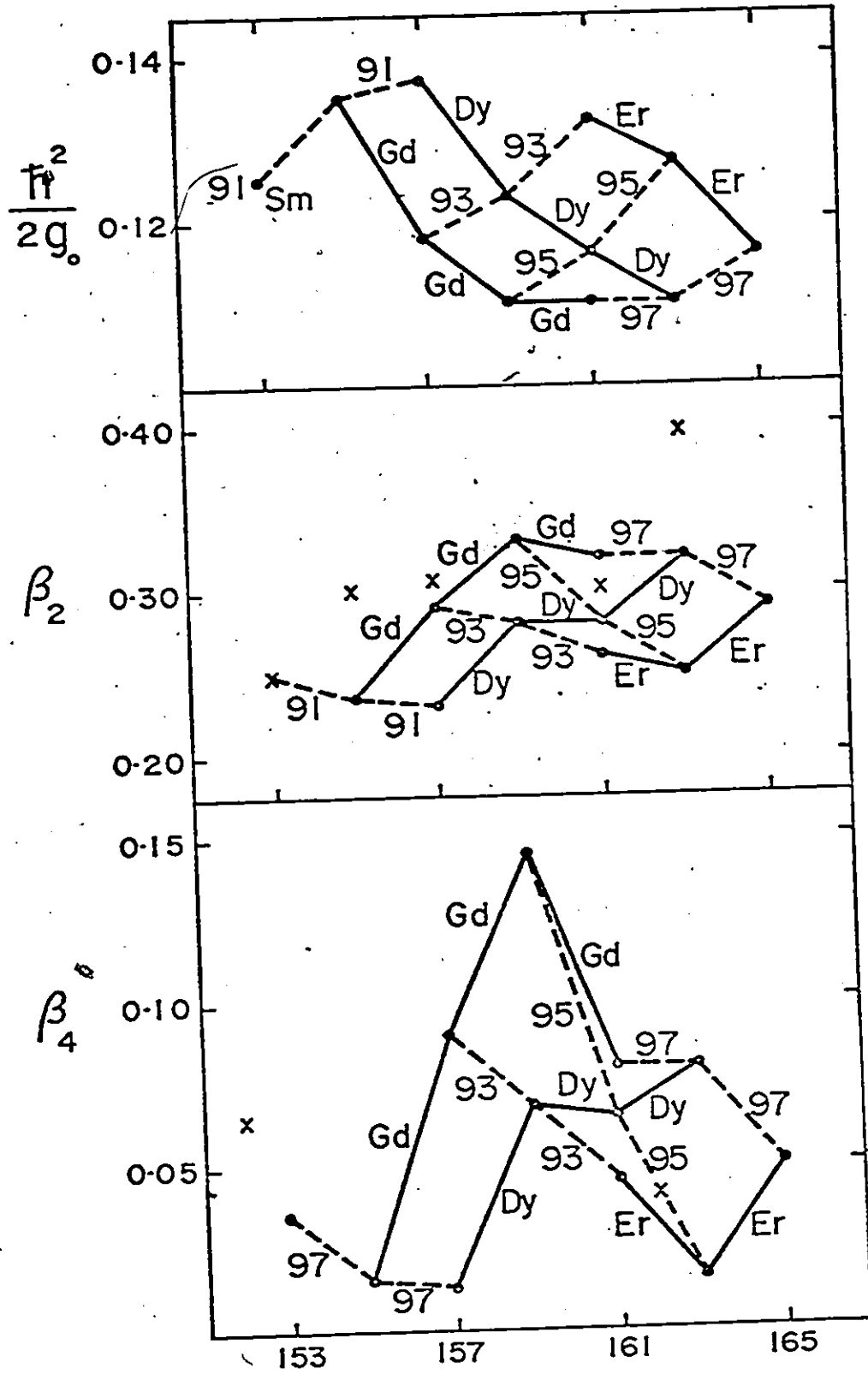


Fig. II



A

Fig. 12

## VI REFERENCES

- Anderson, B. L. 1968, Nucl. Phys. A112, 443.
- Bardeen J., Cooper L. N., and Schrieffer J. R. 1957,  
Phys. Rev. 106, 162.
- Bayman, B. F. and Kallio, A. 1967, Phys. Rev. 156, 1121.
- Becchetti, F. D. and Greenlees, G. W. 1969, Phys. Rev.  
182, 1190.
- Berg V. and Malmskog S. G. 1969, Nucl. Phys. A135, 401.
- Bohr A, 1952, Mat. Fys. Medd. Dan. Vid. Selsk. 26, No. 14.
- Bohr A. and Mottelson B. R. 1953, Mat. Fys. Dan. Vid.  
Selsk. 27, No. 16.
- Bohr A. and Mottelson B. R. 1969, Nuclear Structure Vol. 1.  
Benjamin Inc. New York 1969.
- Bohr N. and Kalekar F. 1937, Mat. Fys. Medd. Dan. Vid.  
Selsk. 14, No. 10.
- Borggreen J. and Sletten G. 1970, Nucl. Phys. A143, 255.
- Burke D. G., Zeidman B., Elbek B., Herskind B., and  
Olesen M. 1966, Kgl. Dan. Vid. Mat. Fys. Medd. 35, No. 2
- Buyrn A. 1972, Nucl. Data Sheets B8, 295.

- Caswell R. S. 1966, NBS Technical Note 410.
- Chi, B. E. and Davidson, J. P. 1963, Phys. Rev. 131, 366.
- Davidson J. P., Close D. A. and Malanify J. J. 1974, Phys. Rev. Lett. 32, 337.
- De-Shalit, A. and Talmi, I. 1963, Nuclear Shell Theory (Academic Press, New York)
- de Swiniarski, R., Glashausser, C., Hendrie, D. L., Sherman, J., Backer, A. D., and McClatchie, A. E. 1969, Phys. Rev. Lett. 23, 317.
- Elbek B. and Tjom P. O. 1969, Advan. Nucl. Phys. 3, 259.
- Erb K. A., Holden J. E., Lee I. Y., Saladin J. X. and Saylor T. K. 1972, Phys. Rev. Lett. 29, 1010.
- Funke L., Graber H., Kaun K. -H., Romer J. and Soden H. 1966, Nucl. Phys. 84, 443.
- Glendenning, N. K. 1965, Phys. Rev. 137, B102.
- Groshev L. V., Demidov A. M. and Sokolovskii 1971, Isv. Akad. Nauk SSSR Ser. Fiz. 35, 1644.
- Grottdal T., Nybo K., and Elbek B. 1970, Mat. Fys. Medd. Dan. Vid. Selsk. 37, No. 12.
- Harada, K. 1964, Phys. Lett. 10, 80.

- Hecht, K. T. and Sachler, G. E. 1962, Nucl. Phys. 32, 286.
- Hendrie D. L., Glendenning N. K., Harvey B. G., Jarvis O. N.,  
 Duham H. H., Saudinos J. and Mahoney J. 1968, Phys. Lett.  
 26B, 127.
- Hird, B. 1971, Can. J. Phys. 49, 302.
- Hird, B. 1973, Comp. Phys. Comm. 6, 30.
- Hird, B. and Huang, K. H. 1973, Can. J. Phys. 51, 956.
- Hird, B. and Huang, K. H. 1975, Can. J. Phys. 53, 559.
- Hird, B. and Huang, K. H. Comp. Phys. Comm. (will be published)
- Hjorth S. A., Ryde H., Nagemann K. A., Lovhoiden G. and  
 Waddington J. C. 1970, Nucl. Phys. A144, 513.
- Hodgson, P. E., 1963, The Optical Model of Elastic Scattering  
 (Oxford University Press)
- Jaskoxa M., Tjom P. O. and Elbek B. 1969, Nucl. Phys. A133, 65.
- Kanestrom, I., Tjom, P. O. and Bang, J., 1971, Nucl. Phys.  
 A164, 664.
- Kean, D. C. and Ollerhead, R. W. 1972, Can. J. Phys. 50, 1539.
- Kerman, A. K. 1956, Mat. Fys. Modd. Dan. Vid. Selsk 30,  
 No. 15.
- Kroger L. A. and Reich C. W. 1973, Nucl. Data Sheets B10, 492.
- Kron, J., Fournier, R. Hodgson, R. J. W., Hird, B.,

- Ollerhead, R. W., and Ingebretsen, F. 1971, Nucl. Phys. A172, 99.
- Lobner K. E. G., Vetter M. and Honig V. 1970, Nucl. Data Tables, A7, 495.
- Lovhoiden G., Waddington J. C., Ellegaard C. and Tjom P. O., 1971, Nucl. Phys. A160, 305.
- Lurio, A. 1962, Phys. Rev. 126, 1768.
- Nathan O. and Nilsson S. G., in Alpha, Beta, and Gamma-Ray Spectroscopy, edited by Seigbahn K. (North-Holland, Amsterdam, 1965) Vol 1, P601.
- Newton, T. D. 1960, Can. J. Phys. 38, 700.
- Nilsson, S. G. 1955, Mat. Fys. Modd. Dan. Veldensk. Selsk 29, No. 16.
- Ogle W., Wahlborn S., Piepenbring R., and Fredriksson S. 1971, Rev. Mod. phys. 43, 424.
- Zebel, H., Schweiner, G. W., Schatz, G., Specht, J., Lohken, R., Hauser, G., Habs, D. and Klewe-Nebius H., 1972, Nucl. Phys. A182, 145.
- Rost, E., 1967, Phys. Rev. 154, 994.
- Bowe, D. J., 1970, Nuclear Collective Motion. Methuen and

Co. LTD. London.

Scharff-Goldhaber G. 1953, Phys. Rev. 90, 587.

Scharff-Goldhaber G. and Wenesez J. 1955, Phys. Ev. 98, 212.

Satchler G. R. 1958, Ann. Phys. (N. Y.) 3, 275.

Tjom P. O. and Elbek B. 1967, Mat. Fys. Medd. Dan. Vid.

Selsk 36 No. 8.

Tuli J. K. 1973a, Nucl. Data Sheets B9, 273.

Tuli J. K. 1973b, Nucl. Data Sheets B9, 435.

Turner, R. J. and Trainor, L. E. H. 1968, Can. J. Phys.

46, 2749.

Vergnes M. N. and Sheline R. K. 1963, Phys. Rev. 132, 1736.

Yagi K., Saji Y., Ishizaki Y. and Ishimatsu T., 1969,

Nucl. Phys. A138, 133.

VII

APPENDIX

(A) The Matrix Elements and Quasi-Particle Transformations.

The state of the odd particle nucleus described as one quasi-particle is

$$\begin{aligned}
 |\alpha_{\mu}^{+}\rangle &= \alpha_{\mu}^{+} \prod_{\nu > 0} (U_{\nu}(\mu) + V_{\nu}(\mu) a_{\nu}^{+} a_{-\nu}^{+}) |0\rangle \\
 &= \alpha_{\mu}^{+} \prod_{\alpha \nu \neq \mu} (U_{\nu}(\mu) + V_{\nu}(\mu) a_{\nu}^{+} a_{-\nu}^{+}) |0\rangle \\
 &= \alpha_{\mu}^{+} \psi_{\mu} \text{----- (A-1)}
 \end{aligned}$$

The matrix of H is

$$\begin{aligned}
 \langle \alpha_{\mu}^{+} | H | \alpha_{\mu}^{+} \rangle &= \sum_{\beta \delta} \langle \alpha_{\mu} | \beta \rangle \langle \beta | H | \delta \rangle \langle \delta | \alpha_{\mu}^{+} \rangle \\
 &= \sum_{\beta \delta} \langle \beta | H | \delta \rangle \langle \alpha_{\mu} | a_{\beta}^{+} a_{\delta} \alpha_{\mu}^{+} \rangle
 \end{aligned}$$

where

$$|\beta\rangle = \chi_{\beta} = a_{\beta}^{+} \psi_{\mu}$$

But

$$\sum_{\beta \delta} \langle | \alpha_{\mu} a_{\beta}^{\dagger} a_{\delta} \alpha_{\mu}^{\dagger} | \rangle = \langle | \alpha_{\mu} a_{\beta=\mu}^{\dagger} a_{\delta=\mu} \alpha_{\mu}^{\dagger} - \alpha_{\mu} a_{\delta=\mu} a_{\beta=\mu} \alpha_{\mu}^{\dagger} | \rangle$$

$$= U(\mu) V(\mu) \prod_{\lambda \neq \mu, \mu'} (U(\mu') U(\lambda) + V(\mu') V(\lambda))$$

$$- V(\mu) V(\mu') \prod_{\lambda \neq \mu, \mu'} (U(\mu') U(\lambda) + V(\mu') V(\lambda))$$

$$\langle | \alpha_{\mu} | H | \alpha_{\mu}^{\dagger} | \rangle = (\langle \mu' | H | \mu \rangle U(\mu) U(\mu') - \langle -\mu' | H | -\mu \rangle V(\mu) V(\mu'))$$

$$\prod_{\lambda \neq \mu, \mu'} (U(\lambda) U(\mu) + V(\lambda) V(\mu))$$

$$= \langle \mu' | H | \mu \rangle (U(\mu) U(\mu') - \tau V(\mu) V(\mu')) \prod_{\lambda \neq \mu, \mu'} (U(\lambda) U(\mu) + V(\lambda) V(\mu))$$

$$= \langle \mu' | H | \mu \rangle P(\mu', \mu) \text{----- (A-2)}$$

where

$$P(\mu', \mu) = (U(\mu) U(\mu') - \tau V(\mu) V(\mu')) \prod_{\lambda \neq \mu, \mu'} (U(\lambda) U(\mu) + V(\lambda) V(\mu)) \text{--- (A-3)}$$

and  $\tau = \pm$  according as  $H$  is -ve under time-reversal. For  $H = H_{rpc}$ , the  $\tau$  is positive.

The matrix  $\langle \mu' | H | \mu \rangle = \langle \chi_{\alpha, \mu'} | H | \chi_{\alpha, \mu} \rangle$  is the expected value of single particle states  $|\mu'\rangle$  and  $|\mu\rangle$  outside the core. From eq (10), one can write the single particle with rotation outside core as following

$$|IMK\mu\rangle = \left(\frac{2I+1}{16\pi^2}\right)^{1/2} [D_{M,K}^I(\theta) \chi_{\alpha, \mu} + (-1)^{I-1/2} D_{M,-K}^I(\theta) \chi_{-\alpha, \mu}]$$

----- (A-4)

Comparing the matrix of  $H_{rpc}$  in eq(18) with eq(A-2), one can write

$$\langle \bar{\Phi}_{\mu', \mu} | H_{rpc} | \bar{\Phi}_{\mu, \mu} \rangle = \langle IMK\mu' | H_{rpc} | IMK\mu \rangle P(\mu', \mu) \text{----- (A-5)}$$

Now

$$\begin{aligned} \langle IMK\mu' | H_{rpc} | IMK\mu \rangle &= \frac{2I+1}{16\pi^2} \langle (D_{M,K'}^I(\theta) \chi_{\alpha, \mu'} + (-1)^{I-1/2} D_{M,-K}^I(\theta) \\ &\cdot \chi_{-\alpha, \mu'}) | -\frac{\hbar^2}{2j_0} (I+j^-+I-j^+) | (D_{M,K}^I(\theta) \chi_{\alpha, \mu} + \\ &(-1)^{I-1/2} D_{M,-K}^I(\theta) \chi_{-\alpha, \mu}) | \rangle \end{aligned}$$

$$\begin{aligned}
&= \frac{2I+1}{16\pi^2} \left[ \langle D_{M,K}^{\pm}(\theta) \chi_{\alpha, \mu} | -\frac{\hbar^2}{2g_0} (I+j^-+I-j^+) | D_{M,K}^{\pm}(\theta) \chi_{\alpha, \mu} \rangle + \right. \\
&\quad \left. \langle D_{M,K}^{\pm}(\theta) \chi_{\alpha, \mu} | -\frac{\hbar^2}{2g_0} (I+j^-+I-j^+) | (-1)^{\pm-1/2} D_{M,-K}^{\pm}(\theta) \chi_{-\alpha, \mu} \rangle \right] \\
&\hspace{15em} \text{----- (A-6)}
\end{aligned}$$

Here  $K=\Omega$  is both in positive and negative. BY using

$$\begin{aligned}
\langle D_{M,K}^{\pm}(\theta) | I^{\pm} | D_{M,K}^{\pm}(\theta) \rangle &= -\frac{\hbar^2}{2I\hbar} [(I\mp K)(I\pm K+1)]^{1/2} \delta_{M,\mu} \delta_{K',K\pm 1} \\
\langle \chi_{\alpha, \mu} | j^{\pm} | \chi_{\alpha, \mu} \rangle &= \sum_j C_{j,\alpha\mu} C_{j,\alpha\mu} \langle j\alpha | j^{\pm} | j\alpha \rangle \\
&= \sum_j C_{j,\alpha\mu} C_{j,\alpha\mu} [(j\mp 1)(j\pm\Omega+1)]^{1/2} \delta_{\alpha, \alpha\pm 1}
\end{aligned}$$

eq(A-6) become

$$\begin{aligned}
\langle IMK' | H_{\text{r.p.c}} | IMK \rangle &= -\frac{\hbar^2}{2g_0} \left\{ [(I\mp K)(I\pm K+1)]^{1/2} \delta_{K,\alpha} \right. \\
&\quad \left. + \sum_j C_{j,\alpha\mu} C_{j,-(\alpha\pm 1)\mu} (-1)^{I-j} [(j\mp 1)(j\pm\Omega+1)]^{1/2} \right\} \text{----- (A-7)}
\end{aligned}$$

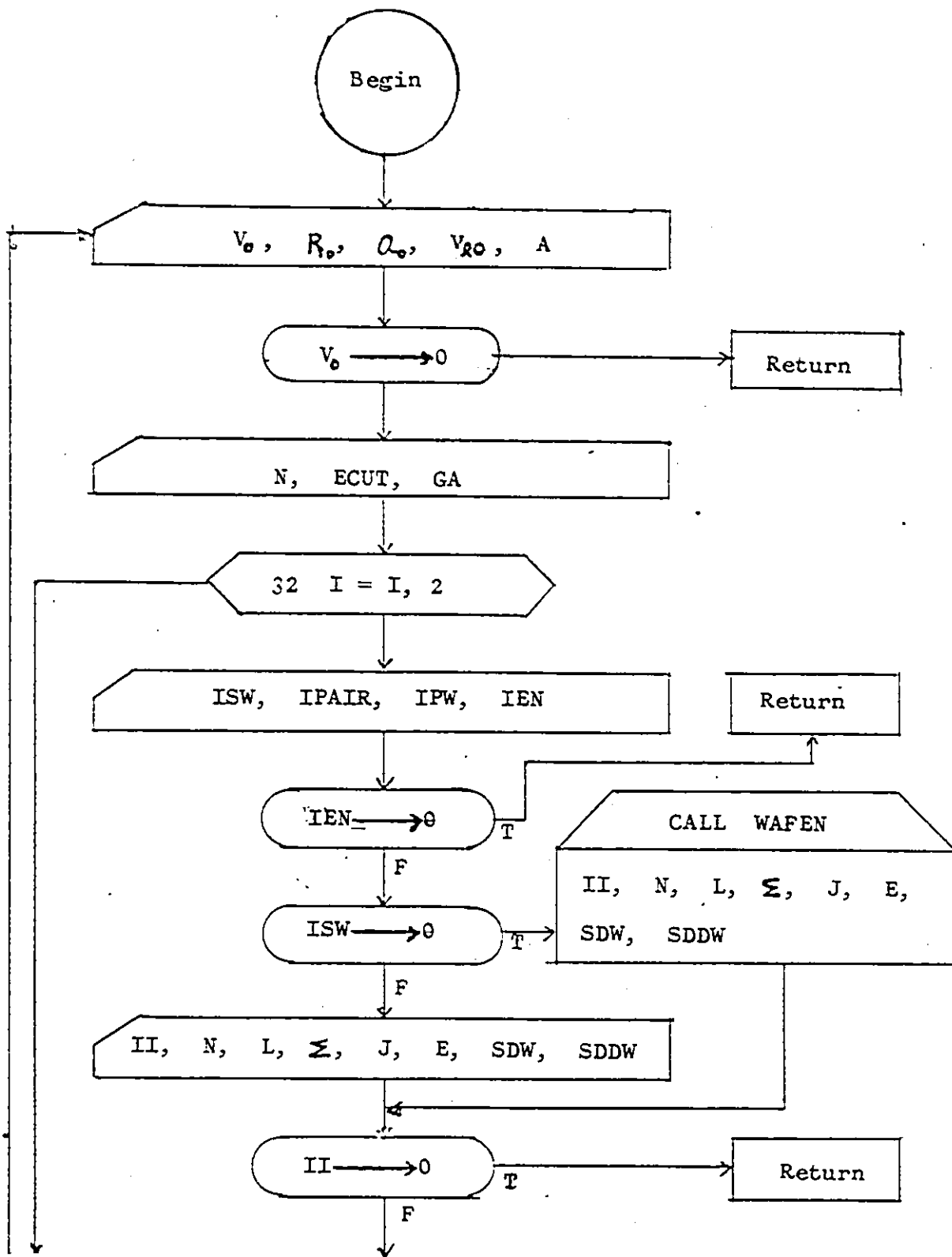
Substitute eq(A-7) into eq(A-5), we get

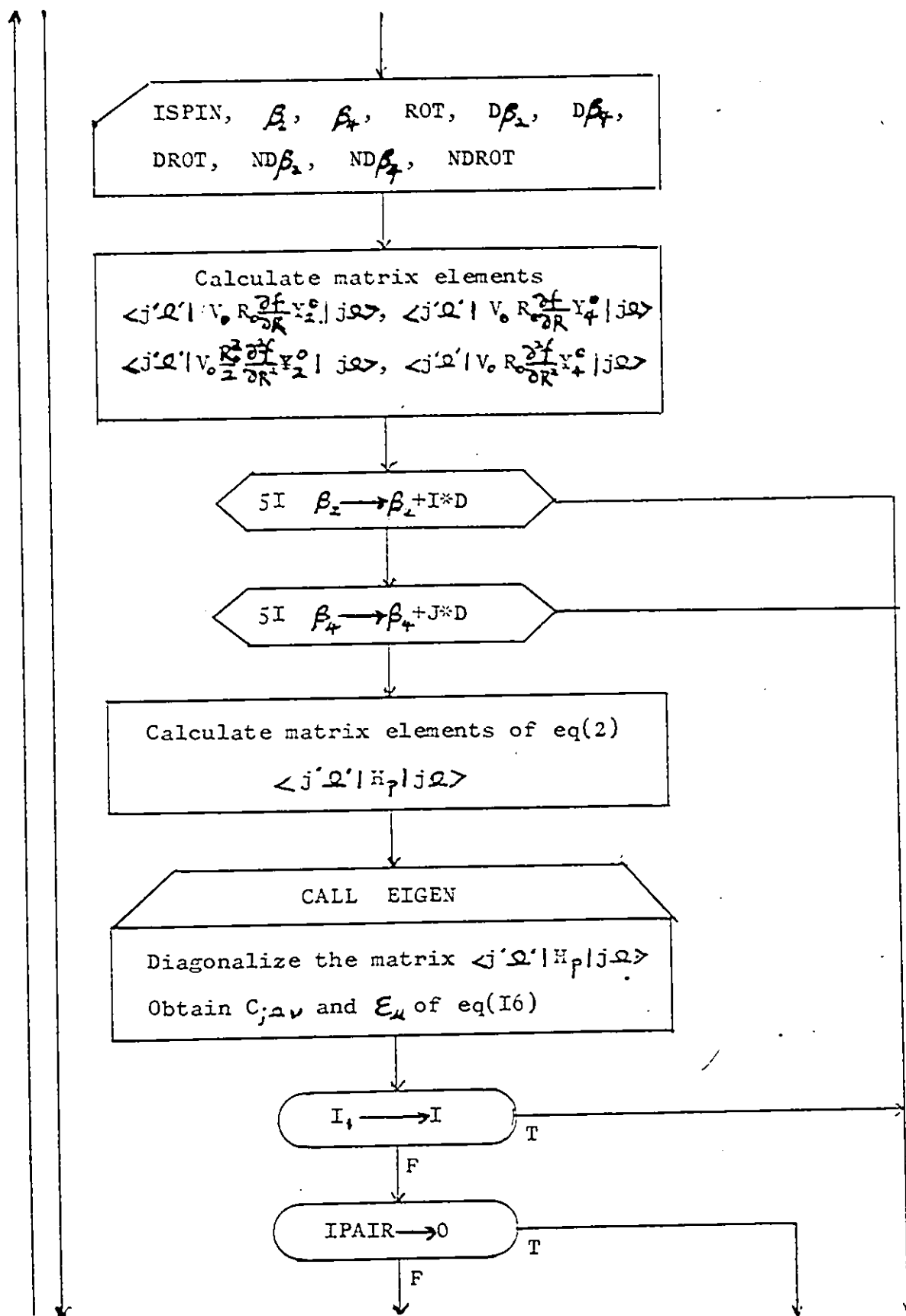
$$\langle \Phi_{K', \mu'} | H_{Tpc} | \Phi_{K, \mu} \rangle = \langle I M K M' | H_{Tpc} | I M - (K \pm 1) \mu \rangle P(K', \mu')$$

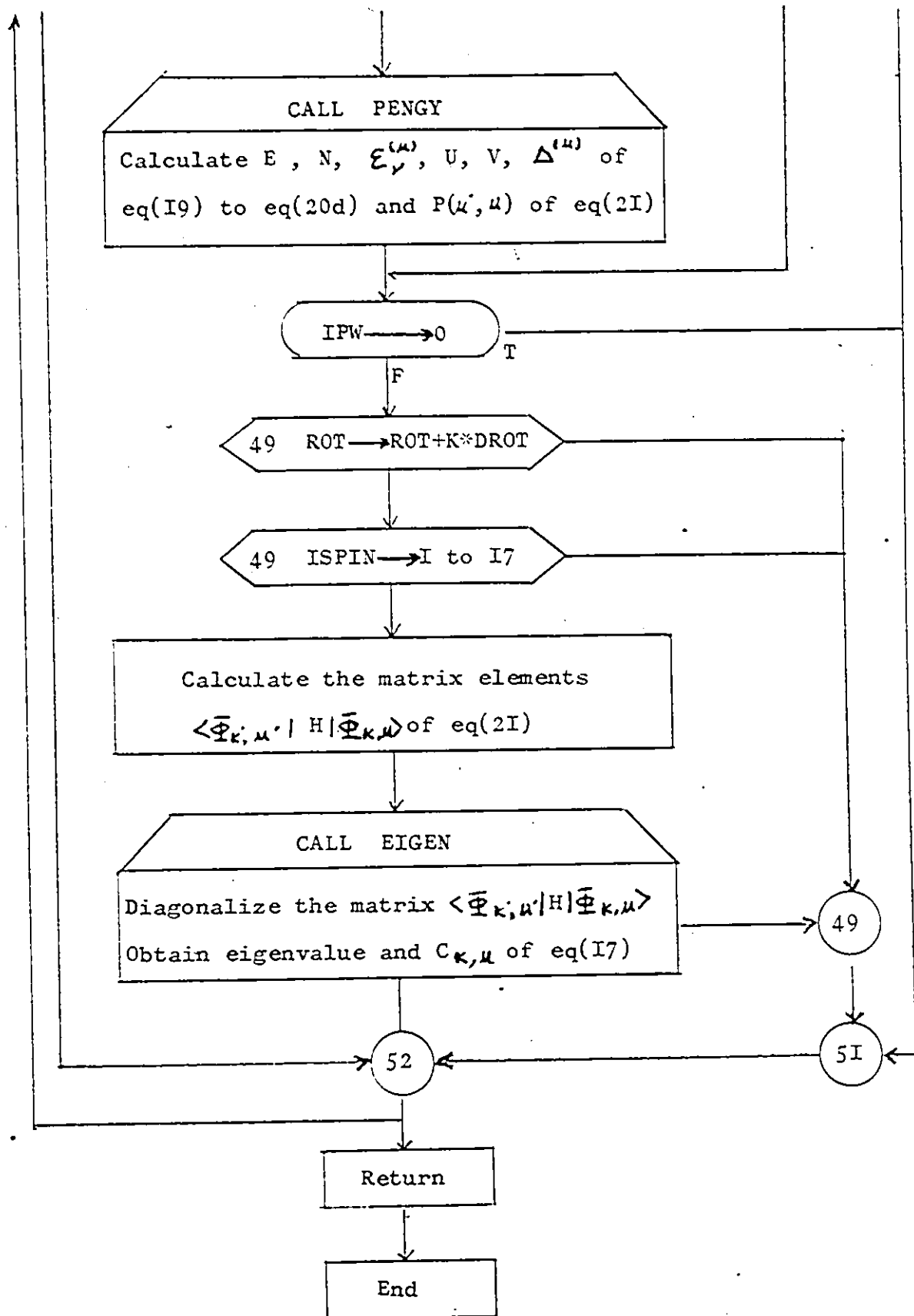
$$= -\frac{\hbar^2}{2g_0} \left\{ [ (I \mp K) (I \pm K + 1) ]^{1/2} \delta_{K, \Omega} \sum_j C_{j, \mu'} C_{j - (\Omega \pm 1) \mu} (-1)^{I-j} \right.$$

$$\left. [ (j \mp 1) (j \pm \Omega + 1) ]^{1/2} P(K', \mu') \right\} \text{----- (A-8)}$$

(B) The Computer Program With Its Flow Chart







THE STARTING OF PROGRAM PAGE = 0  
CALCULATION THE ENERGY LEVELS OF SPHERICAL AND DEFORMED NUCLEI BY  
USING WOODS-SAXON POTENTIAL WITH BCS THEORY.

FIRST SET SUBPROGRAMMES:  
WAFEN TO TEST EIGENV FOR SINGLE PARTICLE EIGENVALUE AND WAVE  
FUNCTION TO CONTROL SUBROUTINE WHICH PERFORMS MATCHING AND EIGEN  
EIGENV TO CONTROL SUBROUTINE WHICH PERFORMS MATCHING AND EIGEN  
-VALUE PREDICTION.  
VR3 TO CALCULATE WOODS-SAXON POTENTIAL V(R) IN EACH POINT.  
INTEG3 TO CONTROL INTEGRATION IN ARDIUS.  
KRRI KUTTA-RUNGE INTEGRATION SUBROUTINE.  
SIMPSON SIMPSON RULE INTEGRATION SUBROUTINE FOR NORMALIZATION  
OF THE WAVE FUNCTION.

SECOND SET SUBPROGRAMMES:  
DIAGONALISE A SQUARE SYMMETRIC MATRIX.  
EIGEN CLEBSCH-GORDAN COEFFICIENT.  
CGC SPHERICAL HARMONIC MATRIX ELEMENT  $\langle L \cdot M \cdot \cdot | Y(L, M) | L \cdot M \cdot \cdot \rangle$ .  
Y MINUS (-1)\*\*J

THIRD SUBPROGRAM:  
TO CALCULATE PROBABILITY (PROBH) OF PAIR NUCLEON IN THE  
PENGY NUCLEUS BY BCS THEORY.

METHOD - MATRIX DIAGONALIZATION.  
FIRST DIAGONALIZATION IS OF DEFORMED HAMILTONIAN WITH SPHERICAL  
WOODS-SAXON EIGENSTATES AS BASIS.  
SECOND DRD DIAGONALIZATION IS OF BAND MIXING AND CORE HAMILTONIAN  
WITH DEFORMED PARTICLE EIGENSTATES AS A BASIS.

REFERENCES:-  
S.G.NILSSON, 1955 MAT.FYS.MEDD.DAN.VID.SELSK. 29 NO 16.  
S.G.NILSSON, 1956 MAT.FYS.MEDD.DAN.VID.SELSK. 30 NO 15.  
A.K.KERMAN, 1956 MAT.FYS.MEDD.DAN.VID.SELSK. 32(1962)286  
K.T.HECHT AND G.R.SATCHLER, NUCLEAR PHYSICS.  
W.SCHOLZ AND F.B.MALIK, PHYS.REV., 176(1968)1355.

NOTATION:-  
LENGTHS IN FM. MASS IN A.M.U. Z IN ELECTRONIC  
ENERGIES IN MEV.  
CHARGE UNITS.  
V0,RO,A0,V0S = WOODS-SAXON PARAMETERS.  
AMU = WEIGHT OF ODD PARTICLE + CORE.  
SNO = NO. OF NUCLEON IN THE SYSTEM FOR (P(U,V) CALCULATION.  
GA = THE PAIRING STRENGTH  
ECUT = LIMIT THE LOWEST ENERGY FOR CALCULATION.  
BETA2 = SPHEROIDAL DEFORMATION  
ROT = UNIT OF ROTATIONAL ENERGY OF THE CORE.  
ROTI(I) = ROTATIONAL ENERGY FOR THIS VALUE OF I ONLY.  
ROTO(OMEGA) = ROTATIONAL ENERGY FOR THIS OMEGA ONLY.  
SPIN = MAXIMUM VALUE OF TOTAL SPIN I OF SYSTEM.  
ALL EIGENSTATES WITH SPINS UP TO INPUT VALUE OF SPIN ARE FOUND.  
N = RADIAL QUANTUM NUMBER.  
L = ANGULAR MOMENTUM QUANTUM OF INTRINSIC SPIN ALONG SYMMETRY AXIS.  
IX2 = 2\*SIGMA = 2\*COMPONENT OF INTRINSIC SPIN.  
JX2 = 2\*J, WHERE J = L + INTRINSIC SPIN.

1  
2  
3  
4  
5  
6  
7  
8  
9  
10  
11  
12  
13  
14  
15  
16  
17  
18  
19  
20  
21  
22  
23  
24  
25  
26  
27  
28  
29  
30  
31  
32  
33  
34  
35  
36  
37  
38  
39  
40  
41  
42  
43  
44  
45  
46  
47  
48  
49  
50  
51  
52  
53  
54  
55



111  
 112  
 113  
 114  
 115  
 116  
 117  
 118  
 119  
 120  
 121  
 122  
 123  
 124  
 125  
 126  
 127  
 128  
 129  
 130  
 131  
 132  
 133  
 134  
 135  
 136  
 137  
 138  
 139  
 140  
 141  
 142  
 143  
 144  
 145  
 146  
 147  
 148  
 149  
 150  
 151  
 152  
 153  
 154  
 155  
 156  
 157  
 158  
 159  
 160  
 161  
 162  
 163  
 164  
 165

```

C 1 IPW IS 0 FOR CALCULATION BAND HEAD WITHOUT BAND MIXING
    IF (V0.EQ.0.0) RETURN
    READ (IR,67) V0,R0,A0,V0S,AMU
    IF (V0.EQ.0.0) RETURN
    READ (IR,65) SNO,ECUT,GA
    WRITE (IW,68) V0,R0,A0,V0S,AMU
    WRITE (IW,66) SNO,ECUT,GA
    -----
C 2 DO 52 I1=1,2
    READ (IR,63) ISW,IPAIR,IPW,IEN
    IF (IEN.EQ.0.0) RETURN
    WRITE (IW,64) ISW,IPAIR,IPW,IEN
    IF (ISW) 2,2,3
    CALL WAFEN (I1,N,L,LA,JX2,E,SDW,SDDW)
    GO TO 5
C 3 READ (IR,57) I1
    READ (IR,58) (N(I),L(I),LA(I),JX2(I),I=1,I1)
    READ (IR,59) (F(I),I=1,I1)
    READ (IR,59) ((SDW(I,J),J=1,I),I=1,I1)
    READ (IR,59) ((SDDW(I,J),J=1,I),I=1,I1)
    WRITE (IW,54) I1
    WRITE (IW,61)
    DO 4 I=1,I1
    WRITE (IW,60) N(I),L(I),LA(I),JX2(I),E(I)
    CONTINUE
C 4 LABELS ARE I=STATE, J=COMPONENT OF STATE.
C 5 WRITE (IW,55)
    DO 6 I=1,I1
    WRITE (IW,62) (SDW(I,J),J=1,I)
    CONTINUE
C 6 WRITE (IW,56)
    DO 7 I=1,I1
    WRITE (IW,62) (SDDW(I,J),J=1,I)
    CONTINUE
C 7 DO 8 I=1,I1
    DO 8 J=1,I1
    SDW(J,I)=SDW(I,J)
    SDDW(J,I)=SDDW(I,J)
    DO 9 I=1,I1
    IF (I.GT.50) GO TO 53
    K5(I)=JX2(I)
    CONTINUE
    KTN=K5(I1)
C 8 II= SIZE OF WOODS-SAXON BASIS FOR DEFORMED STATE DIAGONALIZATION.
C 9 IF (II.EQ.0) RETURN
C 10 LIST EIGENSTATES AND EXPANSION COEFFICIENS. 12 ON ONE LINE.
C 11 IF (2*(N(I1)/2).EQ.N(I1)) GO TO 10
    WRITE (IW,70)
    GO TO 11
  
```



```

10 WRITE (IW,71)
11 DO 12 KKK=1,II,12
   KKKK=II
   IF (KKKK.GT.KKK+11) KKKK=KKK+11
   WRITE (IW,72) (E(I),I=KKK,KKKK)
   WRITE (IW,86) (I,I=KKK,KKKK)
   WRITE (IW,73) (K5(I),I=KKK,KKKK)
12 CONTINUE
   READ (IR,69) SPIN,BETA2,BETA4,ROT,DBETA2,DBETA4,DROT,NBETA2,NBETA4
   1,NROT
   IF (SPIN.EQ.0.0) GO TO 52
   WRITE (IW,74) SPIN,BETA2,BETA4,ROT,DBETA2,DBETA4,DROT,NBETA2,NBETA
   14,NROT
C   NBETA2=NBETA2+1
   NBETA4=NBETA4+1
   NROT=NROT+1
   IF (ABS(SPIN).GT.13.5) SPIN=13.5
   ISX2=ABS(2.*SPIN)
   ISPIN=(ISX2+1)/2
   DO 13 I=1,ISPIN
     ROT(I)=ROT
     ROTO(I)=ROT
   CONTINUE
13   IF (ROT.GT.0.0) GO TO 14
     READ (IR,69) (ROTI(I),I=1,ISPIN)
     WRITE (IW,75) (ROTI(I),I=1,ISPIN)
     READ (IR,69) (ROTO(I),I=1,ISPIN)
     WRITE (IW,76) (ROTO(I),I=1,ISPIN)
     KKK=0
14   KKKK=0
     CYCLE OMEGA IN SERIES (2*INTEGER + 1/2) FROM -SPIN TO +SPIN.
C   IOM=1
     DO 21 IOM=1,ISPIN
       IOM=-IOM-2*MINUS(IOM)
       KKK=0
       DO 15 IJ=1,II
         DO 15 JJ=1,II
           CGCG1(IJ,JJ)=0.0
           CGCG2(IJ,JJ)=0.0
           YSP11(IJ,JJ)=0.0
           YSP12(IJ,JJ)=0.0
           YSP21(IJ,JJ)=0.0
           YSP22(IJ,JJ)=0.0
           SKKW(IJ,JJ)=0.0
           SKW(IJ,JJ)=0.0
15         DO 17 I=1,II
           IF (IABS(IOM).GT.JX2(I)) GO TO 17
           KKK=KKK+1
           NKK(KKK)=N(I)
           LKK(KKK)=L(I)
           LAK(KKK)=LA(I)
           JK2(KKK)=JX2(I)
           KN(IOM,KKK)=I
           KJ=0

```

166  
167  
168  
169  
170  
171  
172  
173  
174  
175  
176  
177  
178  
179  
180  
181  
182  
183  
184  
185  
186  
187  
188  
189  
190  
191  
192  
193  
194  
195  
196  
197  
198  
199  
200  
201  
202  
203  
204  
205  
206  
207  
208  
209  
210  
211  
212  
213  
214  
215  
216  
217  
218  
219  
220

221  
222  
223  
224  
225  
226  
227  
228  
229  
230  
231  
232  
233  
234  
235  
236  
237  
238  
239  
240  
241  
242  
243  
244  
245  
246  
247  
248  
249  
250  
251  
252  
253  
254  
255  
256  
257  
258  
259  
260  
261  
262  
263  
264  
265  
266  
267  
268  
269  
270  
271  
272  
273  
274  
275

```

DO 16 J=1,I
IF (IABS(IOM).GT.JX2(J)) GO TO 16
KJ=KJ+1
SKW(KKK,KJ)=SDW(I,J)
SKKW(KKK,KJ)=SDDW(I,J)
CONTINUE
A1(KKK)=CGC(2*LKK(KKK),2*I IOM,1,-1,JK2(KKK))
A2(KKK)=CGC(2*LKK(KKK),2*(I IOM-1),1,1,JK2(KKK))
CONTINUE

```

16

```

DO 17 I=1,KKK
DO 18 J=1,I
CGCG1(I,J)=A1(I)*A1(J)
CGCG2(I,J)=A2(I)*A2(J)
CGCG1(J,I)=CGCG1(I,J)
CGCG2(J,I)=CGCG2(I,J)
YSP21(I,J)=Y(LKK(I),I IOM,4,0,LKK(J),I IOM)
YSP12(I,J)=Y(LKK(I),I IOM-1,2,0,LKK(J),I IOM-1)
YSP11(I,J)=Y(LKK(I),I IOM,2,0,LKK(J),I IOM)
YSP22(I,J)=Y(LKK(I),I IOM-1,4,0,LKK(J),I IOM-1)
YSP11(J,I)=YSP11(I,J)
YSP12(J,I)=YSP12(I,J)
YSP21(J,I)=YSP21(I,J)
YSP22(J,I)=YSP22(I,J)
CONTINUE

```

18

```

KKKK=KKKK+KKK
IF (KKKK.GT.50) GO TO 53
K1(I IOM)=KKK
IF (KKK.EQ.0) GO TO 21

```

C  
C  
C

CALCULATE DEFORMATION INDEPENDENT PARTS OF THE DEFORMED MATRIX.

```

DO 20 I=1,KKK
DO 20 J=1,I
KK=KK+1
B(KK)=SKW(I,J)*(CGCG1(I,J)*YSP11(I,J)+CGCG2(I,J)*YSP12(I,J))
D(KK)=SKW(I,J)*(CGCG1(I,J)*YSP21(I,J)+CGCG2(I,J)*YSP22(I,J))
YY1=0.0
YY12=0.0
YY21=0.0
YY22=0.0
DO 19 KL=1,KKK
YY1=YY1+YSP11(I,KL)*YSP11(KL,J)*CGCG1(KL,KL)
YY12=YY12+YSP12(I,KL)*YSP12(KL,J)*CGCG2(KL,KL)
YY21=YY21+YSP21(I,KL)*YSP21(KL,J)*CGCG1(KL,KL)
YY22=YY22+YSP22(I,KL)*YSP22(KL,J)*CGCG2(KL,KL)
CONTINUE
B2(KK)=SKKW(I,J)*(CGCG1(I,J)*YY1+CGCG2(I,J)*YY12)
D2(KK)=SKKW(I,J)*(CGCG1(I,J)*YY21+CGCG2(I,J)*YY22)
IF (I.NE.J) GO TO 20
B2(KK)=B2(KK)-(CGCG1(I,I)+CGCG2(I,I))*SKW(I,I)/12.5664
D2(KK)=D2(KK)-(CGCG1(I,I)+CGCG2(I,I))*SKW(I,I)/12.5664
CONTINUE
CONTINUE
KKK1=K1(I)

```

19

20  
21

C



```

331
332
333
334
335
336
337
338
339
340
341
342
343
344
345
346
347
348
349
350
351
352
353
354
355
356
357
358
359
360
361
362
363
364
365
366
367
368
369
370
371
372
373
374
375
376
377
378
379
380
381
382
383
384
385

WRITE (IW,90)
DO 28 NU=1,KKK1
WRITE (IW,89) NU,K5(KN(1,NU)),(S(MU,NU),MU=JJJ,KKKK)
WRITE (IW,85)
-----
C
C
IF (I1.EQ.1) GO TO 51
DO 29 NU=1,KKK1
WRITE (2,91) (S(MU,NU),MU=1,K)
CONTINUE
C
IF (IPAIR.EQ.0) GO TO 30
CALL PENGY (ED,KI,SNO,AMU,PROBH,GA)
IF (IPW.EQ.0) GO TO 51
BAND MIXING
DO 50 MM=1,NROT
DO 31 I1OM=1,IISPIN
RROTI(I1OM)=ROTI(I1OM)+(MM-1)*DROT
RROTO(I1OM)=ROTO(I1OM)+(MM-1)*DROT
MISS.OUT BAND MIXING SECTION IF THERE IS NO ROTATIONAL ENERGY.
IF (RROTO(I1OM).LE.0.0.OR.RROTI(I1OM).LE.0.0) GO TO 50
CONTINUE
CYCLE SPIN VALUES FORM 1/2 UP TO SPIN.
DO 49 IISPIN=1,ISX2,2
C
C
SET UP BAND MIXED MATRIX IN |N,J> BASIS.
KKK=0
KK=0
K=KI(2)
DO 41 MU1=1,K
IF (K3(MU1).GT.IISPIN) GO TO 42
IOM1=K2(MU1)
X1=RROTO((K3(MU1)+1)/2)
KKK=KKK+1
DO 40 MU2=1,MU1
IF (IPAIR.EQ.0) GO TO 32
PH=PROBH(MU1,MU2)
GO TO 33
PH=1.0
IF (K3(MU2).GT.IISPIN) GO TO 41
IOM2=K2(MU2)
KK=KK+1
AM(KK)=0.0
X2=RROTO((K3(MU2)+1)/2)
IF ((IOM1+IOM2)/3.NE.0) GO TO 37
JJOM=K3(MU1)
IF (K3(MU1).GT.K3(MU2)) JJOM=K3(MU2)
DO 36 J=1,I1
IF (JJOM.GT.JX2(J)) GO TO 36
IF (IOM1+IOM2.EQ.-2) X=(JX2(J)-ICM1)*(JX2(J)+IOM1+2)*(IISPIN-IOM1)
1*(IISPIN+IOM1+2)
1*(IOM1+IOM2.EQ.+2) X=(JX2(J)+IOM1)*(JX2(J)-IOM1+2)*(IISPIN+IOM1)
1*(IISPIN-IOM1+2)
IF (X.LT.1.0E-30) X=1.0E-30
X=-SQRT(X*X1*X2)
C
C
32
33

```

```

PAGE = 7
IF (MU1.EQ.MU2.AND.IOM1.EQ.IOM2.AND.JJOM.EQ.1.0) GO TO 34
X=X*MINUS((IISPIN-1)/2)*PH
IF (IOM1.EQ.IOM2.AND.JJOM.EQ.1) X=X*MINUS((JX2(J)-1)/2)
GO TO 35
X=X*MINUS((IISPIN-JX2(J))/2)
AM(KK)=AM(KK)+X*S(MU1,J)*S(MU2,J)
CONTINUE
IF (IOM1.NE.IOM2.OR.MU1.EQ.MU2) GO TO 39
DO 38 J=1,11
AM(KK)=AM(KK)+S(MU1,J)*S(MU2,J)*JX2(J)*(JX2(J)+2)*X1*PH
CONTINUE
AM(KK)=AM(KK)/4.0
CONTINUE
AM(KK)=AM(KK)+RROTI((IISPIN+1)/2)*IISPIN*(IISPIN+2)/4.0-X1*IOM1*IO
IM1/2.0+ED(2,MU1)
CONTINUE
WRITE (IW,79) BBETA2,BBETA4,IISPIN
WRITE (IW,80) RROTI((IISPIN+1)/2)
WRITE (IW,81) (I,I=1,IISPIN,2)
WRITE (IW,82) (RROTO((I+1)/2),I=1,IISPIN,2)
CONTINUE
WRITE OUT MATRIX ELEMENTS. UP TO 12 ON ONE LINE.
WRITE (IW,83)
DO 44 JJ=1,KKK,12
DO 43 JJ=JJ,KKK,12
KKKK=KKK
IF (KKKK.GT.JJ+11) KKKK=JJ+11
DO 43 I=JJ,KKK
JJJJ=I
IF (JJJJ.GT.JJ+11) JJJJ=JJ+11
WRITE (IW,84) K3(I),(AM(I*(I-1)/2+J),J=JJJ,JJJJ)
WRITE (IW,85)
CONTINUE
CALL EIGEN (AM,R,KKK,0)
LIST EIGENSTATES AND EXPANSION COEFFICIENS, 12 ON ONE LINE.
DO 47 JJ=1,KKK,12
KKKK=KKK
IF (KKKK.GT.JJ+11) KKKK=JJ+11
WRITE (IW,72) (AM(I*(I+1)/2),I=JJ,KKKK)
DO 45 I=JJ,KKK
L(I)=KKK-I+1
CONTINUE
WRITE (IW,86) (L(I),I=JJ,KKKK)
WRITE (IW,87)
DO 46 J=1,KKK
WRITE (IW,89) K4(J),K3(J),(R(KKK*(I-1)+J),I=JJ,KKKK)
CONTINUE
KKK7=KKK-11
IF (KKK7.LT.1) KKK7=1
DO 48 I=KKK7,KKK
WRITE (2,91) (R(KKK*(I-1)+J),J=1,KKK)

```

386  
387  
388  
389  
390  
391  
392  
393  
394  
395  
396  
397  
398  
399  
400  
401  
402  
403  
404  
405  
406  
407  
408  
409  
410  
411  
412  
413  
414  
415  
416  
417  
418  
419  
420  
421  
422  
423  
424  
425  
426  
427  
428  
429  
430  
431  
432  
433  
434  
435  
436  
437  
438  
439  
440

34  
35  
36  
37  
  
38  
39  
40  
  
41  
C  
42  
  
C  
C  
  
43  
44  
C  
C  
C  
  
45  
  
46  
47



```

89          PAGE = 9
90          FORMAT ('.214. /2. T16.12F8.3)
          EXPANSION IN SPHERICAL WOODS-SAXON BASIS. / STA
          WRITE (#)
          FORMAT (8(F10.5))
          END

```

```

C          SUBROUTINE WAFEN (IS,N,LL,LA,JX2,ES,SDW,SDDW)
C          MAIN PROGRAM TO TEST EIGENV SINGLE PARTICLE EIGENVALUE AND WAVE
          FUNCTION RPRINT(5), WAVE(5), ENRGY(100), FL(100), N(16), LL(16), LA(16)
          DIMENSION RPRINT(5), WAVE(5), ENRGY(100), FL(100), N(16), LL(16), LA(16)
          1,SDW(16,16), ES(50), JX2(16), SDDW(16,16)
          COMMON/MEIIG/WAVEFN(301),RADIUS,A,VC,ALPHA,AMASS,RMAX,EPS,MODE,
          1NOMAX,NINTVL,L,ELL,K,JDBLD,JPRINT,MPOINT,EN,FLOUT,HI,R,RR,
          2H,VPLUS(599),V,NMAX,F,RMATCH,I,XPLUS,XPLUSP,FRR,INDUT,KSTEP,REFL,
          3XINTGD(301),YINTG,XINT1,XINT2,X,VD(300),WAFN(30,300),II,SEM(16,16)
          4,VDD(300),SDM(16,16)
          II=0
          WRITE (6,1) SEARCH FOR THE EIGENVALUE AND EIGENFUNCTION OF THE WO
          FORMAT (4X, SEARCH FOR THE EIGENVALUE AND EIGENFUNCTION OF THE WO
          100-SAXON POTENTIAL ')
          WRITE (6,2) A VC ALPHA(V50) AMASS
          FORMAT (//, RZERO EPS )
          1RMAX
          READ (1,3) RZERO,A,VC,ALPHA,AMASS,RMAX,EPS
          FORMAT (7F10.5)
          3 RADIUS=RZERO*(AMASS*0.33333)
          IF (AMASS.EQ.0) RETURN
          WRITE (6,3) RZERO,A,VC,ALPHA,AMASS,RMAX,EPS
          READ (1,4) M
          FORMAT (I3)
          WRITE (6,5) M
          FORMAT (//,2X, NO.OF DATA SET FOR WAFEN : M = ,I3)
          5 DO 22 IK=1,M
          ETS=0.0
          WRITE (6,6)
          FORMAT (/, JPRINT')
          6 1JDBLD KZ,MODE,NOMAX,NINTVL,L,JDBLD,JPRINT
          READ (1,7) KZ,MODE,NOMAX,NINTVL,L,JDBLD,JPRINT
          WRITE (6,7) KZ,MODE,NOMAX,NINTVL,L,JDBLD,JPRINT
          FORMAT (7I10)
          7 NPOINT=NINTVL+1
          GO TO (8,11,8), MODE
          WRITE (6,9)
          FORMAT (15H TRIAL ENERGIES)
          8 9 READ (1,10) (ENRGY(KY),KY=1,KZ)
          WRITE (6,10) (ENRGY(KY),KY=1,KZ)
          FORMAT (8F10.5)
          10 KN=0
          GO TO 13
          11 WRITE (6,12)
          12 FORMAT (:ENERGY FLOUT,RMAX')
          READ (1,3) (ENRGY(KY),FL(KY),KY=1,KZ)
          WRITE (6,3) (ENRGY(KY),FL(KY),KY=1,KZ)

```

496  
497  
498  
499  
500-

1  
2  
3  
4  
5  
6  
7  
8  
9  
10  
11  
12  
13  
14  
15  
16  
17  
18  
19  
20  
21  
22  
23  
24  
25  
26  
27  
28  
29  
30  
31  
32  
33  
34  
35  
36  
37  
38  
39  
40  
41  
42  
43  
44  
45  
46  
47

```

13 DO 21 KY=1,KZ
14 IF (MODE-2) 15,14,15
15 FLOUT=FL(KY)
EN=ENRGY(KY)
CALL EIGENV
DEN=ABS(ETS-EN)
IF (DEN.LT.0.1) GO TO 21
IF (ABS(EN)-1.E-10) 21,16,16
16 WRITE (6,17) EN
17 FORMAT (,
ENERGY=,F10.5,'MEV')
RE=HI
II=II+1
ES(II)=EN
ETS=ES(II)
DO 18 I=1,NPOINT
WAFN(II,1)=WAVEFN(I)
R=R+HI
CONTINUE
LL(II)=L
L2=2*L
N(II)=L+2*KN
JX2(II)=JDBLD
LA(II)=1
IF (JDBLD.GT.L2) LA(II)=0
KN=KN+1
GO TO (21,19), JPRINT
19 WRITE (6,20) YINTG
20 FORMAT (7H YINTG=,F12.5)
21 CONTINUE
22 CONTINUE
23 WRITE (6,23) N(I) L(I) LLA(I) JX2(I) ES(I)
FORMAT (,
)
DO 24 I=1,II
WRITE (6,25) N(I),LL(I),LA(I),JX2(I),ES(I)
CONTINUE
24 CONTINUE
25 FORMAT (2X,4(5X,15),5X,F13.6)
IS=II
CALL SUMMA
DO 26 I=1,II
DO 26 J=1,I
SDW(I,J)=SEM(I,J)
SDDW(I,J)=SDM(I,J)
26 WRITE OUT MATRIX FLEMENTS. UP TO 12 ON ONE LINE.
C WRITE (6,27)
C FORMAT (/,
MATRIX OF SDW)
27 DO 28 I=1,II
WRITE (6,31) (SDW(I,J),J=1,I)
CONTINUE
28 WRITE (6,29)
C WRITE (/,
MATRIX OF SDDW)
29 DO 30 I=1,II
WRITE (6,31) (SDDW(I,J),J=1,I)
CONTINUE
30

```

48  
49  
50  
51  
52  
53  
54  
55  
56  
57  
58  
59  
60  
61  
62  
63  
64  
65  
66  
67  
68  
69  
70  
71  
72  
73  
74  
75  
76  
77  
78  
79  
80  
81  
82  
83  
84  
85  
86  
87  
88  
89  
90  
91  
92  
93  
94  
95  
96  
97  
98  
99  
100  
101  
102



103  
104  
106  
107  
108  
109  
110  
111  
112  
113  
114  
115-

PAGE = 11

```

31 FORMAT ('',T10,12F8.3)
32 WRITE (6,32)
33 WRITE (2,33) II
34 WRITE (2,34) (N(J),LL(J),LA(J),JX2(J),J=1,II)
35 WRITE (2,35) (ES(I),I=1,II)
    WRITE (2,35) ((SDW(I,J),J=1,I),I=1,II)
    WRITE (2,35) ((SDOW(I,J),J=1,I),I=1,II)
    FORMAT (6F13.6)
RETURN
END

```

1  
2  
3  
4  
5  
6  
7  
8  
9  
10  
11  
12  
13  
14  
15  
16  
17  
18  
19  
20  
21  
22  
23  
24  
25  
26  
27  
28  
29  
30  
31  
32  
33  
34  
35  
36  
37  
38  
39

```

SUBROUTINE EIGENV
DIMENSION Y(11)
COMMON/MEIG/WAVEFN(301),RADIUS,A,VC,ALPHA,AMASS,RMAX,EPS,MODE,
1NOMAX,NINTVL,L,ELL,K,JDBLD,JPRINT,MPRINT,NPOINT,EN,FLOUT,HI,R,RR,
2H,VPLUS(599),V,NMAX,F,RMATCH,I,XPLUS,XPLUSP,FRR,INOUT,KSTEP,REFL,
3XINTGD(301),YINTG,XINT1,XINT2,X,VD(300),WAFN(16,16)
4,VDD(300),SDM(16,16)
K=L+1
HI=RMAX/FLOAT(NINTVL)
NPOINT=NINTVL+1
RMATCH=(5.*FLOAT(NINTVL/15+1))*HI
IF (ALPHA) 1,2,2
ALPHA=ALPHA*181.1/VC
CALL VR3
KSTEP=1
H=HI
GO TO (3,3,43), MODE
IF (EN) 5,5,4
RMATCH=RMAX
MPRINT=2
IF (NOMAX-1) 6,7,6
KSTEP=5
H=5.*HI
CALL INTEG3
NO=1
ENERGY=EN
IF (EN) 9,9,10
FLOUT=R*XPLUSP/XPLUS
OIF=REFL-FLOUT
GO TO 26
PMOM=SQRT(.04826*F*EN)
GO TO (12,11,12), MODE
DIF=REFL-FLOUT
FLOUT=FLOUT
GO TO (13,26,43), MODE
XX=R*PMOM
KPLUS1=K+1
IF (XX-1.) 14,14,23
NPASS=1

```

31  
32  
33  
34  
35  
  
1  
2  
3  
4  
5  
6  
7  
8  
9  
10  
11  
12  
13  
14

```

40
41
42
43
44
45
46
47
48
49
50
51
52
53
54
55
56
57
58
59
60
61
62
63
64
65
66
67
68
69
70
71
72
73
74
75
76
77
78
79
80
81
82
83
84
85
86
87
88
89
90
91
92
93
94

15 SUM=1.
    TERM=1.
    DO 16 N=1,20
    TERM=-TERM*0.5**XX**2/(FLOAT(N))*FLOAT(2*N-1-2*L)
    SUM=SUM+TERM
    IF (ABS(TERM)-1.E-8) 17,16,16
16 CONTINUE
17 IF (K-1) 18,20,18
18 DO 19 IK=2,K
    AK=IK
    SUM=SUM*(2.*AK-3.)
19 CONTINUE
20 GO TO (21,22), NPASS
21 YL=-SUM/(XX**K)
    K=K+1
    L=L+1
    NPASS=2
    GO TO 15
22 YLPLUS=-SUM/(XX**K)
    K=K-1
    L=L-1
    GO TO 25
23 Y(1)=-COS(XX)/XX
    Y(2)=-COS(XX)/XX**2-SIN(XX)/XX
    DO 24 IK=3,KPLUS
    AK=IK
    Y(IK)=(2.*AK-3.)*Y(IK-1)/XX-Y(IK-2)
    CONTINUE
    YL=Y(K)
24 YLPLUS=Y(KPLUS1)
    FLOMT=FLOAT(L)+1.-XX*YLPLUS/YL
    DIF=REFL-FLOMT
25 IF (NO-NOMAX) 27,31,31
26 IF (NO-2) 28,29,30
27 EN=0.99*EN
28 GO TO 31
    EN=(ENERG1*DIF-ENERGY*DIFM1)/(DIF-DIFM1)
    GO TO 31
29 GO TO 31
    DIFM12=DIFM1-DIFM2
    DIFFM1=DIF-DIFM1
    DIFFM2=DIF-DIFM2
30 IF (ABS(DIFM12).LT.1.0E-30) DIFM12=SIGN(1.0E-30,DIFM12)
    IF (ABS(DIFFM1).LT.1.0E-30) DIFFM1=SIGN(1.0E-30,DIFFM1)
    IF (ABS(DIFFM2).LT.1.0E-30) DIFFM2=SIGN(1.0E-30,DIFFM2)
    EN=((ENERG2*DIFM1-ENERG1*DIFM2)/DIFFM1)
    IFM1)*DIFM2/DIFFM1)-1.)-2) 33,33,32
31 IF (ABS((EN/ENERGY)-1.)) 33,33,32
32 EN=ENERGY+ABS(ENERGY)*SIGN(0.1,(EN-ENERGY))
33 IF (NO-NOMAX) 34,44,44
34 IF (ABS(DIF-DIFM1).EQ.0.0) GO TO 35
    EPP=EPP
    IF (ABS(REFL).GT.1.0E2.OR.ABS(FLOMT).GT.1.0E2) EPP=0.005
    IF (ABS(DIF)-EPP) 35,35,37
    IF (KSTEP-1) 39,36,39
    EN=ENERGY.
35
36

```

```

37 GO TO 43
38 IF (KSTEP-1) 38,40,38
39 IF (ABS(DIF)-.1) 39,40,40
40 KSTEP=1
41 H=HI
42 CALL INTEG3
43 IF (NO-1) 42,42,41
44 DIFM2=DIFM1
45 ENERG2=ENERG1
46 DIFM1=DIF
47 ENERG1=ENERGY
48 NO=NO+1
49 GO TO 8
50 MPRINT=1
51 CALL INTEG3
52 GO TO 46
53 EN=0.
54 DO 45 N=1,NPOINT
55 WAVEFN(N)=0.
56 CONTINUE
57 CONTINUE
58 RETURN
59 END

```

95  
96  
97  
98  
99  
100  
101  
102  
103  
104  
105  
106  
107  
108  
109  
110  
111  
112  
113  
114  
115  
116  
117-

```

1 SUBROUTINE VR3
2 COMMON/MEIMG/WAVEFN(301),RADIUS,A,VC,ALPHA,AMASS,RMAX,EPS,MODE,
3 INOMAX,NINTVL,L,ELL,K,JDBLD,JPRINT,MPRINT,NPOINT,EN,FLOUT,HI,R,RR,
4 1NOMAX,NINTVL,L,ELL,K,JDBLD,JPRINT,MPRINT,NPOINT,EN,FLOUT,HI,R,RR,
5 2H,VPLUS(599),V,NMAX,F,RMATCH,I,XPLUS,XPLUSP,FRR,INOUT,KSTEP,REFL,
6 3XINTGD(301),YINTG,XINT1,XINT2,X,VD(300),WAFN(30,300),II,SEM(16,16)
7 4,VDD(300),SDM(16,16)
8 R=HI
9 H=HI/2.
10 GO TO (3,1), JPRINT
11 WRITE (6,2)
12 FORMAT (25H
13 C=.0110270/A
14 VCA=VC*RADIUS/A
15 VCAA=-VCA*RADIUS/(2.*A)
16 EXPP=EXP(-RADIUS/A)
17 VD(1)=VCA*EXPP/((1.0+EXPP)**2)
18 VDD(1)=VCAA*EXPP*(1.0-EXPP)/((1.0+EXPP)**3)
19 R1=HI
20 DO 4 J=2,NPOINT
21 REXQ=EXP((R1-RADIUS)/A)
22 VD(J)=VCA*REXQ/((1.0+REXQ)**2)
23 VDD(J)=VCAA*REXQ*(1.0-REXQ)/((1.0+REXQ)**3)
24 R1=R1+HI
25 CONTINUE
26 NMAX=2*NINTVL-1
27 DO 11 I=1,NMAX
28 REXP=EXP((R-RADIUS)/A)
29 VCC=VC/(1.0+REXP)
30 VS=ALPHA*VC*C*REXP/((1.0+REXP)**2)*R)

```

1  
2  
3  
4  
5  
6  
7  
8  
9  
10  
11  
12  
13  
14  
15  
16  
17  
18  
19  
20  
21  
22  
23  
24  
25  
26  
27  
28  
29



30  
31  
32  
33  
34  
35  
36  
37  
38  
39  
40  
41-

```

AK=K
IF (JOB LD-2*L) 6,6,5
VPLUS(I)=VCC+VS*(AK-1.0)
GO TO 7
VPLUS(I)=VCC-VS*AK
GO TO (10,8), JPRINT
WRITE (6,9) VPLUS(I),R
FORMAT (E15.7,5X,F7.3)
R=R+H
CONTINUE
RETURN
END

```

5  
6  
7  
8  
9  
10  
11

1  
2  
3  
4  
5  
6  
7  
8  
9  
10  
11  
12  
13  
14  
15  
16  
17  
18  
19  
20  
21  
22  
23  
24  
25  
26  
27  
28  
29  
30  
31  
32  
33  
34  
35  
36  
37  
38  
39  
40

```

SUBROUTINE INTEG3
COMMON/MEMEIG/WAVEFN(301),RADIUS,A,VC,ALPHA,AMASS,RMAX,EPS,MODE,
1NOMAX,NINTVL,L,ELL,K,JDBLD,JPRINT,MPRINT,NPOINT,EN,FLOUT,HI,R,RR,
2H,VPLUS(599),V,NMAX,F,RMATCH,I,XPLUS,XPLUSP,FRR,INOUT,KSTEP,REFL,
3XINTGD(301),YINTG,XINT1,XINT2,X,VD(300),WAFN(30,300),II,SEM(16,16)
4,VDD(300),SDM(16,16)
GO TO (1,3), MPRINT
GO TO (2,2,3), MODE
IF (EN) 19,22,22
WAVEFN(1)=0.0
AK=K
F=AMASS/(AMASS+1.00898)
R=H

```

1  
2  
3

```

RR=R
V=VPLUS(2*KSTEP-1)
XPLUS=R**K
X=XPLUS
ELL=0.
CALL FR
ELL=K-1
XPLUS=XPLUS+FRR**2/(ELL+2.)*(ELL+3.)
WAVEFN(2)=XPLUS
XPLUSP=AK*(R**(K-1))+FRR*R/(ELL+2.)
GO TO (5,5,4), MODE

```

```

NOMAX=2
INOUT=1
DO 11 I=KSTEP,1000,KSTEP
CALL KRRI
R=R+H

```

```

IF (NOMAX-1) 9,6,9
RMATCH=RMAX
IF (R-0.2*RADIUS) 9,7,7
IF (EN-V) 8,8,10

```

```

RMATCH=R
GO TO 12
WAVEFN(I+2)=XPLUS
IF (R-RMATCH+.001) 11,12,12
CONTINUE
REFL=XPLUSP/XPLUS
WMATCH=XPLUS

```

4  
5  
6  
7  
8  
9  
10  
11  
12

```

13 IF (EN) 13,21,21
14 XPLUS=1.
15 WAVEFN(NPOINT)=1.
16 GO TO (14,15,15), MODE
17 XPLUSP=-SQRT(VPLUS(NMAX)-EN)
18 GO TO 16
19 XPLUSP=FLOUT/RMAX
20 H=-H
21 R=RMAX
22 INOUT=-1
23 DO 17 J=1,1000,KSTEP
24 I=NINTVL-J
25 CALL KRR1
26 R=R+H
27 WAVEFN(I+1)=XPLUS
28 IF (R-RMATCH-.001) 18,18,17
29 CONTINUE
30 H=-H
31 GO TO (19,25), MPRINT
32 I=I+1
33 DO 20 J=1,NPOINT
34 WAVEFN(J)=WAVEFN(J)*WMATCH/XPLUS
35 CONTINUE
36 GO TO (22,25), MPRINT
37 YINTG=0.
38 XINT1=0.
39 XINT2=RMAX
40 DO 23 N=1,NPOINT
41 XINTGD(N)=WAVEFN(N)**2
42 CONTINUE
43 CALL SIMPSN
44 DO 24 N=1,NPOINT
45 WAVEFN(N)=WAVEFN(N)/SQRT(YINTG)
46 CONTINUE
47 RETURN
48 END

```

```

1 SUBROUTINE KRR1
2 COMMON/MEIMG/WAVEFN(301),RADIUS,A,VC,ALPHA,AMASS,RMAX,EPS,MODE,
3 NOMAX,NINTVL,L,ELL,K,JDBLD,JPRINT,MPRINT,NPOINT,EN,FLOUT,HI,R,RR,
4 2H,VPLUS(599),V,NMAX,F,RMATCH,I,XPLUS,XPLUSP,FRR,INOUT,KSTEP,REFL,
5 3XINTGD(301),YINTG,XINT1,XINT2,X,VD(300),WAFN(30,300),II,SEM(16,16)
6 4,VDD(300),SDM(16,16)
7 GO TO (3,1), JPRINT
8 WRITE (6,2) H,R,XPLUS,XPLUSP,AI,EN,V,RMATCH
9 FORMAT (3H H=,F8.5,3H R=,F9.5,7H XPLUS=,E12.5,8H XPLUSP=,E12.5,4H
10 1AI=,F9.5,4H EN=,F10.4,3H V=,F9.4,8H RMATCH=,F6.3)
11 RR=R
12 INDEX=2*I-INOUT
13 V=VPLUS(INDEX)
14 X=XPLUS
15 CALL FR
16 AI=FRR*H**2/2.0

```

41  
42  
43  
44  
45  
46  
47  
48  
49  
50  
51  
52  
53  
54  
55  
56  
57  
58  
59  
60  
61  
62  
63  
64  
65  
66  
67  
68  
69  
70  
71  
72  
73  
74  
75  
76-

1  
2  
3  
4  
5  
6  
7  
8  
9  
10  
11  
12  
13  
14  
15  
16

17  
18  
19  
20  
21  
22  
23  
24  
25  
26  
27  
28  
29  
30  
31  
32  
33  
34  
35  
36-

```

RR=R+H/2.0
X=XPLUS+XPLUS*H/2.0+AI/4.0
INDEX=2*I+INOUT*(KSTEP-1)
V=VPLUS(INDEX)
CALL FR
AII=FRR*(H**2)/2.0
RR=R+H
X=XPLUS+XPLUS*H+AII
INDEX=2*I+INOUT*(2*KSTEP-1)
V=VPLUS(INDEX)
CALL FR
AII=FRR*H**2/2.0
XPLUS=XPLUS+H*XPLUS+(AI+2.0*AII)/3.0
XPLUS=XPLUS+(AI+4.0*AII+AII)/(3.0*H)
GO TO (6,A), JPRINT
IF (ABS(RR-RMATCH))-0.01) 5,6,6
WRITE (6,2) H,RR,XPLUS,XPLUS,AI,EN,V,RMATCH
CONTINUE
RETURN
END

```

4  
5  
6

1  
2  
3  
4  
5  
6  
7  
8  
9-

```

SUBROUTINE FR
COMMON/MEIG/WAVEFN(301),RADIUS,A,VC,ALPHA,AMASS,RMAX,EPS,MODE,
INOMAX,NINTVL,L,ELL,K,JDBLD,JPRINT,MPRINT,NPOINT,EN,FLOUT,HI,R,RR,
2H,VPLUS(599),V,NMAX,F,RMATCH,I,XPLUS,XPLUS,FRR,INOUT,KSTEP,REFL,
3XINTGD(301),YINTG,XINT1,XINT2,X,VD(300),WAFN(30,300),II,SEM(16,16)
4,VDD(300),SDM(16,16)
FRR=-.04826*F*(EN-20.721*ELL*(ELL+1.0)/(F*RR**2)-V)*X
RETURN
END

```

1  
2  
3  
4  
5  
6  
7  
8  
9  
10  
11  
12  
13  
14  
15  
16  
17  
18  
19-

```

SUBROUTINE SIMPSN
COMMON/MEIG/WAVEFN(301),RADIUS,A,VC,ALPHA,AMASS,RMAX,EPS,MODE,
INOMAX,NINTVL,L,ELL,K,JDBLD,JPRINT,MPRINT,NPOINT,EN,FLOUT,HI,R,RR,
2H,VPLUS(599),V,NMAX,F,RMATCH,I,XPLUS,XPLUS,FRR,INOUT,KSTEP,REFL,
3XINTGD(301),YINTG,XINT1,XINT2,X,VD(300),WAFN(30,300),II,SEM(16,16)
4,VDD(300),SDM(16,16)
DELINT=(XINT2-XINT1)/FLOAT(NINTVL)
YINTG3=XINTGD(1)
NPT=1
DO 1 NPT=2,NINTVL,2
YINTG3=YINTG3+XINTGD(NPT)*4.0
CONTINUE
DO 2 NPT=3,NINTVL,2
YINTG3=YINTG3+XINTGD(NPT)*2.0
CONTINUE
YINTG3=YINTG3+XINTGD(NPOINT)
YINTG=YINTG+YINTG3*DELINT/3.0
RETURN
END

```

1  
2

```

1 SUBROUTINE SUMMA
2 COMMON/MEIIG/WAVEFN(301),RADIUS,A,VC,ALPHA,AMASS,RMAX,EPS,MODE,
3 INOMAX,NINTVL,L,ELL,K,JDBLD,JPRINT,MPRINT,NPOINT,EN,FLOUT,HI,R,RR,
4 NH,VPLUS(599),V,NMAX,F,RMATCH,I,XPLUS,XPLUSP,FRR,INOUT,KSTEP,REFL,
5 3XINTGD(301),YINTG,XINT1,XINT2,X,VD(300),WAFN(30,300),II,SEM(16,16)
6 4,VDD(300),SDM(16,16)
7 DO 2 I=1,II
8 DO 2 J=1,I
9 SUMEND=0.0
10 SUMMID=0.0
11 SUENDD=0.0
12 SUMIDD=0.0
13 DO 1 N=2,NPOINT,2
14 M=N+1
15 SUMEND=SUMEND+WAFN(I,N)*VD(N)*WAFN(J,N)
16 SUENDD=SUENDD+WAFN(I,N)*VDD(N)*WAFN(J,N)
17 IF (M,GE,NPOINT) GO TO 1
18 SUMMID=SUMMID+WAFN(I,M)*VD(M)*WAFN(J,M)
19 SUMIDD=SUMIDD+WAFN(I,M)*VDD(M)*WAFN(J,M)
20 CONTINUE
21 SUMA=WAFN(I,1)*VD(1)*WAFN(J,1)
22 SUDA=WAFN(I,1)*VDD(1)*WAFN(J,1)
23 SUMB=WAFN(I,NPOINT)*VD(NPOINT)*WAFN(J,NPOINT)
24 SUDB=WAFN(I,NPOINT)*VDD(NPOINT)*WAFN(J,NPOINT)
25 SEM(I,J)=.33333*HI*(2.0*SUMMID+4.0*SUMEND+SUDA+SUMB)
26 SDM(I,J)=.33333*HI*(2.0*SUMIDD+4.0*SUENDD+SUDA+SUDB)
27 CONTINUE
28 RETURN
29 END

```

1  
2

```

1 FUNCTION CGC1(NO)
2 TO USE ABMAGEOMETRICAL COEFFICIENT AS A FUNCTION CGC.
3 CGC(J1,M1,J2,M2,J3) = (2*J1,2*M1,2*J2,2*M2 | 2*J3,2*(M1+M2) ).
4 COMMON FACLOG(500),RAC,IA,IB,IC,ID,IE,IF,IL9(9),U9,KSELC
5 FACLOG(1)=0.0
6 FACLOG(2)=0.0
7 F1=1.0
8 DO 1 N=3,NO
9 F1=F1+1.0
10 FACLOG(N)=FACLOG(N-1)+ALOG(F1)
11 CONTINUE
12 CGC1=0.0
13 RETURN
14 ENTRY CGC(J1,M1,J2,M2,J3)
15 IA=J1
16 IB=J2
17 IC=J3
18 ID=M1
19 IE=M2
20 IF=M1+M2
21 KSELC=1

```

C  
C  
1

CALL CLEB  
CGC=RAC  
RETURN  
END

ABGEOMETRICAL COEFFICIENT GEOMETRICAL COEFFICIENTS, LIKE THE  
THIS PROGRAM CALCULATES THE RACAH COEFFICIENT AND 9-J SYMBOL  
CLEBSCH-GORDON COEFFICIENT, RACAH COEFFICIENT AND 9-J SYMBOL  
OCCURRING IN THE QUANTUM THEORY OF ANGULAR MOMENTUM.

SUBROUTINE CLEB  
COMMON FACLOG(500),RAC,IA,IB,IC,IE,IF,L9(9),U9,KSELC

RAC=0.0  
IGA=IA+IB+IC  
IF (KSELC.EQ.0) GO TO 1  
IF (ID+IE.NE.IF) GO TO 7  
IF (MOD(IGA,2).NE.0) GO TO 7  
IF (IA+IB-IC.LT.0.OR.IC-IABS(IA-IB).LT.0) GO TO 7  
IF (MINO(IA-IABS(ID),IB-IABS(IE),IC-IABS(IF)).LT.0) GO TO 7  
IF (MOD(IB+IE,2).NE.0.OR.MOD(IC+IF,2).NE.0) GO TO 7  
IF (IA.EQ.0.OR.IB.EQ.0) GO TO 2  
IF (IC) 7,3,4

RAC=1.0  
GO TO 7  
FB=IB+1  
RAC=((-1.0)\*\*((IA-ID)/2))/SORT(FB)

GO TO 7  
IF (ID.NE.0.OR.IE.NE.0) GO TO 5  
IG2=IG4/2  
IF (MOD(IG2,2).NE.0) GO TO 7

IG=IG2/2  
I1=(IA+IB-IC)/2+1  
I2=(IC+IA-IB)/2+1  
I3=(IC+IB-IA)/2+1  
I4=IG2+2  
I5=IG+1  
I6=(IG2-IA)/2+1  
I7=(IG2-IB)/2+1  
I8=(IG2-IC)/2+1

F1=EXP(.5\*(FACLOG(I1)+FACLOG(I2)+FACLOG(I3)+FACLOG(I4)))+(FACLOG(I5)  
1)-FACLOG(I6)-FACLOG(I7)-FACLOG(I8))

F2=IC+1  
F2=SORT(F2)  
S1=1-2\*MOD((IG2+IC)/2,2)  
RAC=S1\*F1\*F2  
GO TO 7

FC2=IC+1  
IABCP=IG4/2+1  
IABC=IABCP-IC  
ICAB=IABCP-IB  
IBCA=IABCP-IA  
IAPD=(IA+ID)/2+1  
IAMD=IAPD-ID

22  
23  
24  
25-

1  
2  
3  
4  
5  
6  
7  
8  
9  
10  
11  
12  
13  
14  
15  
16  
17  
18  
19  
20  
21  
22  
23  
24  
25  
26  
27  
28  
29  
30  
31  
32  
33  
34  
35  
36  
37  
38  
39  
40  
41  
42  
43  
44  
45  
46  
47  
48

C  
C  
C  
C

1  
2  
3  
4

5

49  
50  
51  
52  
53  
54  
55  
56  
57  
58  
59  
60  
61  
62  
63  
64  
65  
66  
67  
68  
69  
70  
71  
72  
73  
74  
75  
76-

```

IBPE=(IB+IE)/2+1
IBME=IBPE-IE
ICPF=(IC+IF)/2+1
ICMF=ICPF-IF
SOFCLG=0.5*(ALOG(FC2)-FACLOG(IABCP+1)+FACLOG(IABC)+FACLOG(ICAB)+FA
1CLOG(IBC)+FACLOG(IAPD)+FACLOG(IBPE)+FACLOG(IBM)+FAC
2CLOG(ICPF)+FACLOG(ICMF))
NZMIC2=(IB-IC-ID)/2
NZMIC3=(IA-IC+IE)/2
NZMI=MAX0(0,NZMIC2,NZMIC3)+1
NZMX=MIN0(IABC,IAMD,IBPE)
SI=(-1.0)**(NZMI-1)
DO 6 NZ=NZMI,NZMX
  NZMI=NZ-1
  NZT1=IABC-NZMI
  NZT2=IAMD-NZMI
  NZT3=IBPE-NZMI
  NZT4=NZ-NZMIC2
  NZT5=NZ-NZMIC3
  TERMLG=SOFCLG-FACLOG(NZ)-FACLOG(NZT1)-FACLOG(NZT2)-FACLOG(NZT3)-FA
1CLOG(NZT4)-FACLOG(NZT5)
  SSTERM=SI*EXP(TERMLG)
  RAC=RAC+SSTERM
SI=-SI
CONTINUE
IF (ABS(RAC).LT.0.000001) RAC=0.0
RETURN
END

```

6  
7

1  
2  
3  
4  
5  
6  
7  
8  
9  
10  
11-

```

FUNCTION TO CALCULATE THE MATRIX ELEMENTS OF SPHERICAL HARMONICS.
      M
      < L; LA | Y | L , LA >
      L
FUNCTION Y(LP,LAP,L,M,LL,LA)
X=FLOAT((2*LL+1)*((2*LL+1)))/(12.566375*FLOAT(2*LP+1))
IF (X.LT.1.0E-30) X=0.0
Y=SORT(X)*CGC(2*LL,2*LA,2*L,2*M,2*LP)*CGC(2*LL,0,2*L,0,2*LP)
IF (LAP.NE.M+LA) Y=0.0
RETURN
END
.....

```

C  
C  
C  
C

1  
2  
3  
4  
5  
6  
7  
8  
9  
10  
11  
12  
13

```

SUBROUTINE EIGEN
PURPOSE
  COMPUTE EIGENVALUES AND EIGENVECTORS OF A REAL SYMMETRIC
  MATRIX
USAGE
  CALL EIGEN(A,R,N,MV)
DESCRIPTION OF PARAMETERS
  A - ORIGINAL MATRIX (SYMMETRIC), DESTROYED IN COMPUTATION.

```

C  
C  
C  
C  
C  
C  
C  
C  
C  
C  
C  
C  
C



69  
70  
71  
72  
73  
74  
75  
76  
77  
78  
79  
80  
81  
82  
83  
84  
85  
86  
87  
88  
89  
90  
91  
92  
93  
94  
95  
96  
97  
98  
99  
100  
101  
102  
103  
104  
105  
106  
107  
108  
109  
110  
111  
112  
113  
114  
115  
116  
117  
118  
119  
120  
121  
122  
123

```

DO 4 J=1,N
IQ=IQ+N
DO 4 I=1,N
IJ=IQ+I
R(IJ)=0.0
IF (I-J) 4,3,4
R(IJ)=1.0
CONTINUE
    
```

3  
4  
C  
C  
C  
5

COMPUTE INITIAL AND FINAL NORMS (ANORM AND ANORMX)

```

ANORM=0.0
DO 7 I=1,N
DO 7 J=I,N
IF (I-J) 6,7,6
IA=I+(J-J)/2
ANORM=ANORM+A(IA)*A(IA)
CONTINUE
IF (ANORM) 33,33,8
ANORM=1.414*SQRT(ANORM)
ANORMX=ANORM*RANGE/FLOAT(N)
    
```

6  
7  
8

INITIALIZE INDICATORS AND COMPUTE THRESHOLD, THR

```

INDEF0
THR=ANORM
THR=THR/FLOAT(N)
L=1
M=L+1
    
```

9  
10  
11  
C  
C  
C

COMPUTE SIN AND COS

```

MQ=(M*M-M)/2
LQ=(L*L-L)/2
LM=L+MQ
IF (ABS(A(LM))-THR) 26,13,13
INDEF1
LL=L+LQ
MM=M+MQ
X=0.5*(A(LL)-A(MM))
Y=-A(LM)/SQRT(A(LM)*A(LM)+X*X)
IF (X) 14,15,15
Y=-Y
SINX=Y/SQRT(2.0*(1.0+(SQRT(1.0-Y*Y))))
SINX2=SINX*SINX
COSX=SQRT(1.0-SINX2)
COSX2=COSX*COSX
SINCS=SINX*COSX
    
```

13

14  
15

ROTATE L AND M COLUMNS

```

ILQ=N*(L-1)
IMQ=N*(M-1)
DO 25 I=1,N
IO=(I+I-1)/2
    
```

C  
C  
C

124  
125  
126  
127  
128  
129  
130  
131  
132  
133  
134  
135  
136  
137  
138  
139  
140  
141  
142  
143  
144  
145  
146  
147  
148  
149  
150  
151  
152  
153  
154  
155  
156  
157  
158  
159  
160  
161  
162  
163  
164  
165  
166  
167  
168  
169  
170  
171  
172  
173  
174  
175  
176  
177  
178

```

16 IF (I-L) 16,23,16
17 IF (I-M) 17,23,18
    IM=I+MQ
    GO TO 19
18 IM=M+IQ
19 IF (I-L) 20,21,21
20 IL=I+LQ
    GO TO 22
21 IL=L+IQ
22 X=A(IL)*COSX-A(IM)*SINX
    A(IM)=A(IL)*SINX+A(IM)*COSX
    A(IL)=X
23 IF (MV-1) 24,25,24
24 ILR=ILO+I
    IMR=IMO+I
    X=R(ILR)*COSX-R(IMR)*SINX
    R(IMR)=R(ILR)*SINX+R(IMR)*COSX
    R(ILR)=X
25 CONTINUE
    X=2.0*A(LM)*SINCS
    Y=A(LL)*COSX2+A(MM)*SINX2-X
    Y=A(LL)*SINX2+A(MM)*COSX2+X
    A(LM)=(A(LL)-A(MM))*SINCS+A(LM)*(COSX2-SINX2)
    A(LL)=Y
    A(MM)=X

    TESTS FOR COMPLETION
    TEST FOR M = LAST COLUMN
26 IF (M-N) 27,28,27
27 M=M+1
    GO TO 12

    TEST FOR L = SECOND FROM LAST COLUMN
28 IF (L-(N-1)) 29,30,29
29 L=L+1
    GO TO 11
30 IF (IND-1) 32,31,32
31 IND=0
    GO TO 10

    COMPARE THRESHOLD WITH FINAL NORM
32 IF (THR-ANRMX) 33,33,9
33 SORT EIGENVALUES AND EIGENVECTORS
    IQ=-N
    DO 37 I=1,N
    IO=IO+N
    LL=I+(I*I-1)/2
    JQ=N*(I-2)
    DO 37 J=I,N

```

179  
180  
181  
182  
183  
184  
185  
186  
187  
188  
189  
190  
191  
192  
193  
194  
195-

```

34 JQ=JQ+N
MM=J+(J*J-J)/2
IF (A(LL)-A(MM)) 34,37,37
X=A(LL)
A(LL)=A(MM)
A(MM)=X
IF (MV-1) 35,37,35
35 DD 36 K=1,N
ILR=IQ+K
IMR=JO+K
X=R(ILR)
R(ILR)=R(IMR)
R(IMR)=X
CONTINUE
CONTINUE
RETURN
END
36
37

```

```

SUBROUTINE PENGY (ED,KI,SNO,AMU,PROBH,GA)
DIMENSION EH(60),PROBH(30,30),V2(60),U1(30,60),V1(30,60),KI(2),

```

1  
2  
3  
4  
5  
6  
7  
8  
9  
10  
11  
12  
13  
14  
15  
16  
17  
18  
19  
20  
21  
22  
23  
24  
25  
26  
27  
28  
29  
30  
31  
32  
33  
34  
35

```

1 ED(2,60),EK(120)
M1=KI(2)
M2=KI(1)
M=M1+M2
DO 1 I=1,30
DO 1 J=1,30
PROBH(I,J)=0.0
G=GA/AMU
DO 2 I=1,M1
EK(I)=ED(2,I)
CONTINUE
DO 3 J=1,M2
EK(M1+J)=ED(1,J)
CONTINUE
WRITE (6,15) M1,M2,M,G,(EK(I),I=1,M)
WRITE (6,17)
CP=-7.
DEL=1.5
DO 9 II=1,M1
XCP=CP
DO 5 I=1,M
ECP=EK(I)-XCP
E=SQRT(ECP*ECP+DEL*DEL)
U2=0.5*(1.+ECP/E)
V2(I)=1.-U2
U1(II,I)=SQRT(U2)
V1(II,I)=SQRT(V2(I))
CONTINUE
SN=0.0
DEL=0.0
DO 6 J=1,M
IF (J.EQ.II) GO TO 6
SN=SN+V2(J)

```

1  
2  
3  
4  
5

```

36 DEL=DEL+U1(II,J)*V1(II,J)
37 CONTINUE
38 SN=2.*SN
39 DEL=G*DEL
40 DSN=SN-SNO
41 IF (ABS(DSN).LT.0.01) GO TO 7
42 CP=CP-0.2*DSN
43 GO TO 4
44 EC=0.0
45 DO 8 JJ=1,M
46 IF (JJ.EQ.II) GO TO 8
47 EC=EC+2.*EK(JJ)*V2(JJ)-G*V2(JJ)*V2(JJ)
48 CONTINUE
49 EH(II)=EK(II)+EC-DEL*DEL/G
50 WRITE (6,13) XCP,DEL,SN,U1(II,II),V1(II,II),EK(II)
51 CONTINUE
52 DO 10 I=1,M1
53 ED(2,I)=EH(I)
54 CONTINUE
55 WRITE (3,16) (ED(2,I),I=1,M1)
56 DO 12 I=1,M1
57 DO 12 J=1,I
58 X=U1(I,J)*U1(J,I)-V1(I,J)*V1(J,I)
59 DO 11 K=1,M
60 IF (K.EQ.I.OR.K.EQ.J) GO TO 11
61 X=X*(U1(I,K)*U1(J,K)+V1(I,K)*V1(J,K))
62 CONTINUE
63 PROBH(I,J)=X
64 CONTINUE
65 WRITE (3,14) ((PROBH(I,J),J=1,I),I=1,M1)
66 FORMATS
67 FORMAT (F10.5,5(2X,F10.5))
68 FORMAT (///,10X,PROBH(I,J) ,/8(2X,F10.5))
69 FORMAT (///,2X,M1 = ,13,2X,M2 = ,13,2X,M = ,13,2X,G = ,F8.4
70 /, EK(I) = ,/8(2X,F10.5))
71 /, EK(II) = ,/8(2X,F10.5))
72 FORMAT (///,10X,ED(2,I) = ,/8(2X,F10.5))
73 FORMAT (///, CHEM-POT NO. PART U1-OCUPH V1-0
74 /, CUPP EK
75 /, RETURN
END

```